Ore Geology Reviews xxx (2011) xxx–xxx

Contents lists available at ScienceDirect

Ore Geology Reviews

journal homepage: www.elsevier.com/locate/oregeorev

Felsic magmatic phases and the role of late-stage aplitic dykes in the formation of the world-class Cantung Tungsten skarn deposit, Northwest Territories, Canada

Kirsten L. Rasmussen [a,*], David R. Lentz [b], Hendrik Falck [c], David. R.M. Pattison [d]

[a] Dept. of Earth and Ocean Sciences, University of British Columbia, 6339 Stores Road, Vancouver, British Columbia, Canada V6T 1Z4
[b] Dept. of Earth Sciences, University of New Brunswick, P.O. Box 4400, Fredericton, New Brunswick, Canada E3B 5A3
[c] Northwest Territories Geoscience Office, P.O. Box 1500, Yellowknife, Northwest Territories, Canada X1A 2R3
[d] Dept. of Geosciences, University of Calgary, 2500 University Drive NW, Calgary, Alberta, Canada T2N 1N4

ARTICLE INFO

Article history:
Received 10 September 2010
Received in revised form 24 June 2011
Accepted 24 June 2011
Available online xxxx

Keywords:
Tungsten skarn
Aplite
Dykes
Cantung
Northwest Territories

ABSTRACT

A field and petro-chemical classification of felsic magmatic phases (FMPs) at the world-class Cantung W skarn deposit was undertaken to document the evolution of magmatism and the relationships between different FMPs, metasomatism, and mineralization. Early FMPs include moderately differentiated (Zr/Hf = 18–26, Ti/Zr = 14–15) biotite monzogranitic plutons and early biotite-rich granitic dykes, and compositionally similar quartz–feldspar porphyry dykes. Late, highly fractionated (Zr/Hf = 8–17, Ti/Zr = 3–13) FMPs sourced from a deeper monzogranitic intrusion include: (1) leucocratic biotite- or tourmaline-bearing dykes derived from localized entrapments of residual magma; and, (2) sub-vertical NE-trending aplitic dykes derived from a larger segregation of residual fluid- and incompatible element-enriched magma. The aplitic dykes have textures, morphologies, spatial associations, and a pervasive calcic metasomatic mineral assemblage (Ca-plagioclase + quartz or clinozoisite) indicative of syn-mineralization emplacement. Very late-stage overpressuring and initiation of sub-vertical fractures into the overlying plutonic carapace and country rocks by supercritical magmatic fluid led to an interaction with calcareous country rocks that resulted in an increased $a\mathrm{Ca}^{2+}$ in the fluid and the concurrent precipitation of W skarn. Residual magma also ascended with, and quenched in equilibrium with the magmatic fluid to from the aplitic dykes, then was metasomatized by the fluid as it interacted with calcareous country rocks. Overall, highly fractionated and moderately to very highly undercooled FMPs at Cantung provide evidence for a large and evolving felsic magmatic system at depth that segregated and maintained a stable fluid- and incompatible element-enriched residual magma until the latest stages of crystallization. The detailed study of FMPs associated with magmatic-hydrothermal mineral deposits allow us to refine our understanding of these mineralizing systems and better define metallogenic and exploration models for intrusion-related mineralization.

1. Introduction

The role of felsic intrusions in the formation of most magmatic-hydrothermal mineral deposits types is unquestionable, and mineralization associated with these systems is frequently localized in and proximal to granitic cupolas and (or) zones with a high densities of dykes (e.g., Bineli Betsi and Lentz, 2010; Breiter, 2002; Derre et al., 1986; Lentz, 2005a; Moore, 1975; Štemprok et al., 2008; Vallance et al., 2003). The Cantung W skarn deposit in the northern Canadian Cordillera is one example of the important relationship between magmatic intrusions and the localization of mineralization. At Cantung there is an empirical relationship between higher W grades and a series of fine-grained and frequently highly mineralized felsic dykes (or "aplites" in mine terminology) cutting the country rocks, the main intrusive pluton, and the skarn mineralization (e.g., Atkinson, 1984; Covert, 1983; Crawford, 1963; Mathieson and Clark, 1984). This observation led to the suggestion that these "aplites" could be used as indicators of pathways for W-bearing fluids and that these intrusions may have been important in the formation of mineralized skarn at the Cantung Mine (Atkinson, 1984). However, it wasn't inherently clear whether the "aplites" were pre-mineralization intrusions that provided permeable pathways for later mineralizing fluids, post-mineralization intrusions sealing fractures used by earlier mineralizing fluids, or syn-mineralization magma in equilibrium with the mineralizing fluids (Mathieson and Clark, 1984). With the first closure of the mine in 1986, recommendations by Atkinson (1984) for further study on these intrusions were not acted upon. However, recent re-opening of the mine has provided new opportunities to re-examine the deposit and sample the plutons and felsic dykes. This study documents the field relationships, petrographic textures, and geochemical compositions of these felsic magmatic phases (FMP) at Cantung with the intension of better understanding the petrogenesis of the felsic intrusions. Ultimately, the relationships between felsic dyke phases and metasomatic mineral assemblages,

* Corresponding author. Tel.: +1 778 891 9524; fax: +1 604 822 6088.
E-mail addresses: krasmuss@eos.ubc.ca (K.L. Rasmussen), dlentz@unb.ca (D.R. Lentz), hendrik_falck@gov.nt.ca (H. Falck), pattison@ucalgary.ca (D.R.M. Pattison).

0169-1368/$ – see front matter © 2011 Elsevier B.V. All rights reserved.
doi:10.1016/j.oregeorev.2011.06.011

and the role of these intrusions in the formation of the world-class W skarn deposit at Cantung are discussed.

1.1. Background

The northern Canadian Cordillera is one of the most well endowed W districts in the world (e.g., Dawson, 1996; Dawson and Dick, 1978; Dick, 1979; Dick and Hodgson, 1982; Hart et al., 2004a) and it hosts several notable W skarn occurrences and deposits associated with a broad belt of felsic Cretaceous magmatism emplaced primarily into the Neoproterozoic rifted margin and Paleozoic passive margin rocks of ancestral North America, or Laurentia (Fig. 1). Although only the Cantung deposit has been mined, several others are being actively explored and potentially moved toward production, including Mactung ("the world's largest undeveloped high-grade W skarn"; LaCroix and Cook, 2007). However, the extremely high ore grades at Cantung, one of the largest producers of W outside of Asia (Cathro, 1969; Dawson, 1996), allow it to be classified within the ninetieth percentile of known W skarn deposits in the world and qualify it as a world-class deposit (Menzie and Jones, 1986). Despite several temporary mine closures since the start of mining at Cantung in 1962, by the end 2009 an estimated 6.21 Mt with an average recovered grade of 1.56% WO_3 had been extracted at Cantung for a total value of approximately $1.5 billion (at $200/stu; Dave Tenney, pers. comm., 2010). The most recent estimate of the remaining mineral resource is 1.51 Mt grading 1.27% WO_3 (indicated), with probable mineral reserves of 1.02 Mt grading 1.08% WO_3 (Reid et al., 2009).

1.2. Regional setting

Voluminous Cretaceous magmatism (ca. 124–90 Ma; Mortensen et al., 2000; Hart et al., 2004a) throughout Laurentian and peri-Laurentian rocks in the northern Cordillera (Fig. 1) is the product of subduction of the Farallon Plate and accretion of the Alexander terrane along the ancestral west coast of North America (Nelson and Colpron, 2007). The timing of associated compression and uplift in the northern Cordillera is indicated by limited or poorly preserved east-directed sedimentation through the Late Aptian to Early Albian stages of the Cretaceous (Hadlari et al., 2009; Stott et al., 1991; Yorath, 1991). During this time, Proterozoic rift-related metasedimentary rocks and Cambrian to Devonian passive margin rocks were deformed into a thin-skinned fold and thrust belt, with dextral strain accommodated along transpressional structures active through the Early Cretaceous into the Cenozoic (Gabrielse et al., 2006). The structural grain of deformation trends NW–SE in the Cantung area and the deformation front migrated to the northeast until at least the Tertiary (Aitken et al., 1982; Aitken and Cook, 1974). Most of the Laurentian metasedimentary rocks in the northern portion of the Canadian Cordillera are of sub-greenschist facies metamorphic grade (e.g., Gordey and Anderson, 1993).

Cretaceous magmatism in the northern Cordillera comprises several belts of medium- to high-K calc-alkaline and alkaline magmatism (e.g., Anderson, 1983; Hart et al., 2004a; Lang, 2000; Mortensen et al., 2000). The youngest and most inboard belt of plutonic rocks is the highly metallogenic Tombstone-Tungsten Belt (TTB; Lang, 2000; Hart et al., 2004b), which includes the Tungsten, Mayo, and Tombstone plutonic suites (Fig. 1). The TTB was emplaced as a narrow, 750 km-long belt well inboard of the continental margin and has mineralogical, geochemical, and isotopic characteristics that suggest these intrusions were primarily derived from partial melting of radiogenic crust, although input of melt from enriched lithospheric mantle has been suggested for at least the Tombstone suite intrusions (e.g., Hart et al., 2004a,b; Mortensen et al., 2000). TTB intrusions are very small to moderate-sized, rounded plutons are associated with late felsic and lamprophyric dykes. Metallogenically, the TTB is associated with a range of poly-metallic mineralization types, including distal Ag–Pb–Zn and As–Sb, W–Cu skarns, Au–Bi ± W ± As sheeted veins and replacement-style mineralization, and Au–Cu–Bi skarns/veins and disseminated or vein-controlled U–Th–F disseminations (Hart et al., 2004b). The Cantung deposit has historically been associated with the Tungsten suite of intrusions, which has a metal tenor

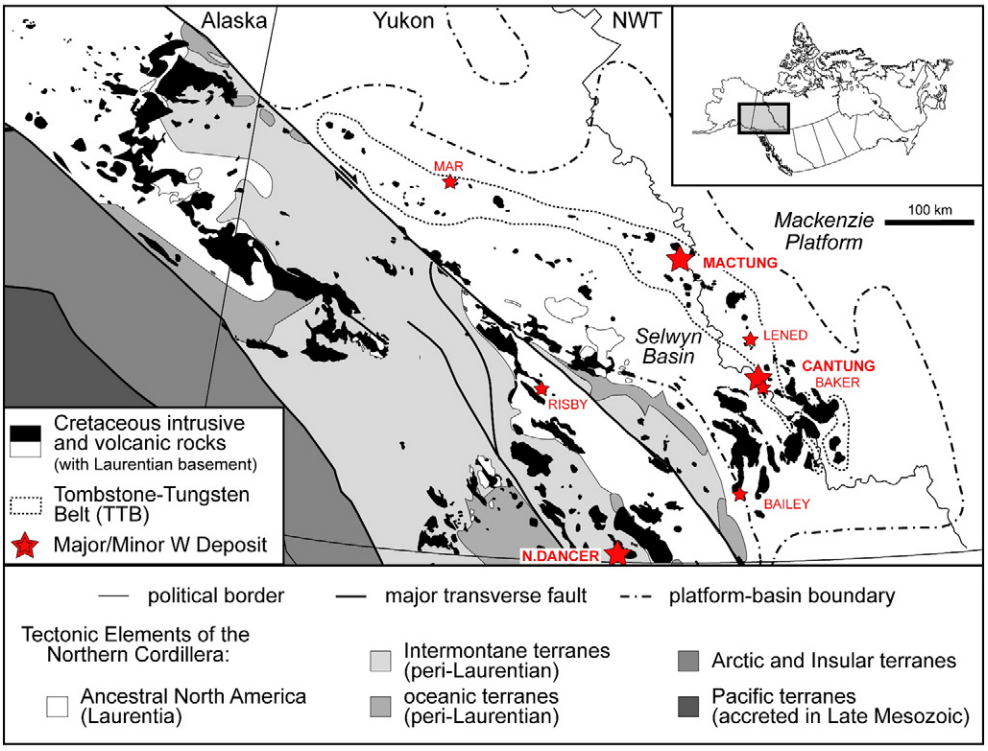

Fig. 1. Distribution of Cretaceous magmatism across ancestral North America (Laurentia) and peri-cratonic (peri-Laurentian) terranes of Yukon and the Northwest Territories (NWT). The locations of the Tombstone-Tungsten Belt, Cantung, and other significant tungsten skarn deposits and occurrences (names capitalized) are indicated. Modified from Gordey and Makepeace (1999) and Nelson and Colpron (2007).

Please cite this article as: Rasmussen, K.L., et al., Felsic magmatic phases and the role of late-stage aplitic dykes in the formation of the world-class Cantung Tungsten skarn deposit, Northwest Territories, Canada, Ore Geol. Rev. (2011), doi:10.1016/j.oregeorev.2011.06.011

consisting of W–Cu–(Zn–Bi–Au–Mo) proximal skarn and Pb–(Ag)–Zn distal manto and veins (Rasmussen et al., 2007).

The Tungsten plutonic suite comprises weakly to moderately peraluminous, reduced, leucocratic monzogranite to quartz monzonite intrusions (e.g., Anderson, 1983; Gordey and Anderson, 1993; Hart et al., 2004a,b; Rasmussen et al., 2007). Biotite- and (or) muscovite (typically sub-solidus) are the main hydrous mineral phases, and minor garnet or tourmaline-bearing leucogranite may be present along plutonic margins (e.g., Anderson, 1983; Hart et al., 2004b; Rasmussen et al., 2007). Tungsten suite plutons are invariably cross-cut by late aplite and pegmatite dykes, although rarer kersantitic lamprophyres have also been observed, particularly at Cantung (Gordey and Anderson, 1993; Rasmussen et al., 2007; Rasmussen et al., 2010). Although the intrusions are typically very small in exposed area (Figs. 1, 2), generally the most economically significant W skarn mineralization occurs in association with Tungsten suite plutons, including some of the more notable examples: Cantung, Mactung (33.0 Mt grading 0.88% WO_3 indicated and 11.3 Mt grading 0.74% WO_3; LaCroix and Cook, 2007), and Lened (0.75 Mt grading 1.17% WO_3 and 0.15% Cu).[1]

1.3. Local geology

The Cantung Mine is located in the Flat River Valley of the Northwest Territories (NWT) within primarily passive margin sedimentary rocks deposited near the transition from deeper water, siliciclastic rocks of the Selwyn Basin into shallower water, calcareous rocks of the Mackenzie Platform (Fig. 1). Mineralization is hosted within a series of strata consisting of turbiditic sandstone, deep-water limestone, chert, and shale (Gordey and Anderson, 1993). The stratigraphic sequence at Cantung has been described by multiple workers (Blusson, 1968; Covert, 1983; Crawford, 1963; Gordey and Anderson, 1993; Mathieson and Clark, 1984) and is only summarized here (Fig. 3). The oldest unit is the Lower Cambrian or older "Lower Argillite" of the Backbone Ranges Formation, which has been co-related to the Proterozoic Hyland Group: a package of thick, quartzo-feldspathic submarine-flows capped by maroon shales in this region of the Cordillera. At Cantung, the Lower Argillite consists of metamorphosed thin, laminated beds of dark gray mudstone to fine-grained sandstone, which is composed primarily of biotite, muscovite, and quartz, with spotted andalusite and cordierite, within a 500-meter contact aureole. Conformably overlying the Lower Argillite is the Lower to Middle Cambrian Sekwi Formation, which was deposited on an open shelf or carbonate ramp during the Lower Cambrian. The lower portions of the Sekwi Formation consist of a deep-water nodular limestone punctuated by debrites, represented at Cantung by the "Swiss Cheese Limestone". The gray to purple-colored Swiss Cheese Limestone has massive, nodular calcareous beds up to 10 cm thick within a finely bedded siltstone, and was contact-metamorphosed to a calc-silicate or siliceous hornfels at Cantung, where it locally hosts what is termed "chert ore." The "Ore Limestone", sharply and conformably overlying the Swiss Cheese Limestone, is a gray, pure, coarsely crystalline, banded marble up to 50 m thick, with minor dolomitic and argillitic horizons and hosts what is termed "skarn ore". Upper portions of the Sekwi Formation consist of shallow-water quartz arenite, dolostone, and multi-colored siltstone, which are represented by the "Upper Argillite" and "Dolostone" units at Cantung. The Upper Argillite is a dark gray to black slate, siltstone, and calcareous argillite interstratified with several massive, medium- to coarse-grained turbiditic quartzite horizons up to 3 m thick, and unconformably overlying the Ore Limestone. It contains corundum within 100 m of the intrusive rocks. The Dolomite is a gray-buff weathering, sandy and sparry, 500 m-thick, finely crystalline, massive dolostone generally lacking mineralized skarn. The Sekwi Formation is unconformably overlain by the Middle to Upper (?) Cambrian Rabbitkettle Formation offshelf carbonate rocks consisting of gray, thinly bedded, silty to graphitic limestone and black shales, which cap the exposed stratigraphy at Cantung.

The local strata were folded into a large, open syncline that forms the NW–SE oriented Flat River Valley (Armstrong et al., 1983; Covert, 1983), parallel to the regional structural grain and probably related to NE-verging fold- and thrust-style deformation. The strata are also folded into a smaller overturned anticline gently plunging to the northeast (Armstrong et al., 1983; Blusson, 1968), but there are no controls on the absolute timing of deformation. Fig. 3b is a generalized NW–SE section through the overturned anticline on the southwest limb of the larger syncline. At the mine scale, five steeply dipping, NE-trending, low-displacement (~6 m) brittle faults and associated splays (<2 m) have cut the country rocks, plutonic rocks, and orebodies (Cummings and Bruce, 1977). These faults were interpreted by McDougall (1977) to have formed during the pluton emplacement, and they closely parallel the sub-vertical tension cracks in the Dolomite unit recorded by Crawford (1963) and the orientations of several plutonic apophysies and dykes (Fig. 4A). The faults tend to be brittle zones 10–50 cm wide infilled with chlorite–carbonate clay-type gouge and pockets of coarse-grained calcite crystals, as well as pyrite and (or) pyrrhotite where they cross-cut skarn mineralization. Both felsic and mafic dykes may also be emplaced in these faults.

Two reduced, sub-alkaline, biotite monzogranite plutons of the Tungsten suite are exposed in the immediate Cantung Mine area (Fig. 3). The "Circular Stock" is a cylindrical body located northwest of the mine. Along the northern contact of the Circular Stock and the Upper Argillite wall rock there is a localized breccia pipe containing mm- to dm-size fragments of sub-rounded coarse-grained (leuco)monzogranite, sub-angular country rocks, and rarer mineralized skarn fragments. The "Mine Stock" is a laterally extensive and flat-topped body exposed in the Flat River Valley southeast of the mine, and it probably underlies the "apical Mine Stock" phase observed in the underground mine workings in contact with mineralization. Background W concentrations for the Mine and Circular stocks are low (0.9–2.6 ppm), but within the range of W concentrations found in other plutons of the Tungsten suite (e.g., 1–12 ppm; Gordey and Anderson, 1993; Hart et al., 2004b; Lang, 2000; Newberry and Swanson, 1986; Rasmussen, 2004; Rasmussen et al., 2007). The low W concentrations in the crystallized plutons near Cantung are thought to be due to a scarcity of Fe–Ti mineral phases (e.g., ilmenite) that can accommodate W in reduced intrusions, and (or) post-crystallization scavenging of W from biotite and ilmenite by sub-solidus magmatic fluid (van Middelaar and Keith, 1990). Most intrusions of the Tungsten plutonic suite in the region are composite bodies with gradational contacts between several highly differentiated intrusive phases (e.g., Anderson, 1983); however, similar leucocratic plutonic phases have not been identified in either the Mine Stock or the Circular Stock near the Cantung Mine (although these may be present at the nearby Baker and Redpath W skarn showings southeast of the Cantung deposit, also underlain by the Mine Stock). The Mine and Circular stocks are very similar mineralogically and geochemically, and it is likely that they are upper-level intrusions derived from one larger, homogenous monzogranitic magma chamber at depth, as exploration drilling would suggest. U-Pb crystallization ages range from as old as 101.15 ± 0.44 Ma (laser ablation-inductively coupled plasma-mass spectrometry, or LA-ICP-MS, on zircon; unpublished results) for the distal Mine Stock where it is exposed on the surface, to 98.2 ± 0.4 Ma for the proximal apical Mine Stock where it underlies the E-zone orebody underground (Rasmussen et al., 2007), and 96.7 ± 0.6 Ma for the Circular Stock where it outcrops on the surface (LA-ICP-MS on zircon; unpublished results). This range of crystallization ages suggests that the intrusions comprise separate magmatic events, although compositional similarities link them to ongoing felsic magmatism over a period of up to 4.5 m.y.

[1] Northern Minerals (NORMIN) Database — a database of mineral occurrences. (http://ntgomap.nwtgeoscience.ca)

Please cite this article as: Rasmussen, K.L., et al., Felsic magmatic phases and the role of late-stage aplitic dykes in the formation of the world-class Cantung Tungsten skarn deposit, Northwest Territories, Canada, Ore Geol. Rev. (2011), doi:10.1016/j.oregeorev.2011.06.011

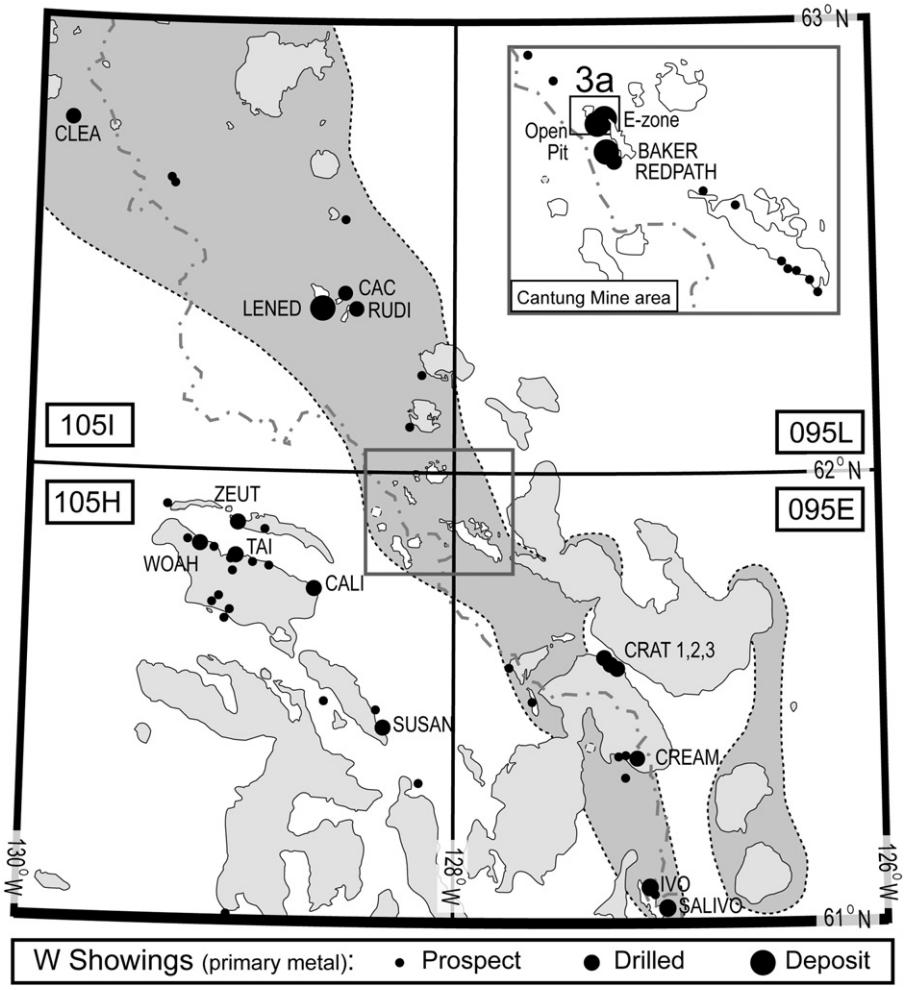

Fig. 2. Distribution of Cretaceous granitoids (grey), Tungsten Suite plutons (white) and mineral showings with W as a primary metal in NTS map sheets 105I, 105H, 095 L, and 095E. The extent of the Tombstone-Tungsten Belt is defined by the darkly shaded area with the dashed outline. The Yukon-NWT border is indicated by the gray stippled line, and the location of Fig. 3A is outlined in the upper right inset of the Cantung Mine area. At Cantung, the two orebodies are labelled "E-zone" and "Open Pit"; mineral occurrence locations are from the (Northern Minerals (NORMIN) Database — a database of mineral occurrences, http://ntgomap.nwtgeoscience.ca) and the Yukon MINFILE database (Yukon MINFILE — a database of mineral occurrences, www.geology.gov.yk.ca/databases_gis.html), and the map is modified from Gordey and Makepeace (1999).

The apical Mine Stock and nearby country rocks are cut by several phases of leucocratic dykes or sills. One biotite-bearing leucocratic dyke and one biotite-free dyke have been dated as 97.3 ± 0.3 Ma and 98.3 ± 0.3 Ma, respectively (Rasmussen et al., 2007). In addition to felsic dykes, late veins and small localized stockworks of quartz ± tourmaline, microcline, calcite, chalcopyrite, coarse-grained scheelite, and trace powellite are found underground cross-cutting the apical Mine Stock, felsic dykes, and skarn mineralization (e.g., Zaw, 1976). Well-mineralized, en-echelon quartz–scheelite veins are also exposed in the Open Pit, where they overprint earlier skarn in the Swiss Cheese Limestone (Yuvan et al., 2007). Kersantitic lamprophyric dykes (<1 m thick) cut the mineralized skarn and all other intrusive phases, and may contain milled clasts of granite, "aplite", quartz vein, and mineralized skarn (Bartlett, 1982; van Middelaar, 1988; van Middelaar and Keith, 1990). Geological relationships and ^{40}Ar–^{39}Ar geochronology (91.0 ± 0.8 Ma; Rasmussen et al., 2007) suggest that the mafic dykes are the last magmatic event at Cantung.

1.3.1. Mineralization

Metallogenic associations at Cantung are typical of reduced W skarn deposits and are dominated by W (as scheelite) and Cu (as chalcopyrite; grading 0.25–0.5%), although locally abundant zinc (as sphalerite in late base metal veins or large pods in the E-zone, or late sphalerite after pyrrhotite in skarn facies), and anomalous Bi (bismuth and bismuthinite) and Au concentrations are also significant (e.g., Zaw, 1976; Cummings and Bruce, 1977; McDougall, 1977; Dick, 1978; Dick and Hodgson, 1982; Amax Internal Report, 1983; Newberry, 1998; B. Mann, pers. comm., 2003; Marshall et al., 2003; Hammarstrom et al., 2004). Due to the very reduced nature of the mineralization Mo is very rare, but molybdenite has been observed in skarn mineralization adjacent to a quartz vein (Newberry, 1998; C. Hart, pers. comm., 2010). As the dominant sulfide species at Cantung, pyrrhotite is generally abundant in all of the skarn facies, forming up to 80% of some skarn facies, and is positively correlated with W grades (Dick and Hodgson, 1982; Zaw, 1976). Skarn mineralization is mainly localized by fractures, faults, and lithological contacts, and usually occurs as irregularly shaped pods or thin lenticular wavy bands following compositional banding (Dawson, 1996; Mathieson and Clark, 1984; Zaw, 1976); high grade mineralization is particularly well-developed in the Ore Limestone within 2–3 m of the upper and lower contacts (B. Mann, pers. comm., 2003). Coarse-grained scheelite may also be found along fractures in unaltered marble and within altered argillaceous country rocks and granitoids intrusions, including the "aplites".

Two large orebodies have been identified at Cantung. The "Open Pit" orebody is hosted by the Swiss Cheese and Ore limestones in the upper limb of the recumbent anticline (Fig. 3b). Here, particularly high W grades occur at the base of the Ore Limestone and (or) in association with late en-echelon quartz veins cutting the Swiss Cheese

Please cite this article as: Rasmussen, K.L., et al., Felsic magmatic phases and the role of late-stage aplitic dykes in the formation of the world-class Cantung Tungsten skarn deposit, Northwest Territories, Canada, Ore Geol. Rev. (2011), doi:10.1016/j.oregeorev.2011.06.011

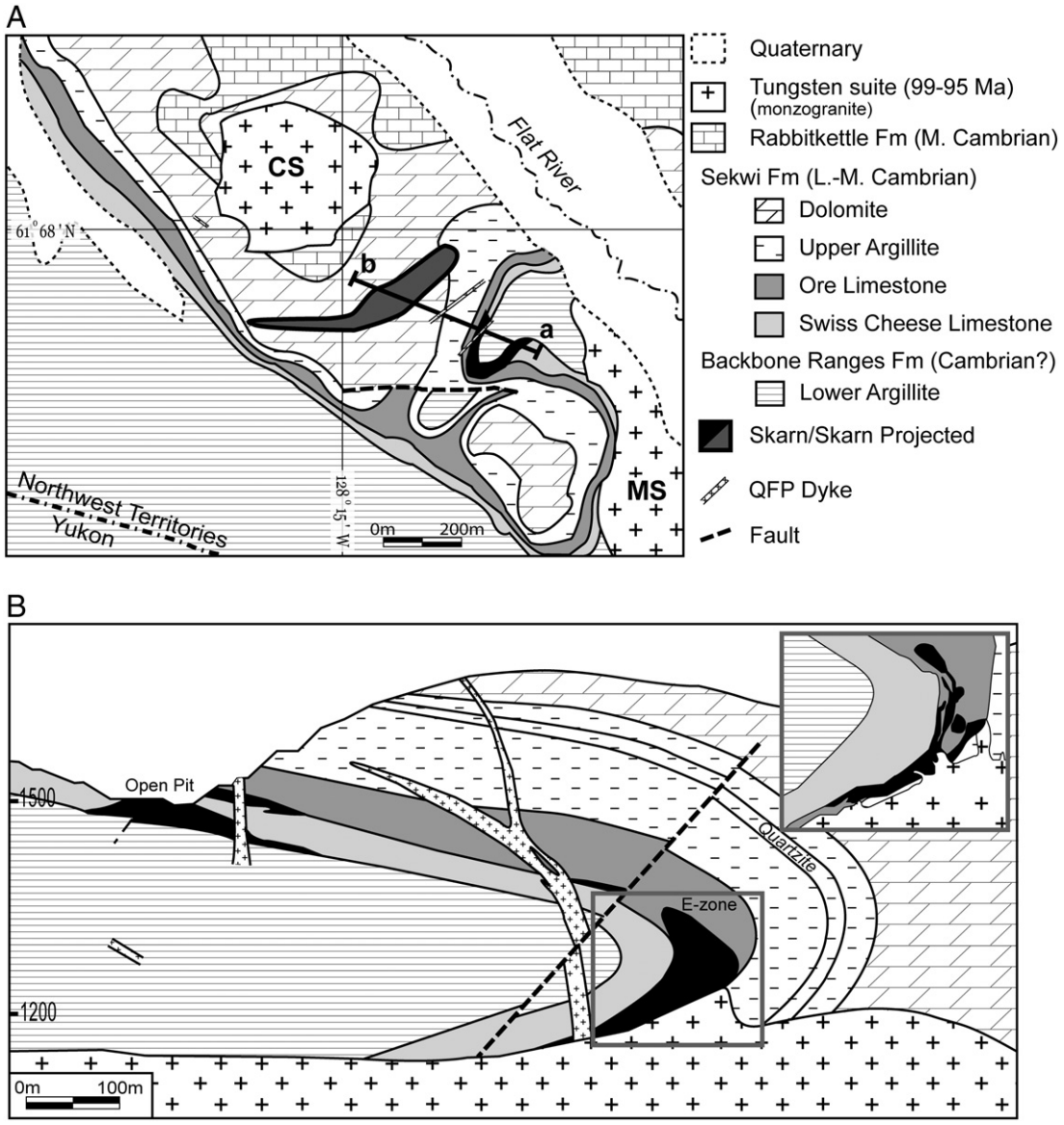

Fig. 3. Local geology at the Cantung Mine. The section line "a–b" on panel A represents the location of the panel B cross-section, and meters above sea level are indicated on the left of panel B. A. Surface geology at the Cantung Mine (modified from Blusson, 1968); the Mine and Circular stocks are denoted by "MS" and "CS", respectively. B. Generalized south to north section at the Cantung Mine showing relative locations of the Open Pit and E-zone orebodies within the folded stratigraphy, and the irregular nature of both the roof of the Mine Stock (MS) and the E-zone ore body (after Cummings and Bruce, 1977; Hodgson, 2000; one cross-sectional detail of E-zone orebody in upper right inset is courtesy of D. Tenney, Cantung internal files, 2003).

Limestone (Adie et al., 1959; Crawford, 1963; Yuvan et al., 2007). Mineralization in the Open Pit is mainly banded to massive, high-temperature grossular-hedenbergite skarn with lesser hydrous actinolite and actinolite–pyrrhotite skarn facies, and contains disseminated scheelite and chalcopyrite (Cummings and Bruce, 1977; Dawson, 1996; Mathieson and Clark, 1984; Zaw, 1976). The underground E-zone orebody is hosted in the Ore Limestone in the hinge zone and the overturned lower limb of the recumbent anticline (Fig. 3b). Anhydrous grossular-hedenbergite skarn is located along the outer fringes of the E-zone orebody and distal to the underlying Mine Stock, whereas hydrous skarn coarsely grades from actinolite, actinolite–pyrrhotite, biotite–(phlogopite)–pyrrhotite, and biotite–(phlogopite) facies towards either the apical Mine Stock (Zaw, 1976; Zaw and Clark, 1978) or the core of the mineralogically zoned underground skarn facies (Dick, 1980; Dick and Hodgson, 1982; Mathieson and Clark, 1984). The biotite–pyrrhotite facies typically contains the coarsest grained scheelite and the highest W grades, both of which have been attributed to solubility changes resulting from temperature and $a\mathrm{Ca}^{2+}$ variations (Dawson, 1996; Dick and Hodgson, 1982; Mathieson and Clark, 1984; Newberry, 1998; Newberry and Einaudi, 1981; Zaw, 1976). Similarly, the coarse zonation exhibited by the skarn facies is thought to reflect a reduction in fluid temperature with distance from the intrusion and (or) a higher $a\mathrm{Ca}^{2+}$ in the more distal anhydrous skarn, as all of the skarn facies are thought to have formed from the same primarily magmatic fluid (Bowman et al., 1985; Dick and Hodgson, 1982; Mathieson and Clark, 1984; Zaw, 1976). Stable isotopic compositions of skarn-forming fluids at Cantung indicate an exceptionally high flux of fluid (average water/rock ratio = 40) with over 90 mol% of the fluid in equilibrium with the late leucocratic dykes (i.e., <10 mol% from country rock or meteoric sources; Bowman et al., 1985).

Early estimates of the depth of mineralization in the E-zone relied on a pressure estimate of 1 kbar using co-existing pyrrhotite, sphalerite, and pyrite geobarometry; this was updated to range from 0.75 to 1.75 kbar by Marshall et al. (2003). However, this sulfide sample was taken from a late base-metal vein of unknown age cross-cutting skarn

Please cite this article as: Rasmussen, K.L., et al., Felsic magmatic phases and the role of late-stage aplitic dykes in the formation of the world-class Cantung Tungsten skarn deposit, Northwest Territories, Canada, Ore Geol. Rev. (2011), doi:10.1016/j.oregeorev.2011.06.011

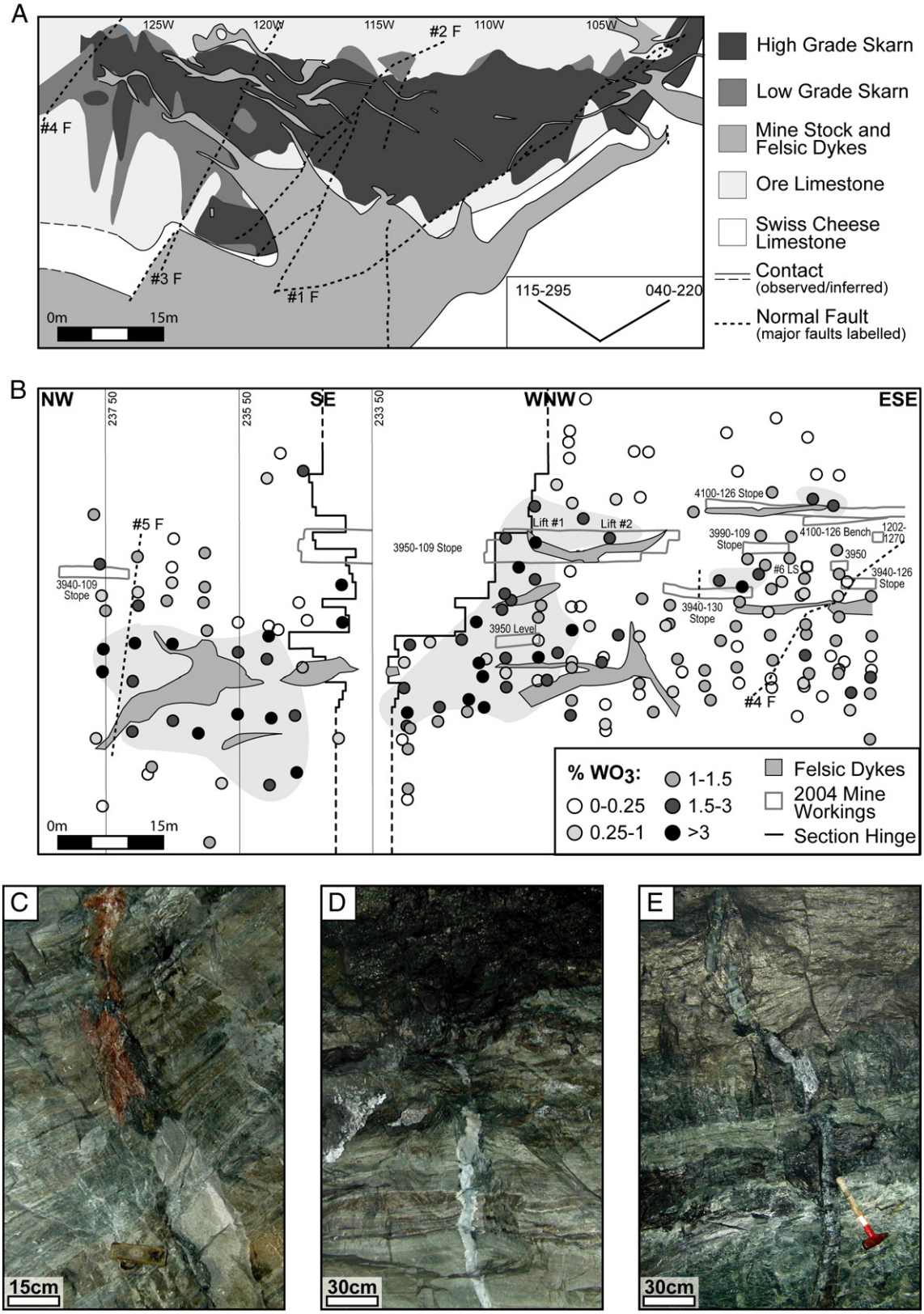

Fig. 4. The empirical relationship between felsic dykes and tungsten mineralization. A. Simplified level plan of the 4000-foot level showing the spatial relationship between high grade ore and large felsic dykes and plutonic apophysies (modified from Watson, 1981). Note the two dominant orientations of the dykes and the apophysies at 115°–295° and 040°–220°, and the orientation of major faults (labeled "F"). B. Simplified long section based on drill intercepts (not to scale) through the West Extension of the E-zone orebody showing the relationship between scheelite grade and aplitic dykes (courtesy of D. Tenney, Cantung internal files, 2003). Zones of higher ore grade are shaded gray. C. Aplitic dyke with zoned calcic metasomatism cutting calc-silicate skarnified Upper Argillite and transitioning into scheelite-chalcopyrite–pyrrhotite-mineralized garnet–diopside skarn within the same fracture that the dyke infills (Survey Point S940, lower West Extension). D. Ribboned calcic-metasomatized aplitic dyke cutting overturned calc-silicate skarnified Upper Argillite and terminating at contact with pyrrhotite-rich W skarn in the Ore Limestone (4100-126E). E. Highly mineralized and calcic-metasomatized aplitic dyke cutting overturned calc-silicate skarnified Upper Argillite and pinching out in high-grade pyrrhotite-rich W skarn in the Ore Limestone (3900–125).

Please cite this article as: Rasmussen, K.L., et al., Felsic magmatic phases and the role of late-stage aplitic dykes in the formation of the world-class Cantung Tungsten skarn deposit, Northwest Territories, Canada, Ore Geol. Rev. (2011), doi:10.1016/j.oregeorev.2011.06.011

mineralization (Mathieson and Clark, 1984; Zaw and Clark, 1978) and as such is not necessarily a reliable estimate of the conditions of W skarn formation. A more recent estimate of 2 to 3.8 kbar, based on fluid inclusion studies and biotite–apatite geothermometry, was provided by Marshall et al. (2003) for the biotite skarn facies. This suggests, along with the presence of andalusite in the contact aureole, a moderately deep level of mineralization and a minimum pressure estimate of ca. 2 kbar, which is more consistent with the pressure conditions and inferred depths of mineralization reported for most W skarns (e.g., Meinert et al., 2005; Newberry, 1998; Newberry and Swanson, 1986).

1.3.2. The empirical relationship between aplite dykes and mineralization

Previous workers such as Crawford (1963) and Atkinson (1984) noted that many felsic or "aplite" dykes at Cantung are mineralized with up to 50% scheelite ± chalcopyrite–pyrrhotite, and that there also exists a strong correlation between dyke localization and the distribution of elevated W grades in the skarn. This empirical relationship between mineralization and the felsic dykes is evident in a level plan and a long section through the E-zone orebody (Fig. 4A, B), which demonstrate that higher grades of skarn mineralization are spatially associated with felsic dykes. Furthermore, several dykes contain skarn-mineralized xenoliths, or transition to scheelite-mineralized calc-silicate skarn assemblages within the same fracture that the dyke infills (Fig. 4C), or pinches out in high-grade skarn mineralization (Fig. 4D, E).

2. Methods

A total of 88 intrusive samples were collected from throughout the mine, and hand specimens were stained for K–feldspar with a sodium cobalt-nitrate solution. Major and minor faults, and 60 dyke orientations were measured and plotted in GEOrient32v.9, and a detailed underground drift map of a 105-meter wide section of the West Incline (leading to the West Extension underground workings) displaying a variety of dyke phases intruding Upper Argillite near the Mine Stock contact was completed (Rasmussen, 2004). Standard and polished thin sections for approximately 40 samples were examined petrographically,

Table 1
Classification of samples that were examined petrographically and geochemically.

Sample (KR-03-)	General mine location	Rock classification	Metasomatic classification[c,d]	Mineralized	Adjacent to mineralization
01-1	3850 Drift	Late Aplite	Calcic 2–**Ser/Cc**	Yes	Yes
01-2	3900-125	Late Aplite	Calcic 2–**Ser/Cc**		Yes
07-8	Mapped Drift[a]	Late Bt-dyke	Unaltered		
07-10	Mapped Drift	Late Bt-dyke	(Potassic?)–Ser/Cc		
07-11/13/5	Mapped Drift	quartz-sulfide vein	n/a		
07-18	Mapped Drift	Early Bt-rich dyke	Potassic		
07-21	Mapped Drift	Late Aplite	(Calcic 1)		
07-22	Mapped Drift	Late Aplite	Calcic 1		
09-1	3850-109	Late Bt-dyke (core)	Potassic–(Ser/Cc)		Yes
09-2	3850-109	Late Bt-dyke (intermediate)	Potassic–Ser/Cc		Yes
09-4	3850-109	Late Bt-dyke (margin)	Potassic–**Ser/Cc**		Yes
09-5	3850-109	Late Aplite (bleached margin of 09–4)	Calcic 2–**Ser/Cc**		Yes
14-1	5 Corners	Late Aplite	Potassic–**Ser/Cc**		
14-2	5 Corners	Late Bt-dyke (core)	Ser/Cc		
14-4	5 Corners	Late Aplite	Potassic–Calcic 1–Ser/Cc		
14-6	5 Corners	Mine Stock-apical	Unaltered		
14-10	1220 W Drift	Late Aplite	Calcic 1		Yes
14-11	1220 W Drift	Late Bt-dyke	Unaltered		
15-3	1102 E Ramp (top)	Late Aplite	Potassic and Calcic 1		
15-4	1102 E Ramp	Late Trm-dyke	Unaltered		
15-5	1102 E Ramp	Late Aplite	Calcic 1–**Ser/Cc**		
15-6	1102 E Ramp	Late Aplite and Bt-dyke	(Potassic)		
15-7c	1102 E Ramp	Late Trm-dyke	Potassic–(Calcic 1)–**Ser/Cc**		
15-8	1102 E Ramp	Late Bt-dyke	Potassic–**Ser/Cc**		
16-1	Open Pit	Early QFP dyke (margin)	Calcic 1		Yes
16-2	Open Pit	Early QFP (upper contact breccia)	n/a	Yes	Yes
16-3	Open Pit	Early QFP (core)	Potassic and Calcic 1		Yes
16-5	Mapped Drift	Late Bt-dyke to Aplite	(Ser/Cc)		
16-11	Mapped Drift	Late Aplite	Potassic–(Ser/Cc)		
27-1	apartment outcrop	Mine Stock-distal	Unaltered		
28-1	central phase	Circular Stock	Unaltered		
28-2	biotite-rich phase	Circular Stock	Unaltered		
28-5	in Dolomite unit	Early QFP (intensely flow-banded)	(Potassic)–Calcic 1		
30-1	Road to Open Pit	Early QFP dyke	Potassic		
30-4	Road to Open Pit	Early QFP dyke	(Potassic)		
31-2	3850; S924	Late Aplite	Calcic 2		Yes
31-3	3900-125	Mine Stock-aplitic margin	Calcic 2–**Ser/Cc**	Yes	Yes
31-4	3900-125	Mine Stock-transition (aplitic to apical)	Potassic and Calcic 1	Yes	Yes
31-5	3900-125	Mine Stock-apical	Unaltered		Yes
31-7	3812	Mine Stock-apical (apophysy/dyke)	Calcic 2	Yes	Yes
99-1	3900-125	Late Aplite	Calcic 2–**Ser/Cc**	Yes	Yes
03M-203[b]	along no. 5 fault	Late Bt-dyke	Ser/Cc		
03M-204	5 Corners; cuts MS	Late Aplite	Calcic 2–(Ser/Cc)		
03M-207	main haulage drift	Mine Stock-apical	Unaltered		
03M-212	Open Pit aplite	Early QFP dyke (sulfide-rich)	Potassic–(Ser/Cc)	Yes	Yes
KR-05-215	Apartment outcrop	Mine Stock-distal	Unaltered		

[a] The "Mapped Drift" comprises a 105-meter section of the West Extention incline for which a detailed geological map of dyke relationships was constructed (Rasmussen, 2004).
[b] *Italicized* samples are not preceeded by "KR-03-".
[c] Ser/Cc — sericite–calcite alteration (vein or disseminated).
[d] Brackets = only minor development of alteration type; **bolded** = intense development of alteration type.

Please cite this article as: Rasmussen, K.L., et al., Felsic magmatic phases and the role of late-stage aplitic dykes in the formation of the world-class Cantung Tungsten skarn deposit, Northwest Territories, Canada, Ore Geol. Rev. (2011), doi:10.1016/j.oregeorev.2011.06.011

Please cite this article as: Rasmussen, K.L., et al., Felsic magmatic phases and the role of late-stage aplitic dykes in the formation of the world-class Cantung Tungsten skarn deposit, Northwest Territories, Canada, Ore Geol. Rev. (2011), doi:10.1016/j.oregeorev.2011.06.011

Table 2
Geochemical data with relevant calculated geochemical parameters. A. Preliminary XRF and ICP-MS data. B. XRF and ICP-MS data for representative samples.

A

Sample (KR-03-)	01-1	01-2	07-22	09-2	07-11/13/5	14-10	14-6	15-3	15-7c	15-8	16-2	16-3	27-1	28-1	28-5	30-1	31-3	99-1
Alteration type	Cal-2	Cal-2	Cal-1	Pot	n/a	Cal-1	Unalt'd	Pot + Cal-1	Pot (+Cal-1)	Unalt'd-Pot	n/a	Pot + Cal-1	Unalt'd	Unalt'd	Cal-1	Pot	Cal-1	Cal-2
XRF																		
SiO_2 (%)	nd	45.84	76.53	74.55	nd	75.16	70.39	72.66	74.37	74.17	nd	75.98	71	71.16	62.24	74.12	77.38	nd
TiO_2 (%)	nd	0.27	0.046	0.119	nd	0.115	0.322	0.04	0.1	0.097	nd	0.107	0.335	0.318	0.08	0.112	0.075	nd
Al_2O_3 (%)	nd	30.56	13.55	13.8	nd	14.19	15.4	16.63	14.6	13.58	nd	13.09	14.91	14.79	22.23	13.51	13.42	nd
CaO (%)	nd	14.79	3.53	1.04	nd	7.22	2.9	8.85	0.72	1.32	nd	6.01	2.25	1.84	10.41	1.65	3.35	nd
K_2O (%)	nd	1.195	1.881	4.985	nd	0.674	3.243	0.183	7.108	5.551	nd	0.982	4.58	4.35	1.716	5.328	1.749	nd
Na_2O (%)	nd	2.28	3.24	3.58	nd	1.15	3.31	0.61	1.36	2.51	nd	1.06	3.11	2.92	1.65	3.03	3.26	nd
MgO (%)	nd	0.43	0.17	0.29	nd	0.24	0.74	0.07	0.2	0.17	nd	0.35	0.78	0.7	0.13	0.29	0.19	nd
MnO (%)	nd	0.051	0.019	0.025	nd	0.021	0.05	0.006	0.02	0.014	nd	0.012	0.036	0.046	0.004	0.011	0.017	nd
P_2O_5 (%)	nd	0.75	0.13	0.09	nd	0.14	0.17	0.24	0.11	0.09	nd	0.06	0.13	0.11	0.08	0.11	0.16	nd
Fe_2O_3 (%)	nd	1.526	0.861	1.356	nd	0.851	2.75	0.68	0.9	1.52	nd	1.875	2.593	2.975	0.554	0.7	0.956	nd
Zn (ppm)	nd	24	6	10	nd	7	29	3	7	8	nd	8	22	40	9	10	13	nd
Ba (ppm)	nd	70	70	187	nd	86	548	14	186	262	nd	143	628	663	1499	331	86	nd
Ce (ppm)	nd	63	10	44	nd	44	96	6	23	35	nd	79	89	72	55	41	30	nd
Co (ppm)	nd	2	4	4	nd	2	13	3	7	4	nd	1	6	8	3	5	7	nd
Cr (ppm)	nd	13	40	25	nd	41	25	28	29	22	nd	41	30	18	37	11	38	nd
Ga (ppm)	nd	97	22	15	nd	35	20	32	20	16	nd	28	19	19	29	12	22	nd
La (ppm)	nd	24	8	21	nd	26	43	12	10	25	nd	36	32	16	26	25	<2	nd
Nb (ppm)	nd	19	15	12	nd	11	12	26	13	10	nd	16	11	12	20	12	3	nd
Nd (ppm)	nd	23	<1	20	nd	20	38	<2	3	21	nd	29	40	29	24	18	7	nd
Ni (ppm)	nd	<16	<12	<16	nd	<18	<15	<16	<14	<11	nd	<18	<10	<12	<18	<17	<14	nd
Pb (ppm)	nd	<3	11	67	nd	<6	25	<9	46	36	nd	<5	37	31	<8	25	11	nd
Rb (ppm)	nd	108	105	199	nd	25	153	10	242	214	nd	46	195	187	59	200	77	nd
Sr (ppm)	nd	345	107	71	nd	296	285	370	62	117	nd	290	245	178	422	148	173	nd
Th (ppm)	nd	4	<2	6	nd	1	11	<9	<4	4	nd	15	15	13	7	6	0	nd
U (ppm)	nd	14	16	9	nd	7	3	8	27	15	nd	4	5	4	6	5	5	nd
V (ppm)	nd	14	8	9	nd	8	30	3	16	4	nd	12	26	35	14	11	7	nd
Y (ppm)	nd	20	6	18	nd	9	13	4	18	13	nd	22	12	18	13	13	8	nd
Zr (ppm)	nd	136	21	61	nd	61	137	33	35	51	nd	87	135	127	102	57	40	nd
LOI	nd	4.6	0	0.6	nd	0.6	1.1	0.2	0.8	1.1	nd	0.8	0.6	1.3	0.9	0.2	0.5	nd
Sum (%)	nd	97.79	99.99	99.93	nd	99.84	99.43	100.02	99.56	99.10	nd	99.62	99.88	99.35	99.95	100.61	99.47	nd
ICP-MS																		
Ag (ppm)	10.8	0.2	0.3	0.2	0.4	0.2	0.2	0.2	0.1	0.1	0.9	0.2	0.1	0.1	0.2	0.2	0.2	0.7
Al (%)	11.14	10.03	5.74	6.69	0.18	6.49	7.33	8.09	7.13	6.7	3.11	6.66	8.02	7.21	8.93	6.41	5.86	5.15
As (ppm)	1	2	3	2	<1	2	3	3	2	2	7	3	2	13	3	2	2	4
Ba (ppm)	41	70	60	177	7	67	529	15	164	248	26	126	686	662	1257	369	90	7
Be (ppm)	35	11	10	5	<1	3	6	8	7	7	11	16	3	5	3	7	18	24
Bi (ppm)	637.6	5	1.7	0.5	298.2	0.7	0.7	0.4	0.1	1.8	356.7	1.4	0.2	0.4	0.2	0.1	18.3	549.4
Ca (%)	10.84	9.57	2.45	0.61	0.27	5.13	2.01	6.36	0.43	0.82	5.54	4.17	1.56	1.18	6.95	1.19	2.21	7.99
Cd (ppm)	2.1	0.1	<0.1	0.1	<0.1	<0.1	0.1	0.1	<0.1	<0.1	0.2	0.1	0.1	<0.1	<0.1	0.1	0.1	0.1
Ce (ppm)	127	26	5	45	3	22	71	4	14	22	47	59	78	70	29	23	13	90
Co (ppm)	13	1	<1	1	70	<1	2	<1	1	1	17	<1	3	3	<1	<1	<1	37
Cr (ppm)	9.1	3.7	11	13.4	16.1	12.5	16.5	11.1	20.5	9.7	14	43.1	18.7	16.8	17.2	5.2	20.6	67.3
Cu (ppm)	15721.9	177.1	11.7	6.3	359.3	9.7	4.2	4	6.2	30.8	1297.9	36.3	3.6	6	2.5	49.3	21.7	768.4
Fe (%)	3.25	0.84	0.56	0.98	21.05	0.51	2.08	0.39	0.48	0.91	25.71	1.24	1.74	2.02	0.33	0.48	0.57	21.81
Hf (ppm)	2.6	2.1	1.4	1.9	<0.1	1.3	1.5	2.2	1.3	1.4	1.2	1.8	1.7	1.6	2.6	2	1.1	1.3
Hf_{recalc} (ppm)[c]	n/a	8.25	2.67	3.74	n/a	4.15	7.31	4.75	2.94	3.05	n/a	4.72	5.20	5.81	6.05	2.69	3.17	n/a
K (%)	1.15	0.78	1.5	4.07	0.08	0.5	2.58	0.15	5.82	4.61	1.01	0.66	3.67	3.55	1.13	4.93	1.48	0.11
La (ppm)	61.7	10.5	1.6	21.7	1.3	10.6	33.8	1.9	5.5	9.9	25.6	28	39.7	35.9	12.8	11	6.5	45.6
Li (ppm)	39.5	49.3	8	32.6	9.6	6.2	72.2	3.7	16.7	25.8	57.5	10.8	77.6	71.7	11	22.6	12.3	16.3
Mg (%)	0.04	0.14	0.05	0.14	0.07	0.09	0.35	0.01	0.06	0.07	1.2	0.15	0.42	0.35	0.03	0.15	0.08	2.05

Mn (ppm)	368	398	145	191	37	155	401	50	139	111	305	87	294	357	33	81	140	4258
Mo (ppm)	4	0.5	1.4	2.4	1.1	0.7	0.7	2.8	1.1	0.5	9.1	1.1	0.3	0.5	0.2	0.6	20.8	7
Na (%)	0.602	1.506	2.2	2.559	0.068	0.687	2.247	0.351	0.805	1.815	0.147	0.606	2.312	2.139	0.919	2.359	2.262	0.275
Nb (ppm)	2.3	13.7	13.2	10.3	0.3	8.8	10.7	19.2	9.2	6	5.6	13.1	9.9	10.4	13.8	8.5	3.9	32.1
Ni (ppm)	0.8	2.1	1.2	1.6	175.2	0.2	1.7	<0.1	2.2	1.1	6.2	1.1	3.3	2	0.7	1.7	1.5	18.9
P (%)	0.177	0.331	0.047	0.033	0.001	0.052	0.066	0.104	0.038	0.033	0.008	0.019	0.053	0.04	0.023	0.042	0.068	0.347
Pb (ppm)	6.4	14.1	19.7	76.1	3.9	6.4	35.2	5.1	50.9	41.4	18.2	4	38.9	35.6	4.5	39.7	24.7	2.6
Rb (ppm)	93	24.9	94.7	218.4	9.4	13.4	142.7	5.1	226.4	223.8	106	26.6	201.8	187	31.3	224.3	74.7	8.7
S (%)	1.9	0.3	<0.1	<0.1	8.1	0.1	<0.1	0.1	<0.1	0.1	12.8	0.4	<0.1	<0.1	<0.1	<0.1	0.1	8.4
Sb (ppm)	2.7	0.1	0.1	0.1	0.4	<0.1	<0.1	0.1	<0.1	0.1	2.3	0.1	0.1	0.1	0.1	0.2	0.1	0.2
Sc (ppm)	1	3	2	4	<1	3	5	<1	3	2	2	3	5	6	2	2	1	11
Sn (ppm)	29.6	9.9	0.8	1.4	1.5	2.4	1.9	0.9	5.5	9	7.2	10.7	1.7	3.8	2.2	6	4.8	48
Sr (ppm)	359	275	93	68	8	244	276	337	56	107	129	232	236	163	317	145	1.55	149
Ta (ppm)	0.2	2.5	10.7	2.3	<0.1	2.6	1.5	28.7	4.3	1.3	0.9	1.6	1.2	1.2	2.2	1.6	0.8	1.5
Th (ppm)	7.9	8	1.9	10	0.3	6.5	15.4	2.9	4.1	5.8	6	16	18	17.3	11.8	12.1	2.9	10.2
U (ppm)	41	8.3	12.2	8.2	0.1	9.3	4	14.3	24.8	10.8	7.3	5.7	4.2	2.3	5.3	6.8	8.5	5.2
V (ppm)	7	20	4	6	2	14	25	9	6	6	4	12	33	30	10	10	6	88
W (ppm)	>200	>200	0.9	1.6	55.2	12.3	1	1.4	2.2	1.8	>200	6.2	1	2.3	0.9	1.2	3.2	>200
Y (ppm)	29	11.3	6	6.4	1	7.1	8.5	4.8	7.4	6.7	21.5	17.4	7.7	14.4	10.3	11.2	6.2	40.8
Zn (ppm)	137	28	6	14	4	7	32	3	6	8	39	10	26	43	8	13	16	164
Zr (ppm)	28.7	34.6	11	31	1.9	19.1	28.1	15.3	15.5	23.4	24.3	33.2	44.1	35	43.8	42.4	13.9	28.9
$Zr_{correction\ factor}$[c]	*n/a*	*3.93*	*1.91*	*1.97*	*n/a*	*3.19*	*4.88*	*2.16*	*2.26*	*2.18*	*n/a*	*2.62*	*3.06*	*3.63*	*2.33*	*1.34*	*2.88*	*n/a*
Total S (%)	2.39	0.24	0.05	0.02	13.49	0.05	<0.02	0.02	0.04	0.22	16.81	0.56	<0.02	<0.02	<0.02	<0.02	0.12	13.78
ASI[a]	0.69	0.96	0.98	1.05	n/a	0.90	1.08	0.96	1.30	1.08	n/a	0.95	1.05	1.15	0.95	0.98	1.01	0.46
Nb/Y	nd	0.95	2.50	0.67	n/a	1.22	0.92	6.50	0.72	0.77	n/a	0.73	0.92	0.67	1.54	0.92	0.38	nd
Ti/Zr	nd	11.90	13.13	11.70	n/a	11.30	14.09	7.27	17.13	11.40	n/a	7.37	14.88	15.01	2.76	11.78	11.24	nd
Zr/Hf	11.04	16.48	7.86	16.32	n/a	14.69	18.73	6.95	11.92	16.71	20.25	18.44	25.94	21.88	16.85	21.20	12.64	22.23
Ab_{CIPW}[b]	nd	19.24	28.11	31.71	n/a	10.17	30.71	5.27	12.09	22.59	n/a	9.51	28.78	27.80	14.54	26.65	28.28	nd
An_{CIPW}	nd	73.21	17.08	4.79	n/a	32.98	14.56	43.01	6.13	6.34	n/a	29.76	11.28	7.93	50.17	7.76	15.97	nd
Mc_{CIPW}	nd	7.55	11.40	30.84	n/a	4.16	21.02	1.10	44.14	34.89	n/a	6.16	29.44	28.93	10.46	32.73	10.60	nd
Qtz_{CIPW}	nd	0.00	43.42	32.66	n/a	52.70	33.71	50.61	37.64	36.19	n/a	54.56	30.50	35.33	24.83	32.86	45.15	nd

[a]Aluminum saturation index: Al/(Ca + Na + K).
[b]Normalized to Ab + An + Mc + Qtz = 100.
[c] see Section 3.5.2 for discussion of the Zr correction factor and recalculated Hf concentrations.

B

Sample	03M-203	03M-204	03M-207	03M-212	07-18	KR-05-215
Alteration type	Unalt'd	Cal-1	Unalt'd	Pot	Pot	Unalt'd
XRF						
SiO_2 (%)	75	74.56	70.5	75.02	70.83	71.53
Al_2O_3 (%)	14.3	13.92	15.6	13.48	14.74	15.04
CaO (%)	0.86	2.54	2.4	1.22	2.28	1.93
K_2O (%)	4.74	2.54	3.93	5.79	4.84	4.26
Na_2O (%)	2.9	2.8	2.82	2.1	2.41	3.26
MgO (%)	0.17	0.16	0.68	0.16	0.59	0.53
MnO (%)	0.03	0.02	0.04	<0.01	0.03	0.04
P_2O_5 (%)	0.11	0.15	0.13	0.05	0.119	0.1
Fe–O_T (%)[a]	1.01	0.54	2.74	1.17	2.08	2.2
Fe_2O_3 (%)	0.10	0.05	0.08	−0.07	nd	0.05
FeO (%)[b]	0.82	0.44	2.39	1.11	nd	1.93
SrO (%)	0.01	0.02	0.04	0.03	0.03	nd
TiO_2 (%)	0.1	0.07	0.35	0.13	0.29	0.26
F (ppm)	70	340	470	150	nd	nd
LOI	0.53	2.54	0.41	0.61	1.19	0.43
Sum (%)	99.77	99.88	99.71	99.79	99.55	99.66

(continued on next page)

Table 2 (*continued*)

B						
Sample	03M-203	03M-204	03M-207	03M-212	07-18	KR-05-215
Alteration type	Unalt'd	Cal-1	Unalt'd	Pot	Pot	Unalt'd
ICP-MS (research quality dissolution)						
Ba (ppm)	97.9	189.5	666	422	1025	584
Ce (ppm)	22.5	13.3	88	76.3	80.6	79.3
Co (ppm)	0.6	0.5	3.3	0.8	4.8	2.8
Cs (ppm)	3.2	11.8	7.1	2.3	5.22	9.8
Cu (ppm)	<5	10	<5	27	18	1.2
Dy (ppm)	2.7	1.3	3.1	3.4	2.46	4
Er (ppm)	1.4	0.7	1.7	1.9	1.3	2.2
Eu (ppm)	0.2	0.4	1.2	0.9	1.34	1
Ga (ppm)	18	17	19	14	17	17
Gd (ppm)	2.4	1.2	5.2	5	4.35	5
Hf (ppm)	6	6	7	12	7.5	7
Ho (ppm)	0.5	0.3	0.6	0.7	0.41	0.7
La (ppm)	10.5	6.6	46.2	39.4	41.8	40.6
Lu (ppm)	0.2	0.1	0.2	0.3	0.16	0.2
Nb (ppm)	17	6	12	17	13	11
Nd (ppm)	9.3	5.3	34.3	29	29.9	31.2
Pb (ppm)	54	23	39	25	32	41
Pr (ppm)	2.6	1.5	10	8.6	8.32	8.4
Rb (ppm)	193	146	173	199	173	203
Sm (ppm)	2.5	1.2	6.3	5.7	5.25	5.5
Sn (ppm)	2	6	3	6	16	3
Sr (ppm)	47.7	146	314	184	292	201
Ta (ppm)	4	1.7	1.2	1.8	1.5	1.3
Tb (ppm)	0.5	0.2	0.7	0.7	0.52	0.7
Th (ppm)	6	3	19	23	21	18
Tl (ppm)	0.5	<0.5	0.5	0.7	0.6	0.5
Tm (ppm)	0.2	0.1	0.2	0.3	0.17	0.3
U (ppm)	21.1	10.8	9.2	7.6	5.82	8.8
V (ppm)	5	<5	25	5	21	23
W (ppm)	3	2	1	4	5	6
Y (ppm)	15.5	7.8	17.2	19.2	12.3	20.9
Yb (ppm)	1.4	0.8	1.5	1.8	1.13	2
Zn (ppm)	11	17	40	10	30	33
Zr (ppm)	186	232	288	467	309	268
ASI[c]	1.25	1.16	1.18	1.13	1.10	1.12
Fe_2O_3/FeO	0.134	0.341	0.054	0.045	nd	0.026
[d]Ab_{CIPW}	26.19	25.39	26.59	18.73	22.43	30.03
An_{CIPW}	3.79	12.45	12.46	6.13	11.69	9.71
Mc_{CIPW}	29.89	16.09	25.87	36.07	31.46	27.40
Qtz_{CIPW}	40.13	46.07	35.08	39.07	34.41	32.86

[a] Total iron oxide.
[b] Ferrous iron by HF–HCl acid digestion and titimetric finish.
[c] Aluminum saturation index: $Al/(Ca + Na + K)$.
[d] Normalized to $Ab + An + Mc + Qtz = 100$.

several of which were also examined on the scanning electron microscope (SEM).

Twenty samples underwent geochemical analysis by fused disc lithium borate fusion X-Ray fluorescence (XRF) spectrometry for major element oxides, plus fourteen trace elements at the University of Ottawa (Ottawa), and HF-based 4-acid total digestion inductively coupled plasma-mass spectrometry (ICP-MS) at Acme Analytical Laboratories (Vancouver). CANMET standards SY-4 (diorite gneiss), BH-1 (W ore), and GTS-2 (Au tailings) were also analyzed (see results in Rasmussen, 2004). An additional six representative intrusive samples were later analyzed for major-element oxides by lithium borate fusion and XRF spectroscopy, trace-element concentrations by lithium borate fusion ICP-MS (with attention to complete dissolution), and ferrous iron by HF–HCl acid digestion and titrimetric finish at ALS Chemex (Vancouver). Data quality of the latter samples was monitored with internal standards, sample duplicates, and selected high resolution ICP-MS analyses done at the Pacific Centre for Isotopic and Geochemical Research, University of British Columbia (Vancouver). Characteristics of geochemical samples are summarized in Table 1, and geochemical data with relevant calculated geochemical parameters are presented in Table 2.

Polished thin sections from eight samples also underwent electron probe micro-analysis (EPMA) for feldspar composition at the University of British Columbia, using a fully automated CAMECA SX-50 instrument operating in wavelength-dispersion mode under the following conditions: excitation voltage, 15 kV; beam current, 20 nA; peak count time, 20 s; background count-time, 10 s; spot diameter, 5 μm. Data reduction was done using the 'PAP' $\phi(\rho Z)$ method (Pouchou and Pichoir, 1985). For the elements considered, the following standards, X-ray lines and crystals were used: albite, Na$K\alpha$, TAP; anorthite, Al$K\alpha$, TAP; diopside, Mg$K\alpha$, TAP; orthoclase, Si$K\alpha$, TAP; orthoclase, K$K\alpha$, PET; anorthite, Ca$K\alpha$, PET; synthetic fayalite, Fe$K\alpha$, LIF; barite, Ba$L\alpha$, PET. Representative feldspar compositional data are presented in Table 3.

3. Felsic magmatic phases (FMP)

3.1. Plutonic phases

The Mine Stock is a relatively homogenous, medium-grained, hypidiomorphic granular, biotite (7–10%) monzogranite with minor amounts of sub-solidus muscovite and very fine-grained garnet in trace quantities (Fig. 5A, C, D). Exposures of the Mine Stock are limited to apical portions adjacent to the E-zone orebody in the underground mine workings, and more distal portions exposed on the surface southeast of the mine (Fig. 3). Where exposed on the surface, the Mine Stock has a medium-grained K-feldspar-phyric texture (<2 cm long) with smaller euhedral plagioclase sub-phenocrysts. Underground and more proximal to the E-zone orebody, the apical portion of the Mine Stock is finer grained and relatively equigranular in texture, with only sparse and small K-feldspar (<1 cm) phenocrysts. Contacts with country rock are typically discordant to bedding and (or) pre-existing fold structures, and foliated biotite hornfels and emplacement-related disharmonic folding in the country rocks along the apical Mine Stock contact is present locally (Mathieson and Clark, 1984). Large granitic apophysies and smaller dykes branch off the apical Mine Stock (e.g., Fig. 3b) and an unmineralized thin quartz margin (generally <5 cm, but up to 50 cm thick) fed by sub-vertical quartz veins cutting the Mine Stock frequently lines the contacts of the apical Mine Stock with siliceous country rocks (Fig. 5B; van Middelaar and Keith, 1990).

Microcline, with predominantly coarse and patchy tartan twins is present as euhedral Carlsbad-twinned megacrysts with abundant perthite, and anhedral grains with lesser perthite in the groundmass. Film perthite is typical, but is locally overprinted by coarser and shorter flame perthite associated with patches of minor sericitization and tartan twinning (Fig. 5E). Rare examples of anhedral microcline in the groundmass intergrown with rounded irregular blebs of quartz, or micropoikilitic texture (Fig. 5F), are observed and ascribed to recrystallized spherulitic K-feldspar with interstitial quartz. Magmatic and euhedral (sub-phenocrystic to phenocrystic) to subhedral (groundmass) plagioclase may have sharp fine albite twinning, and simple twins are abundant. Plagioclase is typically unzoned or normally zoned, although coarse reverse or finely developed oscillatory zoning may be observed in larger euhedral crystals thought to represent xenocrysts (Fig. 5D). These xenocrysts may also have unzoned sieve-textured cores or rounded and irregular calcic cores, frequently with more sodic unzoned to normal-zoned rims (Fig. 5G, H). Otherwise, euhedral plagioclase xenocrysts have anhedral margins that are typical of late stage grain boundaries in plutonic rocks (Fig. 5G, H). Quartz forms both large anhedral composite grains with slightly undulating extinction and sharp to consertal, planar to coarse-skeletal (mosaic-like) intergrain boundaries, and smaller anhedral to euhedral, slightly elongate prismatic to coarse-skeletal grains throughout the groundmass. Magmatic biotite is Ti-rich, typically dark red-brown, and is moderately low-Fe/(Fe + Mg) annite–siderophyllite (unpublished results), although bleached Ti-poor biotite ± chlorite with rutile needles occurs along some biotite grain margins (see Fig. 11A). Inclusions of accessory euhedral fluorapatite (unpublished results) and zircon are typical of fresh biotite and are particularly abundant in plutonic samples; trace ilmenite and very rare monazite are also associated with magmatic biotite.

The pipe-shaped Circular Stock is mineralogically very similar to the Mine Stock, with the exception of larger microcline phenocrysts (up to 2 × 3 cm) and composite quartz grains (1 cm). However, despite macroscopically appearing to be a hypidiomorphic-granular, K-feldspar megacrystic, coarse-grained biotite granite not unlike other Tungsten suite intrusions in the region, the Circular Stock has a strongly seriate texture defined by a very fine-grained, inhomogeneous quartz–feldspar groundmass.

3.2. Dyke phases

The majority of the felsic dykes (and sills) are found near the margins of the apical Mine Stock in the underground mine workings, with the exception of a series of quartz–feldspar–(biotite) porphyry (QFP) dykes exposed only at the surface. The dykes (and sills) are generally <1 m thick, locally bifurcate or have frequent jogs or offsets along joint and bedding planes, and locally contain angular rafts of wall rock materials. For simplicity, these intrusions will be herein referred to as dykes. Inter-dyke and dyke-pluton relationships are complicated by a lack of visible crosscutting relationships exposed underground and by difficulties discerning original magmatic textures and compositions, which are frequently overprinted or destroyed by partial to pervasive metasomatism in some of the dykes. However, several generalized intrusive phases have been identified using petrographic mineral associations and primary textures, where present, and these have been subdivided into "early" and "late" dyke phases.

3.2.1. Early dykes

A series of "biotite-rich" (7–15% biotite, but irregularly distributed) dykes intruded the country rocks as narrow (<15 cm-thick) dykes with shallow dips (<30°; Fig. 6A, B). Biotite-rich dykes are characterized by distinct cm-thick bleached margins where biotite and K-feldspar are lacking in favor of plagioclase and quartz (Fig. 6B). These intrusions are not particularly abundant as only of these dykes (with sheeted narrower equivalents) were observed underground. The biotite is also frequently foliated so that it is sub-horizontal. Texturally and mineralogically the biotite-rich dykes are nearly indistinguishable from the sparsely K-feldspar porphyritic apical Mine Stock (see the petrographic description in Section 3.1), except for higher biotite concentrations (see

Please cite this article as: Rasmussen, K.L., et al., Felsic magmatic phases and the role of late-stage aplitic dykes in the formation of the world-class Cantung Tungsten skarn deposit, Northwest Territories, Canada, Ore Geol. Rev. (2011), doi:10.1016/j.oregeorev.2011.06.011

Table 3
Representative feldspar compositional data for unaltered and metasomatized (potassic, calcic-1, and calcic-2) samples, as determined by EPMA.

Sample	Rock	Alteration	Na_2O[a]	MgO	Al_2O_3	SiO_2	K_2O	CaO	MnO	FeO	Total	Na[b]	Mg	Al	Si	K	Ca	Mn	Fe	∑Cat.	An[c]	Ab	Or	Fsp[d]
KR-05-215	Mine Stock-distal	Unalt'd	7.74	0.00	25.15	60.48	0.22	6.61	0.02	0.00	100.23	0.666	0.000	1.316	2.686	0.013	0.315	0.001	0.000	4.996	31.69	67.00	1.31	And-(Ol)
KR-05-215	Mine Stock-distal	Unalt'd	8.28	0.00	24.44	61.62	0.26	5.92	0.02	0.00	100.54	0.710	0.000	1.273	2.724	0.015	0.280	0.001	0.000	5.002	27.86	70.65	1.49	Ol-(An)
KR-05-215	Mine Stock-distal	Unalt'd	0.86	0.01	18.51	65.24	16.11	0.02	0.00	0.00	100.74	0.076	0.001	1.001	2.994	0.943	0.001	0.000	0.000	5.015	0.10	7.45	92.45	Mc
KR-05-215	Mine Stock-distal	Unalt'd	0.53	0.00	18.59	64.85	16.38	0.01	0.00	0.03	100.39	0.048	0.000	1.010	2.989	0.963	0.000	0.000	0.001	5.011	0.10	7.45	92.45	Mc
KR-05-215	Mine Stock-distal	Unalt'd	0.64	0.01	18.43	65.08	16.37	0.02	0.01	0.02	100.59	0.057	0.001	0.999	2.994	0.961	0.001	0.001	0.001	5.015	0.00	4.75	95.25	Mc
03M-207	Mine Stock-apical	Unalt'd	6.68	0.00	26.86	58.36	0.19	8.31	0.03	0.05	100.48	0.576	0.000	1.409	2.597	0.011	0.396	0.001	0.002	4.992	0.10	5.59	94.31	Mc
03M-207	Mine Stock-apical	Unalt'd	1.34	0.00	18.57	64.20	14.92	0.08	0.00	0.00	99.11	0.121	0.000	1.017	2.984	0.885	0.004	0.000	0.000	5.011	0.10	7.29	92.61	Mc
03M-207	Mine Stock-apical	Unalt'd	7.21	0.00	25.63	59.38	0.23	7.26	0.02	0.01	99.74	0.625	0.000	1.350	2.654	0.013	0.348	0.001	0.001	4.990	40.28	58.60	1.12	And
03M-207	Mine Stock-apical	Unalt'd	7.15	0.00	25.39	59.65	0.26	7.24	0.02	0.02	99.72	0.619	0.000	1.337	2.665	0.015	0.346	0.001	0.001	4.983	35.29	63.39	1.32	And
03M-207	Mine Stock-apical	Unalt'd	0.81	0.00	18.65	63.87	15.58	0.03	0.05	0.04	99.02	0.073	0.000	1.025	2.979	0.927	0.001	0.002	0.001	5.009	35.31	63.16	1.53	And
KR-03-07-18	Early Bt-rich dyke	Potassic	0.99	0.00	18.49	65.31	15.65	0.07	0.00	0.01	100.51	0.088	0.000	1.000	2.997	0.916	0.003	0.000	0.000	5.005	0.30	8.74	90.96	Mc
KR-03-07-18	Early Bt-rich dyke	Potassic	1.03	0.01	18.58	65.20	15.81	0.09	0.01	0.03	100.76	0.091	0.001	1.004	2.990	0.925	0.005	0.001	0.001	5.016	0.49	8.91	90.60	Mc
KR-03-07-18	Early Bt-rich dyke	Potassic	1.07	0.00	18.56	65.27	15.78	0.07	0.01	0.02	100.77	0.095	0.000	1.003	2.992	0.923	0.003	0.000	0.001	5.016	0.29	9.30	90.40	Mc
KR-03-07-18	Early Bt-rich dyke	Potassic	1.18	0.00	18.79	65.18	15.53	0.04	0.00	0.00	100.72	0.105	0.000	1.014	2.985	0.907	0.002	0.000	0.000	5.014	0.20	10.36	89.45	Mc
KR-03-07-18	Early Bt-rich dyke	Potassic	0.72	0.01	18.57	65.08	16.22	0.02	0.02	0.00	100.65	0.064	0.001	1.006	2.991	0.951	0.001	0.001	0.000	5.014	0.10	6.30	93.60	Mc
KR-03-07-18	Early Bt-rich dyke	Potassic	0.28	0.00	18.53	65.39	16.78	0.02	0.00	0.02	101.02	0.025	0.000	1.001	2.997	0.981	0.001	0.000	0.001	5.006	0.10	2.48	97.42	Mc
KR-03-07-18	Early Bt-rich dyke	Potassic	0.35	0.00	18.36	64.80	16.38	0.03	0.03	0.00	99.96	0.031	0.000	1.001	2.998	0.967	0.002	0.001	0.000	5.000	0.20	3.10	96.70	Mc
KR-03-07-18	Early Bt-rich dyke	Potassic	7.73	0.00	24.73	61.61	0.21	6.23	0.00	0.05	100.56	0.662	0.000	1.286	2.719	0.012	0.295	0.000	0.002	4.975	30.44	68.32	1.24	And-(Ol)
KR-03-07-18	Early Bt-rich dyke	Potassic	7.97	0.00	24.91	61.04	0.09	6.43	0.03	0.01	100.49	0.683	0.000	1.299	2.700	0.005	0.305	0.001	0.001	4.994	30.72	68.78	0.50	And-(Ol)
KR-03-07-18	Early Bt-rich dyke	Potassic	7.96	0.00	24.69	61.32	0.20	6.34	0.02	0.01	100.54	0.682	0.000	1.286	2.711	0.011	0.301	0.001	0.000	4.993	30.28	68.61	1.11	And-(Ol)
KR-03-07-18	Early Bt-rich dyke	Potassic	6.55	0.01	26.67	58.20	0.15	8.59	0.00	0.01	100.17	0.566	0.000	1.403	2.598	0.009	0.411	0.000	0.000	4.988	41.68	57.40	0.91	And
KR-03-07-22	Late aplite	Calcic-1	7.35	0.01	25.40	60.07	0.13	7.28	0.00	0.00	100.24	0.633	0.001	1.330	2.669	0.008	0.346	0.000	0.000	4.987	35.06	64.13	0.81	And
KR-03-07-22	Late aplite	Calcic-1	7.54	0.00	25.24	60.44	0.10	7.12	0.00	0.00	100.45	0.648	0.000	1.318	2.679	0.006	0.338	0.000	0.000	4.989	34.07	65.32	0.60	And
KR-03-07-22	Late aplite	Calcic-1	8.12	0.01	24.57	61.62	0.08	6.12	0.00	0.00	100.51	0.695	0.001	1.279	2.721	0.004	0.289	0.000	0.000	4.989	29.25	70.34	0.40	Ol-(And)
KR-03-14-10	Late aplite	Calcic-1	0.61	0.00	36.02	44.57	0.00	19.23	0.04	0.07	100.54	0.054	0.000	1.951	2.048	0.000	0.947	0.001	0.003	5.004	0.40	11.98	87.62	Mc
KR-03-14-10	Late aplite	Calcic-1	0.54	0.00	35.84	43.91	0.01	19.20	0.00	0.05	99.55	0.048	0.000	1.961	2.039	0.000	0.955	0.000	0.002	5.005	94.61	5.39	0.00	An
KR-03-14-10	Late aplite	Calcic-1	0.46	0.00	36.14	44.05	0.00	19.56	0.00	0.05	100.26	0.041	0.000	1.965	2.032	0.000	0.967	0.000	0.002	5.006	95.21	4.79	0.00	An
KR-03-14-10	Late aplite	Calcic-1	0.57	0.00	35.71	44.77	0.00	19.09	0.01	0.09	100.24	0.051	0.000	1.938	2.061	0.000	0.942	0.000	0.004	4.995	95.93	4.07	0.00	An
KR-03-14-10	Late aplite	Calcic-1	0.62	0.00	35.60	44.29	0.01	19.22	0.01	0.01	99.76	0.055	0.000	1.943	2.051	0.001	0.954	0.000	0.001	5.005	94.86	5.14	0.00	An
KR-03-14-10	Late aplite	Calcic-1	0.74	0.01	35.27	44.45	0.01	18.94	0.00	0.05	99.47	0.066	0.001	1.930	2.064	0.001	0.942	0.000	0.002	5.005	94.46	5.45	0.10	An
KR-03-14-10	Late aplite	Calcic-1	0.46	0.01	35.64	43.97	0.00	19.54	0.01	0.10	99.73	0.041	0.001	1.949	2.040	0.000	0.971	0.000	0.004	5.006	93.36	6.54	0.10	An
KR-03-14-10	Late aplite	Calcic-1	0.46	0.01	35.60	43.56	0.00	19.20	0.02	0.04	98.88	0.041	0.001	1.961	2.036	0.000	0.962	0.001	0.002	5.004	95.95	4.05	0.00	An
KR-03-31-3	Late aplite	Calcic-2	5.64	0.00	27.75	55.65	0.10	9.88	0.00	0.01	99.03	0.496	0.000	1.482	2.523	0.006	0.480	0.000	0.000	4.987	95.95	4.05	0.00	An
KR-03-31-3	Late aplite	Calcic-2	1.16	0.01	34.58	45.75	0.03	18.08	0.03	0.02	99.65	0.104	0.000	1.882	2.113	0.002	0.895	0.001	0.001	4.998	86.76	12.94	0.30	By
KR-03-31-3	Late aplite	Calcic-2	1.66	0.01	33.77	47.11	0.01	17.27	0.00	0.00	99.84	0.148	0.001	1.829	2.165	0.001	0.850	0.000	0.000	4.994	89.41	10.39	0.20	By
KR-03-31-3	Late aplite	Calcic-2	6.72	0.00	26.44	58.21	0.10	8.43	0.00	0.00	99.91	0.583	0.000	1.394	2.605	0.006	0.404	0.000	0.000	4.993	85.09	14.81	0.10	By
KR-03-31-3	Late aplite	Calcic-2	0.97	0.01	34.95	44.98	0.02	18.65	0.04	0.01	99.63	0.087	0.001	1.908	2.083	0.001	0.925	0.001	0.001	5.007	88.24	11.76	0.00	By
KR-03-31-3	Late aplite	Calcic-2	1.03	0.00	34.54	45.39	0.02	18.22	0.00	0.03	99.23	0.093	0.000	1.889	2.106	0.001	0.906	0.000	0.001	4.996	91.31	8.59	0.10	An
KR-03-31-3	Late aplite	Calcic-2	0.88	0.00	35.02	44.88	0.01	18.52	0.01	0.02	99.34	0.079	0.000	1.915	2.083	0.001	0.921	0.000	0.001	5.000	90.60	9.30	0.10	An
KR-03-31-3	Late aplite	Calcic-2	5.63	0.00	27.28	56.15	0.13	9.96	0.02	0.00	99.17	0.494	0.000	1.455	2.541	0.007	0.483	0.001	0.000	4.982	92.01	7.89	0.10	An
KR-03-31-3	Late aplite	Calcic-2	2.49	0.01	32.31	48.73	0.07	15.78	0.01	0.00	99.40	0.222	0.001	1.751	2.241	0.004	0.777	0.000	0.000	4.997	89.00	10.81	0.20	By-(An)
KR-03-31-3	Late aplite	Calcic-2	8.37	0.00	23.63	62.02	0.07	5.29	0.00	0.00	99.38	0.722	0.000	1.240	2.762	0.004	0.252	0.000	0.000	4.981	77.47	22.13	0.40	By
KR-03-31-3	Late aplite	Calcic-2	1.33	0.00	34.45	45.73	0.00	18.02	0.01	0.06	99.60	0.119	0.000	1.877	2.114	0.000	0.893	0.000	0.002	5.007	40.68	58.71	0.60	An
KR-03-31-3	Late aplite	Calcic-2	6.26	0.00	27.12	57.02	0.14	8.93	0.00	0.03	99.50	0.546	0.000	1.439	2.567	0.008	0.431	0.000	0.001	4.991	48.88	50.51	0.61	And
KR-03-31-3	Late aplite	Calcic-2	1.44	0.01	34.31	46.28	0.05	17.51	0.04	0.05	99.69	0.129	0.001	1.865	2.134	0.003	0.865	0.001	0.002	4.999	43.76	55.43	0.81	And
KR-03-31-3	Late aplite	Calcic-2	1.23	0.00	34.55	45.42	0.03	18.26	0.01	0.00	99.50	0.110	0.000	1.886	2.104	0.002	0.906	0.000	0.000	5.009	49.09	50.20	0.71	And-(La)

[a] wt.%.
[b] Number of ions on the basis of 8 oxygen.
[c] mol%.
[d] Fsp = Feldspar type: Mc = microcline, Ol = oligoclase, And = andesine, La = labradorite, By = bytownite, An = anorthite.

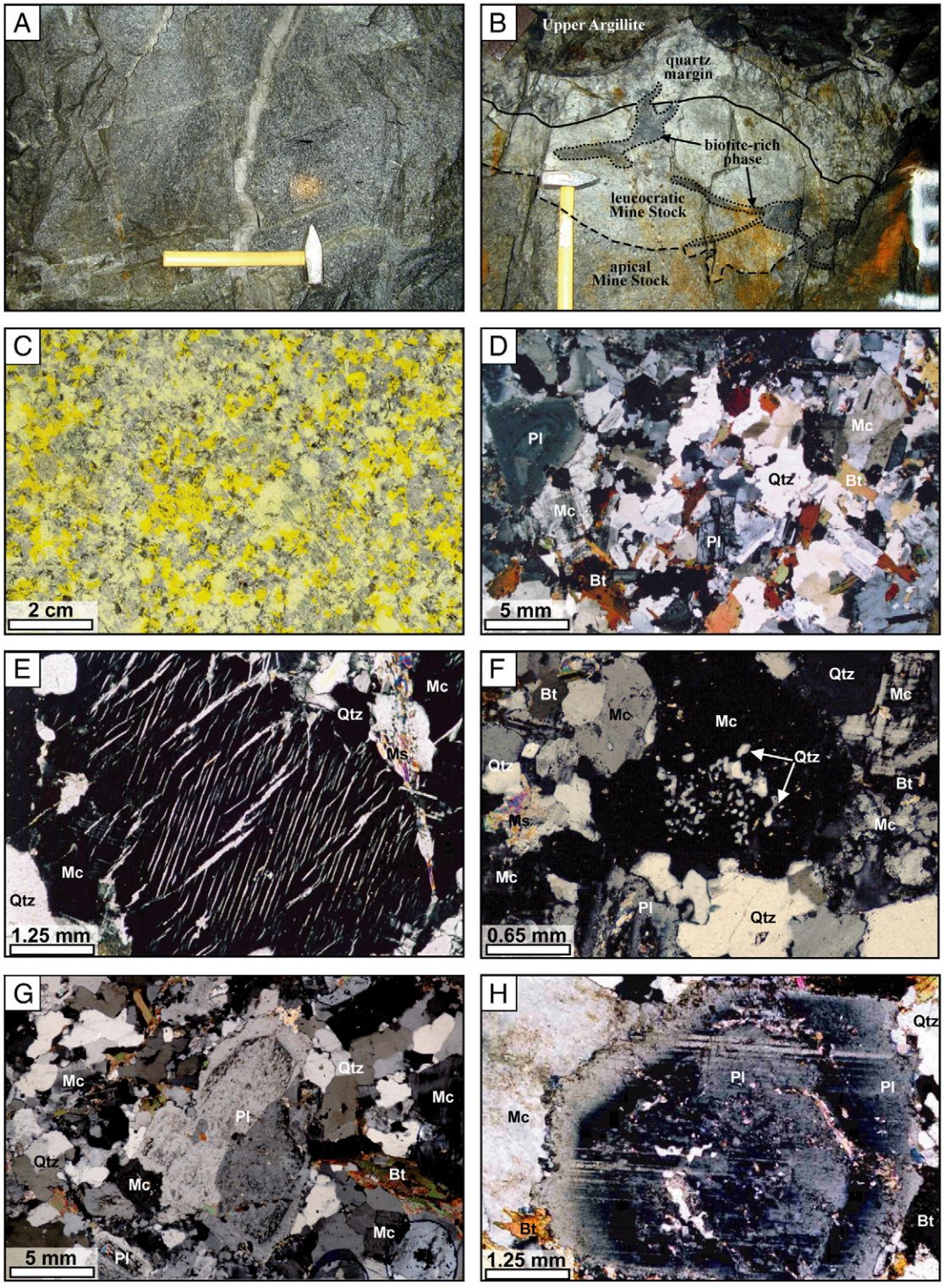

Fig. 5. Representative textures and mineralogy of the plutonic phases at Cantung. A. Hypidiomorphic-granular apical Mine Stock cut by quartz vein. B. Contact zone of apical Mine Stock with thick quartz margin with irregular biotite-rich phase similar to nearby off-shooting dykes and mantled by a wide envelope of bleached metasomatized Mine Stock. C. Polished thin section off cut showing fine- to medium-grained hypidiomorphic-granular texture with large composite quartz grains and 5–7% biotite. D. Photomicrograph (CPL; cross polarized light) showing typical hypidiomorphic-granular texture of biotite-bearing monzogranite, and a large complexly zoned plagioclase xenocryst in the upper left. E. Photomicrograph (CPL) of film perthite overprinted by flame perthite in microcline. The veinlet of muscovite represents minor manifestation of sericitic–calcic metasomatism (described in Section 3.4.4). F. Photomicrograph (CPL) of intergrown quartz (blebs) and microcline (at extinction) indicative of recrystallized spherulitic K-feldspar in micropoikilitic quartz. Note the presence of fine-grained sub-solidus muscovite. G. Photomicrograph (CPL) of simple-twinned xenocrystic plagioclase displaying sieve-textured core and thin normally zoned magmatic rim, with primary igneous biotite and minor sub-solidus muscovite. Groundmass plagioclase displays typical sericitization with muscovite along cleavage planes, and quartz has subhedral-euhedral prismatic to coarse-skeletal intergrain boundaries. H. Photomicrograph (CPL) of euhedral xenocryst of plagioclase displaying sieve-texture with a more calcic core and a normally zoned sodic rim. Rock-forming mineral notations are after Kretz (1983).

Please cite this article as: Rasmussen, K.L., et al., Felsic magmatic phases and the role of late-stage aplitic dykes in the formation of the world-class Cantung Tungsten skarn deposit, Northwest Territories, Canada, Ore Geol. Rev. (2011), doi:10.1016/j.oregeorev.2011.06.011

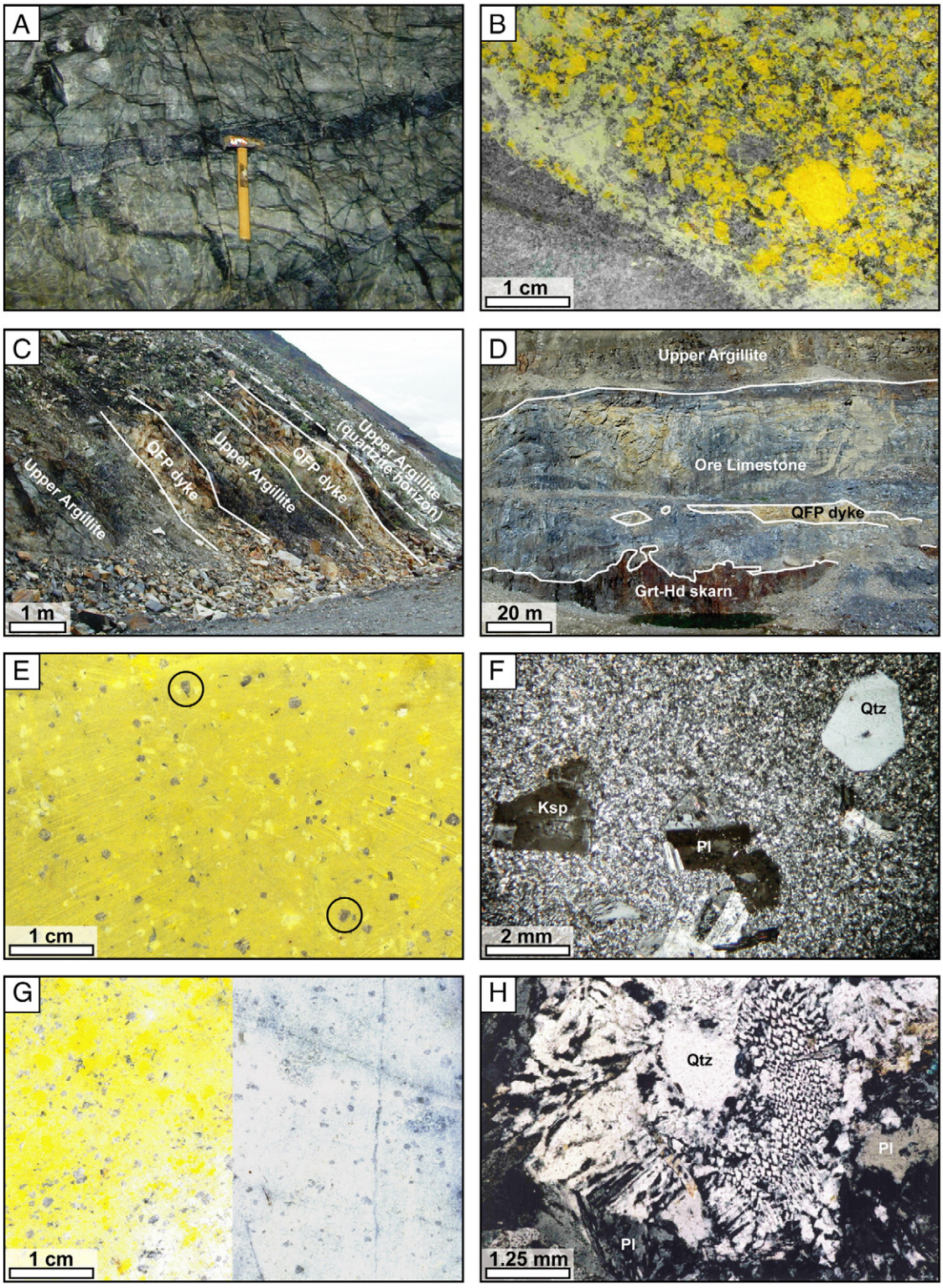

Fig. 6. Representative textures and mineralogy of the early dyke phases at Cantung. A. Shallow-dipping biotite-rich dyke and associated dykelet with bleached margins cutting a quartzite horizon in the Upper Argillite unit. B. Polished slab of shallow-dipping biotite-rich dyke stained for K-feldspar (bright yellow); note the lack of K-feldspar and biotite along the bleached contact with quartzite (bottom left) of the Upper Argillite unit. C. Exposure of two felsic QFP dykes in the Upper Argillite unit, approximately 300 m above the apical Mine Stock. D. Open Pit QFP dyke cutting the Ore Limestone above scheelite–chalcopyrite mineralized skarn. E. Stained polished slab of QFP dyke comprising dark gray quartz phenocrysts preserving dipyramidal beta-quartz morphologies and with rare embayments (some embayed examples are circled), euhedral plagioclase (pale yellow), and rarer euhedral microcline (deep yellow) and lath-like biotite phenocrysts. F. Photomicrograph (CPL) of QFP dyke with quartz, plagioclase, and K-feldspar phenocrysts in a microcrystalline quartz-feldspar-biotite groundmass. G. Two polished slabs stained for K-feldspar (bright yellow) from the Open Pit QFP dyke displaying variable degrees of calcic metasomatism: the left slab is taken from the dyke core and the right slab is taken from the dyke margin. H. Photomicrograph (CPL) of the QFP dyke in the Open Pit with pervasive micrographic and (or) coarse-granophyric to skeletal quartz intergrown with axiolitic spherulitic plagioclase replacing K-feldspar (lower left) and mantling a resorbed quartz phenocryst. Rock-forming mineral notations are after Kretz (1983). (For interpretation of the references to color in this figure legend, the reader is referred to the web version of this article.)

Please cite this article as: Rasmussen, K.L., et al., Felsic magmatic phases and the role of late-stage aplitic dykes in the formation of the world-class Cantung Tungsten skarn deposit, Northwest Territories, Canada, Ore Geol. Rev. (2011), doi:10.1016/j.oregeorev.2011.06.011

Section 3.4.5) and a finer-grained groundmass. In one locality at the contact of the apical Mine Stock with the Upper Argillite, an irregular and discontinuous biotite-rich 'phase' is haloed by bleached Mine Stock (Fig. 5B) and nearby biotite-rich dyke phases are seen off-shooting from the apical Mine Stock.

Four relatively thick (2–5 m), steeply dipping quartz–feldspar porphyry (QFP) dykes with biotite phenocrysts and a microcrystalline groundmass were observed and sampled from surface exposures 300–700 m above the apical Mine Stock and underground mine workings, including a large dyke found in the Open Pit (Fig. 6C, D). These dykes were not observed underground and are texturally distinct from all of the underground dykes. Angular biotite granite xenoliths of similar texture and mineralogy to the Mine Stock are found in at least one QFP dyke. The QFP dykes do not have chilled margins and they are enclosed by hornfelsed haloes extending 10–20 cm into the country rock. Their groundmass contains up to 10% phenocrysts. About 4% of the phenocrysts are quartz, which are generally 1.5–2 mm in size and have four pronounced crystal faces preserving a dipyramidal beta-quartz morphology. Sharp grain boundaries and rare embayments in the phenocrysts are suggestive either skeletal growth or resorption (Fig. 6E, F). Also present are euhedral plagioclase (4%) and microcline (1%) phenocrysts, both of which display evidence for either dissolution along grain margins or skeletal textures, and are moderately altered to sericite-muscovite (Fig. 6E, F). Biotite (1%) phenocrysts are locally altered to chlorite. The groundmass in the QFP dykes is microcrystalline and appears to be composed primarily of K-feldspar with lesser amounts of plagioclase and quartz, and minor biotite. However, a 3–4 meter thick QFP dyke emplaced into the Open Pit orebody is unique in that it is characterized by microcline and locally resorbed quartz phenocrysts mantled by pervasively developed magmatic micrographic to granophyric quartz–microcline intergrowths with marginal skeletal quartz and spherulitic or axiolitic feldspar (Fig. 6H). Although the QFP dyke in the Open Pit was also originally relatively potassic in composition, encroaching hydrous high-temperature calcic metasomatism from the contacts inwards (Fig. 6G) has replaced microcline phenocrysts and intergrowths with calcic plagioclase. A narrow (< 20 cm-wide) zone of massive and disseminated pyrrhotite-chalcopyrite-scheelite mineralized QFP is brecciated and cemented by quartz along the high-angle hanging-wall contact of the Open Pit QFP dyke; saussuritization of metasomatic calcic plagioclase is associated with this late breccia.

3.2.2. Late dykes

A series of very abundant, relatively large, and fine-grained hypidiomorphic-equigranular, but locally texturally heterogeneous, "biotite-bearing" (3–5%) leucocratic dykes and sills were also emplaced underground at Cantung (Fig. 7A, B). These late biotite-bearing dykes typically have moderately steep dips and are generally 20–50 cm thick. Although macroscopically similar in texture and mineralogy to the apical Mine Stock, these intrusions are finer grained and more leucocratic. Local pooling of fluids along dyke margins is evidenced by dm-scale pockets of albitic plagioclase and tourmaline with minor quartz (Fig. 7B), and bleached fractures and (or) quartz–tourmaline veins with bleached selvages frequently cross-cut these dykes. Anhedral to subhedral microcline has well-defined tartan twins and film perthite is overprinted by flame perthite. Equigranular subhedral to euhedral plagioclase is albite twinned, and complexly zoned xenocrystic grains were not observed. Quartz is typically anhedral with lesser coarse-skeletal grain boundaries, but rare irregular quartz blebs in microcline suggesting recrystallized micropoikilitic quartz interstitial to spherulitic K-feldspar is also present (Fig. 12C). Up to 5% primary magmatic muscovite has been observed in these dykes, and fine-grained magmatic biotite is a lighter brown color and has evolved to near-end-member siderophyllitic compositions (unpublished results). Compared to the Mine Stock and the early biotite-rich dykes, fewer inclusions of accessory zircon, apatite, and ilmenite are present, and monazite was not observed.

A relatively rare, but distinct set of moderately dipping, fine-grained, "tourmaline-bearing" (<3%) leucocratic dykes and sills (Fig. 7C) with pegmatitic equivalents are also recognized at Cantung, particularly in drill core intersections. Only four examples of such dykes were observed and sampled, but despite their limited distribution at least one tourmaline-bearing dyke was observed to cross-cut a biotite-bearing dyke at one locality. This dyke phase contains scattered small pockets of tourmaline in association with coarse-grained magmatic muscovite ± apatite displaying open-space filling textures (Fig. 7D), although graphic and granophyric textures are typical of pegmatitic equivalents. Large pockets of matted tourmaline with thick aplitic margins are also found along dyke margins and are broadly similar to the miarolitic cavities described by Sinclair and Richardson (1992) in felsic intrusions at the Northern Dancer (or "Logtung") W–Mo porphyry (located in Fig. 1). Similar examples of these leucocratic phases, but with the addition of minor garnet were also observed in drill holes under the nearby Baker W skarn prospect (Fig. 1; 0.12 Mt grading 1.4% WO_3; Dawson, 1996). Although texturally comparable to the late biotite-bearing dykes, these dykes are unique in that they contain magmatic tourmaline and muscovite ± garnet, lack biotite, and have pegmatitic equivalents.

A series of fine-grained, typically sub-vertical, narrow (<25 cm) "aplitic" dykes and sheeted dykelets (<3 cm wide) essentially lacking magmatic biotite and tourmaline is locally observed to cut and offset biotite-rich dykes in a normal sense (Fig. 7E–H). These aplitic dykes are also the only phase of dykes observed cutting the Mine Stock (Fig. 7G). Ribboned aplite ± quartz vein textures may be present in some of these dykes, indicating repeated fracture openings with alternating injections of magma and/or fluid (Fig. 7H). Some aplitic dykes are also zoned by metasomatic mineral assemblages and have central tourmaline stringers or veins. Sub-angular to angular fragments of argillaceous and calcareous rafts may be found in the aplitic dykes, and these clasts are sometimes affected by anhydrous skarnification ± mineralization. Aplitic dykes comprise the vast majority of intrusions seen adjacent to, cross-cutting, or pinching-out in skarn mineralization and they may be intensely mineralized with sulfides and scheelite (Fig. 4C–E). Furthermore, the association between sheeted clusters of aplitic dykelets and mineralized skarn has been used to indicate proximity to mineralization in mine exploration (B. Mann, pers. comm., 2004). Magmatic microcline is not abundant in these dykes, but may have simple twins when present. Quartz may or may not be present; however, where present it forms fine-grained subhedral to euhedral, interlocking equant to slightly elongate prisms that appear to be transitional from hexagonal dipyramidal to skeletal morphologies in the groundmass (Fig. 12D). These dykes are nearly ubiquitously metasomatized such that plagioclase is almost always an unzoned neoformed mineral phase. A single example of a partially altered, haplogranitic aplitic dyke found near the contact of the apical Mine Stock with Upper Argillite in an unmineralized drift has relict unaltered zones that are texturally and mineralogically similar to the biotite-bearing dykes except that fine-grained, ragged biotite ± muscovite are present in much lower abundances (<1%) and garnet is present in trace quantities (Fig. 7E).

3.3. Structural orientations

Structurally, the felsic intrusions at Cantung display considerable scatter on an equal area stereonet; however, most of the dyke orientations may be subdivided into two broad categories: shallowly to moderately dipping dykes, and sub-vertical dykes (Fig. 8A). Within the "shallow- to moderate-dipping" category, three general clusters of data are observed (Fig. 8A). The first comprises a phi-girdle, oriented 116/49 with the pole plunging gently NE-ward, and defined by the orientations of biotite-rich, biotite-bearing, and tourmaline-bearing intrusions found mainly in the upper mine workings near the hinge zone of the recumbent anticline. These intrusions may have been emplaced mainly along bedding planes in the overturned anticline, which also plunges gently to the north–northeast (Fig. 8A; upper inset).

Please cite this article as: Rasmussen, K.L., et al., Felsic magmatic phases and the role of late-stage aplitic dykes in the formation of the world-class Cantung Tungsten skarn deposit, Northwest Territories, Canada, Ore Geol. Rev. (2011), doi:10.1016/j.oregeorev.2011.06.011

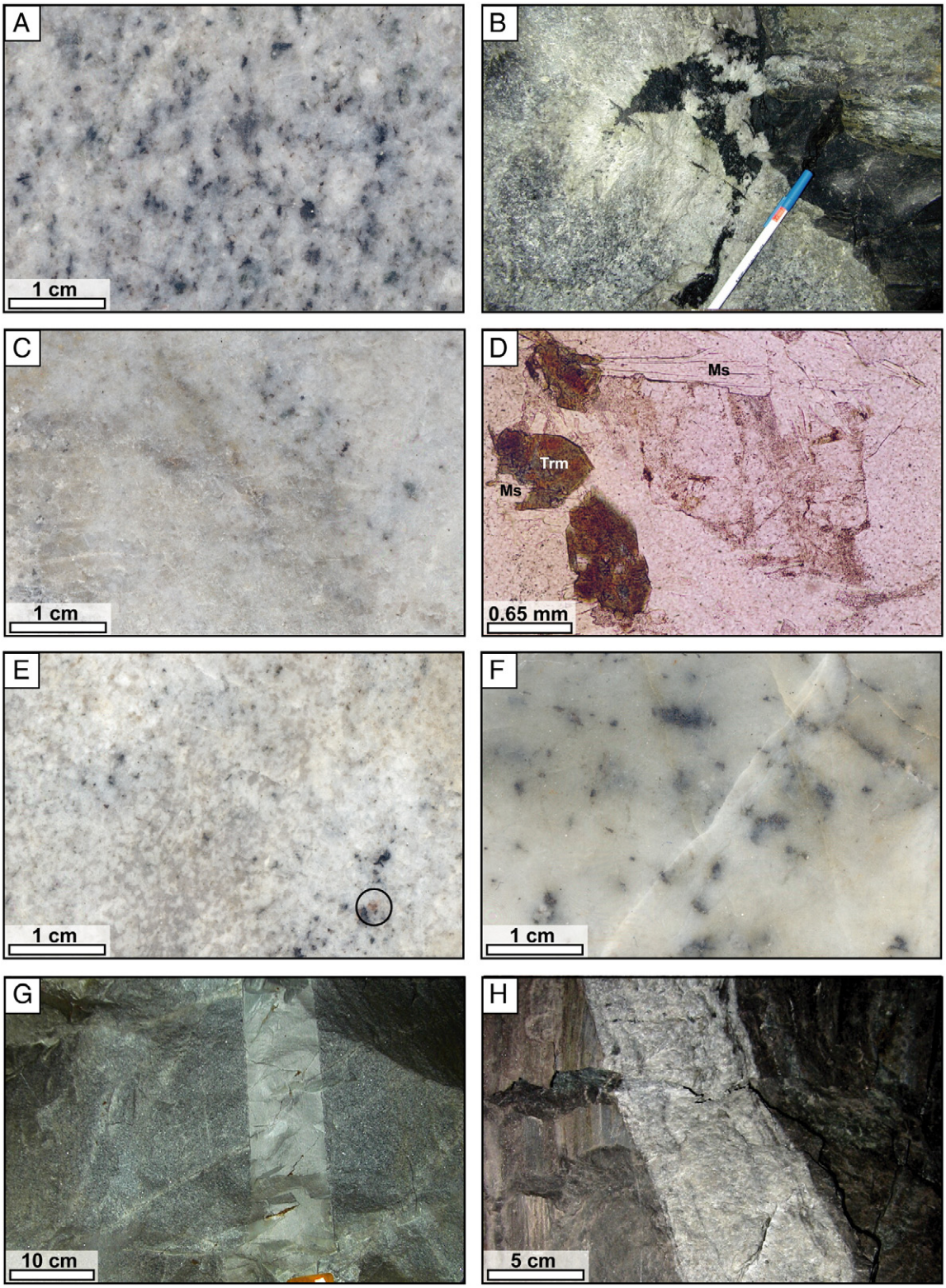

Fig. 7. Representative textures and mineralogy of the late dyke phases. A. Polished thin section off cut of a fine-grained hypidiomorphic-equigranular biotite-bearing dyke. B. Miarolitic cavity infilled by tourmaline with an aplitic (mainly albite–quartz) margin in a biotite-bearing dyke with the Upper Argillite. C. Polished thin section off cut of a fine-grained leucocratic tourmaline-bearing dyke with small scattered tourmaline and muscovite pockets. D. Photomicrograph (PPL; plane polarized light) of a small tourmaline and muscovite pocket displaying open-space filling textures. E. Quartz-bearing aplitic dyke with relict unaltered patches containing magmatic biotite (black) and trace garnet (circled). F. Very fine-grained or sugary, quartz-absent aplitic dyke with sulfide-bearing micro-veins and dark gray patches of epidote-group minerals. G. Steeply dipping aplitic dyke cutting the apical Mine Stock near the Mine Stock-Upper Argillite Contact (notebook is 11 cm wide); the texture of this dyke is very similar to that in E. H. Steeply dipping ribboned aplitic dyke in skarnified Swiss Cheese Limestone; the texture of this dyke is very similar that in to F. Rock-forming mineral notations are after Kretz (1983).

Please cite this article as: Rasmussen, K.L., et al., Felsic magmatic phases and the role of late-stage aplitic dykes in the formation of the world-class Cantung Tungsten skarn deposit, Northwest Territories, Canada, Ore Geol. Rev. (2011), doi:10.1016/j.oregeorev.2011.06.011

The other two data clusters at 115°–295° and 040°–220° are comparable to the two trends of dykes previously reported by Watson (1981), and together they comprise a 'near-conjugate' dyke set with averaged poles separated by 50° and a sub-vertical principal stress axis (Fig. 8A):

1) 115°–295°, or 123/32 (Fig. 8A; middle inset): defined by SE-striking, biotite- and tourmaline-bearing dykes that have moderate to shallow dips and are found predominantly in the lowermost mine workings, west of the Mine Stock contact with country rocks. This 115°–295° orientation is sub-parallel to bedding in the lower fold limb, thought to be the primary control on the orientation of these dykes. However, a small proportion of minor faults and splays also have a similar orientation (Fig. 8B).
2) 040°–220°, or 239/24 (Fig. 8A; lower inset): defined by SW-striking, biotite-bearing dykes that have moderate to shallow dips and are found throughout the mine workings cutting bedding along high-angle joint surfaces.

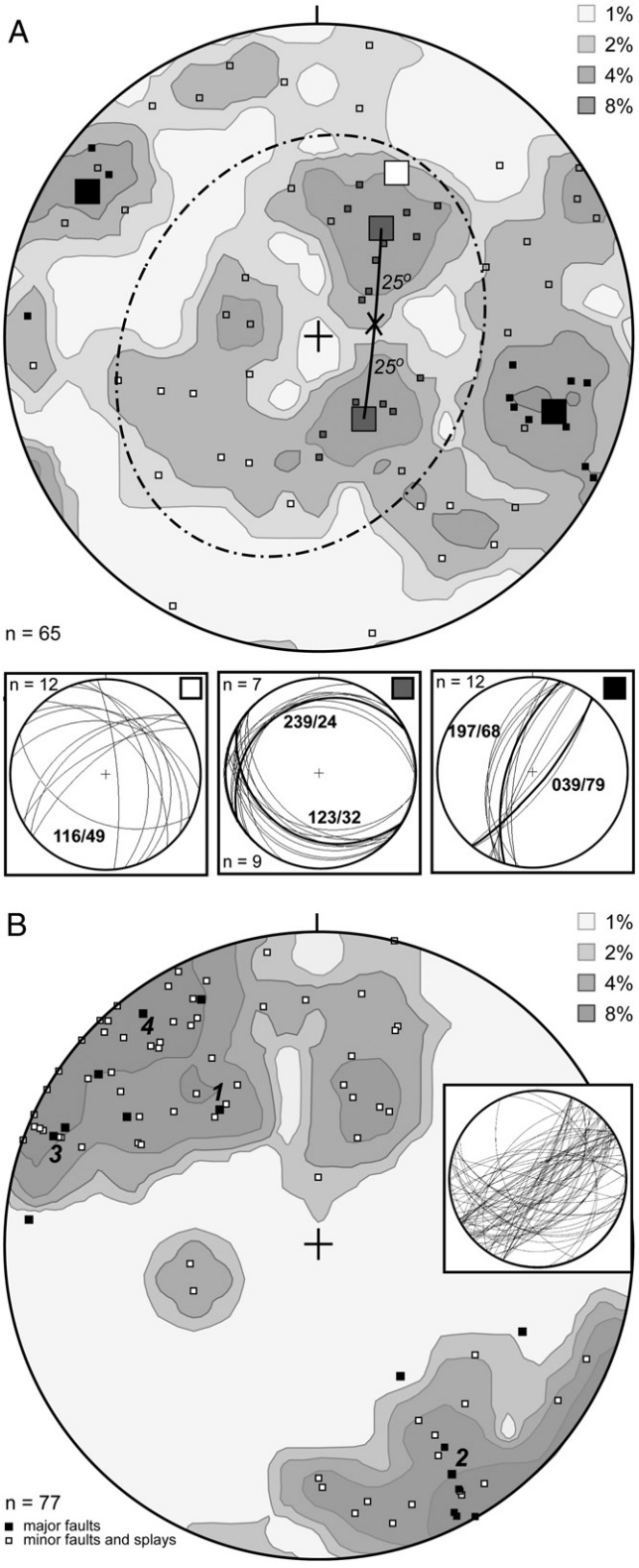

The "sub-vertical" dykes are characterized by NE-striking aplitic dykes that have been emplaced sub-parallel to steeply dipping normal faults and associated minor faults and splays underground (Fig. 8A, B), mainly within or along the Mine Stock near its margins and in the uppermost eastern mine workings.

3.4. Metasomatism of the FMP

All of the felsic intrusive phases described above display evidence for some degree of metasomatism, particularly textures indicative of minor sub-solidus flow or trapping of late-stage sodic magmatic fluids (e.g., very fine-grained ragged muscovite, flame perthite, myrmekite, local chloritization of biotite). However, most of these intrusions have preserved their magmatic textures, mineralogies, and compositions, with the exception of the aplitic dykes. Additionally, previous workers have reported more intense, but localized alteration in felsic intrusions, ranging from small bodies of greisenization at plutonic contacts with country rocks to potassic and (or) greisenized halos around fractures and as selvages for late quartz–microcline–calcite–tourmaline–pyrrhotite–apatite ± scheelite–molybdenite veins (e.g., Mathieson and Clark, 1984; van Middelaar, 1988). The most detailed petrographic study of the Cantung intrusive phases, documenting sub-solidus re-equilibration textures (e.g., myrmekite, granoblastic quartz, K-feldspar megacrysts, graphic intergrowths, titano-magnetite to magnetite, microclinitization, and perthite development), was completed by van Middelaar (1988) and it defined several other types of alteration in intrusive samples:

1) Pervasive metasomatic alteration (deuteric, or late-stage magmatic) causing oligoclase overgrowths (and replacements of cores) on plagioclase, biotite altered to muscovite–pyrrhotite–rutile or low-Ti hydrothermal biotite, and ilmenite altered to pyrrhotite-rutile;
2) Vein-controlled alteration, with bleached selvages comprising quartz–sericite/muscovite–rutile/titanite–tourmaline–pyrrhotite/pyrite–calcite/scheelite; and
3) Greisenization comprising a similar mineral assemblage to the vein selvages, but with the addition of albite.

This classification of alteration appears to be most applicable to the relatively unaltered Mine Stock and some dykes phases preserving magmatic mineralogies and textures. However, this is difficult to extend to all of the dykes, many of which have experienced more intense or pervasive metasomatism, and of different types than what was previously described by van Middelaar (1988).

Relying on petrographic observations from over 45 intrusive samples, primarily dykes (Table 1), a revised metasomatic classification

Fig. 8. Equal area stereoplots. A. All measured dyke and sill orientations plotted as poles to the plane, with statistical concentrations indicated (1 measurement equals 1.54%; maximum of 9.23%). Measurements from sampled dykes are indicated by the sample number, and the dashed line circles the "shallow- to moderate-dipping dykes and sills." Color-coded symbols (black, dark gray, and white) are used for data in the insets and average poles for each cluster are indicated by a larger symbol. Insets illustrate the planes and the average plane orientations for each of the data clusters discussed in the text. The "X" indicates the location of the principal stress axis upon emplacement of the near-conjugate dykes indicated by the dark gray squares. Measurements not used for statistical calculations are unfilled. B. All measured underground fault orientations plotted as poles to the plane, with statistical concentrations indicated (1 measurement equals 1.30%; maximum of 14.29%). Major fault measurements are indicated by black symbols and the fault number.

Please cite this article as: Rasmussen, K.L., et al., Felsic magmatic phases and the role of late-stage aplitic dykes in the formation of the world-class Cantung Tungsten skarn deposit, Northwest Territories, Canada, Ore Geol. Rev. (2011), doi:10.1016/j.oregeorev.2011.06.011

Table 4
Characteristics of alteration types affecting the felsic magmatic phases.

Alteration	Protolith	Mineral assemblage	Minor minerals	Trace minerals	±	Replacement	Textures	Feldspar	Perthite	Twins	Geochemical signature	Relationship to mineralization
Unaltered	Plutonic, bt-bearing, trm-bearing, v. rare aplitic	Pl>Qtz>Mc>Bt (red-brown> bleached)	Ms ($\delta = 3o$)	Ap, Zrn, (Ilm, Mnz)	Rt in bleached Bt, Trm, (allanite)	minor Ser–Sauss–Chl–Cal after Pl, Chl–Ms or Ms–phengite after Bt	Hypidiomorphic-granular (primary igneous porphyritic, megacrystic, seriate, equigranular)	An (28–31); Or (92–95)	Film overprinted by flame	Tartan: coarse-patchy; albite: fine-pervasive; pericline: present in most grains	Peraluminous (A/CNK = 1.05–1.25); 70–72 (75 in late dykes) wt.% SiO_2	Unrelated
Potassic	QFP, bt-rich, bt-bearing, trm bearing; rare aplitic	Mc>Qtz>Pl>Bt (red-brown); or in aplitic dykes: Mc = Qtz	Ms ($\delta = 3°$), Bt (pale green), Alb	Ap, Zrn, (Ilm, Mnz)	Bt (red-brown)	Ms ± phengite or Chl–Ep–Ilm–Rt after Bt; Ser–Sauss–Ms–Chl after Pl	Primary hypidiomorphic-granular textures preserved; consertal fsp contacts; intergranular Alb at Pl–Ksp boundaries	ca. An (30); Or (89–97); late Ab	Dominantly short blebs with tails	Tartan: coarse-patchy to sharp-pervasive; albite ± pericline: fine but largely overprinted by alteration	Peraluminous (A/CNK = 0.98–1.3); K_2O>4.8 wt.%; SiO_2 = 74–75 (70 in early dykes) wt.%	Unrelated
Calcic 1	aplitic, rare plutonic, rare QFP, rare bt-bearing	Pl = Qtz	Ap, Cal	Bt (pale brown), Zrn	Bt (red-brown)	An after Mc and And; minor Ser after Mc (when rarely present); Chl–Ep–Ilm–Rt after Bt (red-brown)	f–gr seriate aplitic; 2–5 mm Pl pseudomorphs of euhedral Ksp and <1 mm Pl and Qtz in groundmass; Trm 'stringer' veins	An (29–35; distal) to An (93–96; proximal); rare Or (87)	Rare; short blebs with tails	Tartan: coarse-patchy, with Ser; Ab: patchy to pervasive and fine to coarse ± herringbone pattern; pericline: present; deformation: rare	Metaluminous (A/CNK<0.96); CaO>3 wt.%; SiO_2 = 74–77 wt.%; lower Rb, Ti, Zr, Ba, Pb; higher Sr, W, Cu, Zn, Mo, Bi	Less altered equivalent of calcic-2 alteration; distal to mineralization
Calcic 2	aplitic, rare plutonic, rare bt-bearing	Pl>>>Qtz, Mc	Czo/Zo, Cal, Ap,	Bt (pale brown), (Mnz), Qtz, Mc, Zrn	Sulfide (Po–Py–Cpy), Chl, Ep, Rt, Ttn, Scheelite	An after Mc + Qtz and And	very f–gr seriate xenomorphic aplitic; <1 mm Pl and <0.2 mm (clino)zoisite; sulfide ± scheelite disseminated or in Fe–Mg–CO_3 veins with Ttn–Ap–Chl–Ep–Rt; Trm 'stringer' veins	An (77–96) and minor An (41–49)	n/a	Albite: patchy to pervasive and fine to coarse ± herringbone pattern; pericline: present	Metaluminous (A/CNK<0.96); CaO>3 wt.% (usually); SiO_2 = ~50 wt.%; lower Rb, Ti, Zr, Ba, Pb; higher Sr, W, Cu, Zn, Mo, Bi	Characteristic of all dykes cutting or adjacent to mineralization; may be mineralized
Sericitic–Calcic	Unaltered or potassic-altered intrusions	Ser ± Ms ($\delta = 1°$ and/or 3°), Mc, Qtz	Cal	Sauss		Ser/Ms–(Sauss) after Pl; Chl after Bt	Primary hypidiomorphic-granular texture; pervasive Ser ± Sauss of Pl from the margins inwards; veinlets of Ms–Mc–Qtz–Cal	ca. An (30); Or (89–97); late Ab	Dominantly short blebs with tails; absent in secondary Mc	Tartan: coarse-patchy or sharp-pervasive in secondary Mc; albite ± pericline: overprinted by alteration	Peraluminous (A/CNK = 0.98–1.3); K_2O>5 wt.%; SiO_2 = 74–75 wt.%	Rarely in direct contact with mineralization
	Calcic-altered intrusions	Cal, Ser	Ap		Ms ($\delta = 1°$ and/or 3°), Trm	n/a	f–gr to v. f–gr seriate aplitic; pervasive unidirectional discontinuous blebs of Cal and Ser ± Ms	An (77–96) ± An (40–49)	n/a	albite: patchy to pervasive and fine to coarse ± herringbone pattern; pericline: present	Metaluminous (A/CNK<0.96); CaO>3 wt.% (usually); SiO_2 = 50–77 wt.%	Frequently, but not always, in direct contact with mineralization

Please cite this article as: Rasmussen, K.L., et al., Felsic magmatic phases and the role of late-stage aplitic dykes in the formation of the world-class Cantung Tungsten skarn deposit, Northwest Territories, Canada, Ore Geol. Rev. (2011), doi:10.1016/j.oregeorev.2011.06.011

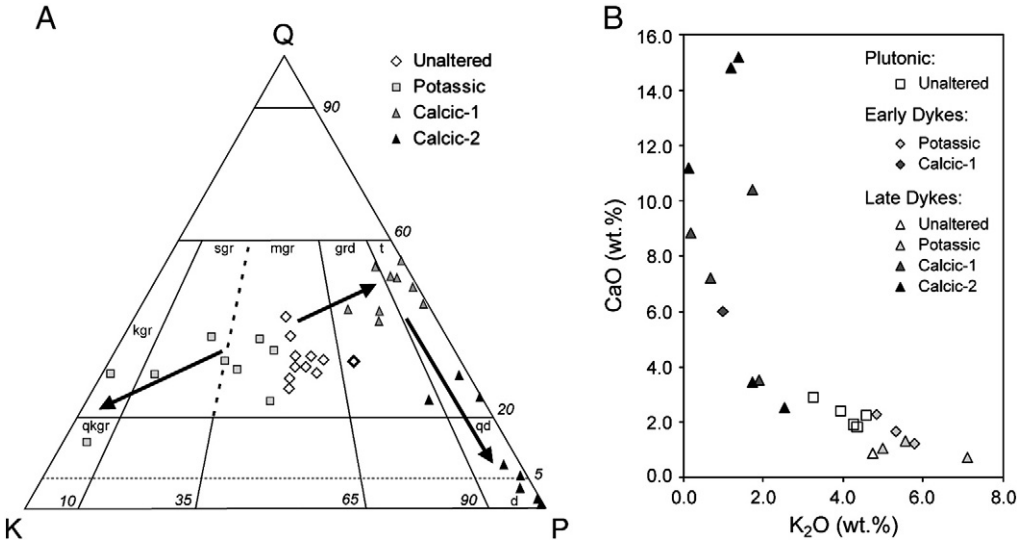

Fig. 9. Major element geochemistry and alteration type. A. Quartz–K–feldspar–plagioclase ternary plot after Streckeisen (1976) showing mineralogical trends away from unaltered plutons and dykes (monzogranitic) to potassic dykes (K-feldspar granitic), and two types of calcic dykes (tonalitic and dioritic); kgr = K-feldspar granite, sgr = syenogranite, mgr = monzogranite, grd = granodiorite, t = tonalite, qkgr = quartz K-feldspar granite, qd = quartz diorite, d = diorite. B. K_2O vs. CaO (wt.%) demonstrating the range of compositions associated with unaltered, potassic, and calcic samples.

is suggested for felsic intrusions at Cantung (Table 4). Most of these are easily recognized on the basis of mineralogical assemblages and textural relationships in stained hand slabs or by chemical composition, and their defining mineral assemblages are clearly evident on a quartz–K-feldspar–plagioclase (QKP) ternary diagram (Fig. 9A). Unaltered samples are monzogranitic, but QKP ratios trend towards K-feldspar-rich or 'potassic' mineral assemblages, and towards two plagioclase-rich or 'calcic' mineral assemblages: a tonalitic assemblage with roughly equal amounts of plagioclase and quartz ('calcic-1'); and a dioritic assemblage with very little to no quartz and microcline ('calcic-2'). K_2O vs. CaO (wt.%) also distinguishes the unaltered intrusive phases from those that have undergone potassic or calcic metasomatism (Fig. 9B). The third type of metasomatism observed in the dykes is a late-stage overprinting assemblage of sericite or muscovite, with calcite ± microcline ± quartz ('sericitic–calcic') that seems to have affected many of the different dyke phases to varying degrees. Characteristic mineral assemblages and modal percentages, megascopic and microscopic textures, and basic geochemical features of each metasomatic type are detailed below and summarized in Table 4.

3.4.1. Unaltered

Unaltered intrusions have hypidiomorphic-granular magmatic textures and are characterized by a monzogranitic mineral assemblage of microcline (20–27%), plagioclase (30–35%), quartz (28–32%), and biotite (1–10%) with primary accessory apatite and zircon, and rarer ilmenite and monazite. Anorthite content in plagioclase for unaltered plutonic samples is bimodal (Table 3): magmatic plagioclase is typically oligoclase-andesine with An_{28} to An_{32}, and euhedral xenocrysts are andesine with An_{35} to An_{40} (Table 3). Microcline is <8% albite-anorthite (Table 3). Unaltered examples of intrusions are represented mainly by the plutonic samples, although a few examples of the late biotite-bearing, tourmaline-bearing, and one aplitic dyke are also considered to be relatively unaltered (Table 1).

As the petrography of the unaltered plutonic phases has already been described in detail, here we note a few additional features that apply to the unaltered late dykes. Most of the magmatic minerals in these dykes are relatively pristine. However, plagioclase has undergone slightly more intense (variably low to moderate) saussuritization or sericitization, and secondary muscovite, chlorite, and (or) calcite may be present along cleavage and twin planes (Fig. 5G). Microcline may have very minor patchy myrmekite (Fig. 10A). Bleached Ti-poor biotite (± chlorite) with inclusions of rutile needles along margins is relatively abundant (Fig. 11A), or biotite may be partially replaced by chlorite, muscovite, and (or) pale green phengite (Fig. 11B; van Middelaar, 1988). Minor, very fine-grained and ragged sub-solidus muscovite is typically present in the groundmass of the relatively unaltered late dykes (Fig. 5F).

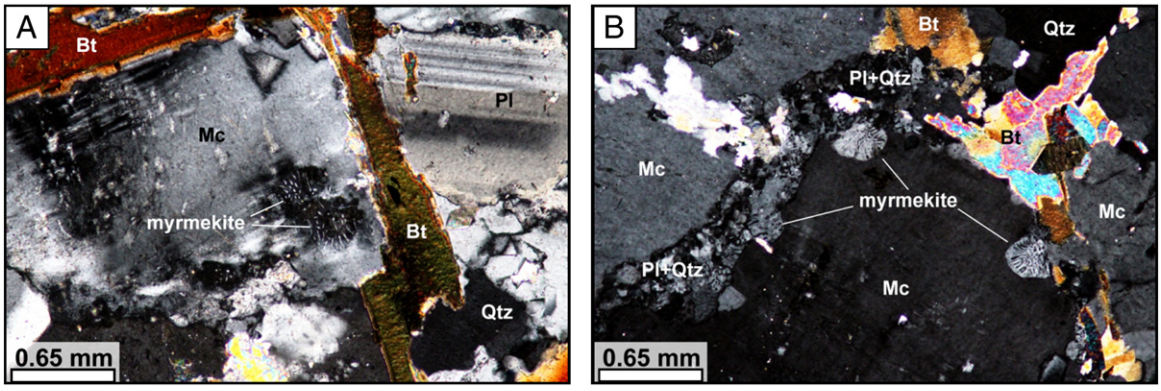

Fig. 10. Myrmekite development in "unaltered" samples. A. Patchy myrmekite developed in microcline grain with marginal rim myrmekite (not shown; apical Mine Stock). B. Wart-like myrmekite developed along microcline grain boundaries in contact with very fine-grained intergranular quartz–plagioclase (early biotite-rich dyke). Rock-forming mineral notations are after Kretz (1983).

Please cite this article as: Rasmussen, K.L., et al., Felsic magmatic phases and the role of late-stage aplitic dykes in the formation of the world-class Cantung Tungsten skarn deposit, Northwest Territories, Canada, Ore Geol. Rev. (2011), doi:10.1016/j.oregeorev.2011.06.011

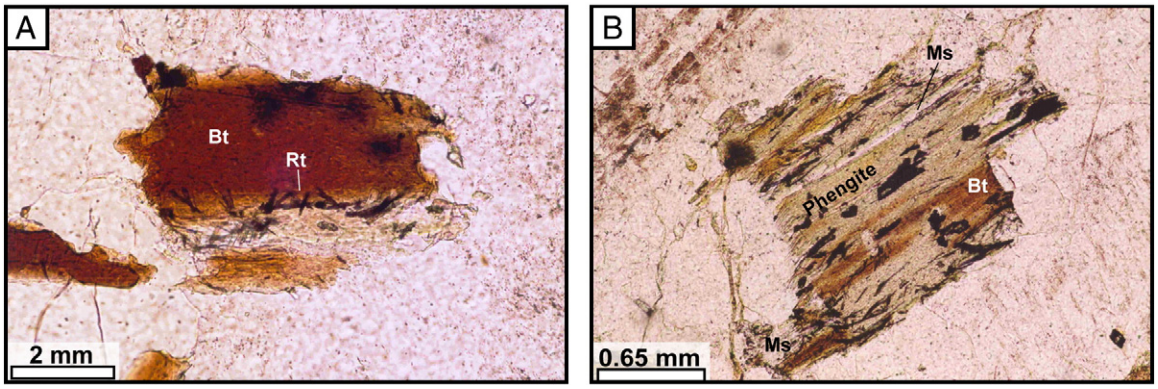

Fig. 11. Typical alteration of biotite in "unaltered" samples. A. Bleached Ti-poorer biotite with abundant rutile "needle" inclusions. B. Biotite largely replaced with pale green phengite and lesser muscovite. Rock-forming mineral notations are after Kretz (1983).

3.4.2. Potassic metasomatism

Varying degrees of development of potassic mineral assemblages, also referred to as potassic metasomatism here, are the result of late-stage magmatic fluid loss in the early biotite-rich dykes, many of the later biotite-bearing and tourmaline-bearing dykes, and less frequently although more pervasively in some aplitic dykes. Potassic dykes are characterized by an assemblage of microcline (>30%, but up to 80% in aplitic dykes; Fig. 12A, B), plagioclase (5–35%), quartz (15–50%), and reddish-brown magmatic biotite (0–15%, depending on the dyke phases described earlier) with secondary ragged muscovite in biotite (<1%, rarely up to 5%). Plagioclase is andesine-(oligoclase) with ca. An_{30}, although xenocrystic plagioclase in biotite-rich dykes is up to An_{42} (Table 3).

Microcline is <10% albite–anorthite (Table 3) and is typically very fresh in appearance, although tartan twins range from pervasive and sharply defined to coarse, turbid, and patchy. Perthite is either less abundant than in unaltered samples or absent. When present, film and overprinting flame perthite morphologies are still present in some grains, the latter being locally coarse enough to display albite twins; however, short discontinuous bleb perthites (±tails) predominate, particularly in the presence of nearby secondary sericite or muscovite (Fig. 12C). Inclusions of round quartz grains and secondary white micas are common in larger microcline grains, suggesting a very late overgrowth by K-feldspar. Plagioclase cores are moderately to highly sericitized and partially saussuritized, and secondary

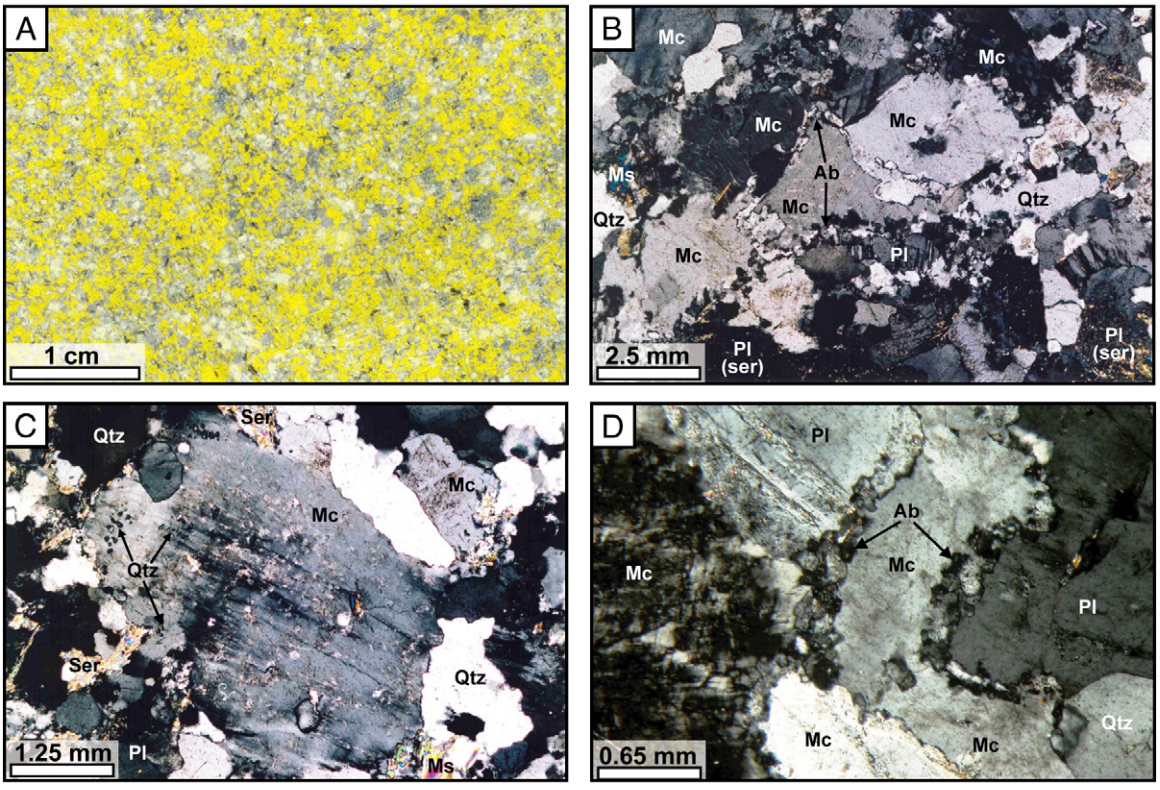

Fig. 12. Characteristic textures and mineral assemblages of potassic metasomatism. A. Polished slab of potassic fine-grained biotite-bearing dyke stained for K-feldspar, comprising abundant microcline (dark yellow), plagioclase (white), quartz (gray), and biotite (black). B. Photomicrograph (CPL) of equigranular texture and microcline>quartz–plagioclase mineral assemblage with strongly sericitized plagioclase, ragged secondary muscovite, and bleb-type perthite in K-feldspar; note the interweaving very fine-grained masses of untwinned consertal albitic plagioclase along intergrain boundaries. C. Photomicrograph (CPL) of short discontinuous bleb perthite (±tails) typical of microcline, and secondary muscovite-sericite in potassic samples; note the presence of irregular quartz blebs at extinction in the large microcline grain, which are indicative of a recrystallized micropoikilitic quartz interstitial to spherulitic K-feldspar. D. Photomicrograph (CPL) of interweaving very fine-grained masses of untwinned consertal albitic plagioclase along microcline-oligoclase/andesine (Pl) grain boundaries. Rock-forming mineral notations are after Kretz (1983) and "Ser" = sericite. (For interpretation of the references to color in this figure legend, the reader is referred to the web version of this article.)

Please cite this article as: Rasmussen, K.L., et al., Felsic magmatic phases and the role of late-stage aplitic dykes in the formation of the world-class Cantung Tungsten skarn deposit, Northwest Territories, Canada, Ore Geol. Rev. (2011), doi:10.1016/j.oregeorev.2011.06.011

muscovite and (or) chlorite grains are frequently found in altered cores and along cleavage planes. Zoning, and fine or sharp albite and pericline twins are present in plagioclase, although these features are typically partially obscured by sericitization. In some samples, interweaving masses of very fine-grained, anhedral, granular to consertal albitic plagioclase are localized at microcline-oligoclase grain boundaries (Fig. 12B, D). Inter-feldspar contacts are fuzzy or consertal and all mineral phases, but particularly biotite and microcline, may have sutured grain boundaries. Quartz is present in slightly lower abundances than in unaltered samples, although it can comprise up to 50% of the aplitic dykes displaying potassic mineral assemblages. Moderate to relatively high (<1 to 2 modal %) rim and wart-like myrmekite are developed in microcline along feldspar–quartz–biotite intergrain boundaries and are frequently associated with very fine-grained intergranular quartz and albitic plagioclase (Fig. 10B) and (or) with increased proximity to zones of calcic metasomatism. Biotite may or may not be a significant mineral depending on the intrusive phase affected by potassic metasomatism, although the relatively high, but heterogeneous abundance of this mineral in the early biotite-rich dykes is one manifestation of potassic metasomatism. A significant proportion of the biotite in the leucocratic biotite-bearing dyke phase (up to 2% of the rock) is partially to completely replaced by clots of chlorite–epidote-opaque–(rutile), or by muscovite and (or) a pale green-brown Ti-poor phengite (Fig. 11B; van Middelaar, 1988; van Middelaar and Keith, 1990). Rarer examples of pervasive potassic metasomatism comprising 50–80% microcline and 20–50% quartz in the steeply dipping aplitic dykes are adjacent to pervasive calcic zones of calcic metasomatism (Fig. 13A). Generally, potassic mineral assemblages are difficult to distinguish in hand specimen without staining for K-feldspar, although it may be identified geochemically by a relative enrichment in K_2O (Fig. 9B), or by anomalously high biotite concentrations in the case of the early biotite-rich dykes.

3.4.3. Calcic metasomatism

Although evidence for partial calcic metasomatic overprinting of other alteration styles exists, dykes that have undergone pervasive calcic metasomatism are characterized by a true aplitic texture and mineralogy (e.g., fine-grained or sugary groundmass comprising only quartz and feldspar). This type of metasomatism rarely affects intrusive phases other than the steeply dipping aplitic dykes; however, along the contact with exoskarn mineralization the apical Mine Stock may have a gradational of increasingly calcic mineral assemblages with proximity to exoskarn. Patchy to pervasive calcic metasomatism also affects the Open Pit QFP dyke from the margins inward, a distal intensely flow-banded QFP dyke in the Dolomite unit, and one of the tourmaline-bearing dykes (Table 1). There are two main metasomatic assemblages typified by calcic mineralogies, which are easily distinguished by the presence or absence of quartz.

Roughly equal quantities of plagioclase (~50%) and quartz (~50%) are characteristic of the 'dioritic' mineral assemblage referred to as calcic-1 metasomatism (Figs. 9, 13a). Plagioclase is anorthite (An_{93-96}), although less pervasive manifestations of this metasomatism may have relict early-formed micro-phenocrysts of K-feldspar that are partially to fully pseudomorphed by oligoclase-andesine (An_{29-35}) with irregular remnants of microcline still present in some grain cores (Table 3; Fig. 13B). The only microcline grain analyzed in a calcic dyke has <13% albite-anorthite (Table 3). K-feldspar destruction in favor of calcic plagioclase and quartz is explained by the simplified Eq. (1), which requires a fluid with high Ca activity (aCa^{2+}) and produces a potassic fluid:

$$2K-\text{feldspar} + Ca(OH)_{2(aq)} \rightarrow \text{anorthite} + \text{quartz} + 2KOH_{(aq)} \quad (1)$$

Eq. (1) also explains the relationship between potassic mineral assemblages and adjacent calcic-1 mineral assemblages in the metasomatically zoned aplitic dykes (Fig. 13A). While appearing to be fine-grained and equigranular in hand specimen, at the microscopic scale a seriate texture dominates in calcic-1 dykes, with very fine-grained quartz and plagioclase in the groundmass (<0.2–1 mm) and coarser grained plagioclase replacing earlier-formed microcline ± oligoclase micro-phenocrysts (2–5 mm; Fig. 13B–D). In the rare cases that K-feldspar is present, it is observed as small anhedral grains lacking perthite in the groundmass, and tartan twins are coarse, turbid, and associated with sericitization. Plagioclase is unzoned and not affected by sericitization or saussuritization, and it forms either anhedral to subhedral grains in the groundmass, or larger euhedral grains that have skeletal to boxy cellular (inclusion-rich) morphologies. Albite and pericline twins are present in skeletal portions of grains, which have been mostly infilled by untwinned to poorly twinned anhedral plagioclase resulting in a patchy appearance (Fig. 13C). Larger composite grains frequently have coarser and pervasive twins that may display a distinctive 'herringbone' pattern (Fig. 13D). Carlsbad twins are typically lacking, but isolated wedge-shaped polysynthetic deformation twins are associated with micro-fractures in plagioclase. Inclusions in boxy cellular plagioclase are microcline and large rounded quartz grains, as well as secondary mineral phases such as epidote and chlorite, and rare (magmatic?) monazite and zircon. Quartz occurs as very fine-grained, subhedral to euhedral, equant to slightly elongate prismatic grains in the groundmass. Less than 3% biotite may be present, but it is almost invariably replaced by chlorite–epidote–ilmenite ± rutile needles. Calcic-1 alteration is not observed in direct contact with mineralization, nor are such dykes mineralized despite very intense metasomatism in some of them; however, they may be cored by tourmaline veins suggesting a high B-rich fluid flux (Fig. 13A).

Calcic-2 metasomatism is composed primarily of calcic plagioclase (~70–98%) and aluminous epidote-group minerals, such as clinozoisite ± zoisite (2–30%; Fig.13E, F, G). Quartz is notably rare or absent, as are microcline and biotite. Anorthite content in plagioclase determined by EPMA is bimodal, with andesine (An_{41-49}) and bytownite to anorthite (An_{77-96}; Table 3). Micron-scale patches of the andesine plagioclase are visible using SEM-BSE imaging of some of the more sodic samples (Table 3), and this small andesine population is thought to be the result of incomplete or semi-pervasive reaction of andesine to anorthite. Destruction of andesine and quartz may be accomplished by interaction with a calcic fluid with high aAl^{3+} to produce the calcic-2 mineral assemblage and a sodic fluid, based on the simplified Eq. (2):

$$An_{40} + \text{quartz} + Ca(OH)_{2(aq)} \pm Al^{3+} \rightarrow \text{anorthite} + NaOH_{(aq)} \pm \text{clinozoisite} \quad (2)$$

Calcic-2 dykes also appear to have a more microcrystalline texture in hand specimen (Fig. 7) than those that have undergone calcic-1 metasomatism, but at the microscopic scale a seriate texture also dominates with respect to plagioclase (0.2–1 mm), (clino)zoisite (<0.2 mm), and apatite (typically <0.5 mm). Plagioclase also forms tabular skeletal to anhedral grains (Fig. 13F, G ,H) and may overgrow secondary epidote, muscovite, and calcite from the groundmass within boxy cellular plagioclase. Albite and pericline twins are present in most grains, and albite twins range from fine to coarse lamellae and are typically patchy and suggestive of early skeletal morphologies, but may also be pervasive and (or) may exhibit a 'herringbone' pattern (Fig. 13G). Clots of epidote and interstitial xenomorphic clinozoisite ± zoisite may make up a significant portion of the groundmass in dykes in direct contact with mineralized skarn (Fig. 13E, H). Secondary, Ti-rich, pale brown annitic biotite has been observed as ragged disseminations present in small abundances (typically <2% modal) and associated with pyrrhotite and even as inclusions in scheelite. This biotite is nearly phlogopitic (unpublished results) and is compositionally very similar to biotite described in the mineralized biotite-facies skarn and the late

Please cite this article as: Rasmussen, K.L., et al., Felsic magmatic phases and the role of late-stage aplitic dykes in the formation of the world-class Cantung Tungsten skarn deposit, Northwest Territories, Canada, Ore Geol. Rev. (2011), doi:10.1016/j.oregeorev.2011.06.011

lamprophyre dykes (van Middelaar, 1988; van Middelaar and Keith, 1990). Relatively coarse-grained end-member fluorapatite (unpublished results) is abundantly disseminated through the groundmass (up to 5% modal; Fig. 13H), and aggregates of very coarse-grained fluorapatite (up to several mm in size) and chlorite–epidote–pyrrhotite (±chalcopyrite–pyrite)–rutile–(±titanite) are associated with scheelite-mineralized Fe–Mg–CO_3 veinlets (Fig. 13E, G; Fig. 14D). Fluorapatite is also found in all of the mineralized skarn facies at Cantung (Marshall et al., 2003; Mathieson and Clark, 1984) and this association between fluorapatite and scheelite has been documented in many other W-mineralizing systems, which is consistent with experimental data suggesting a role for phosphate species in the transport of W (Manning and Henderson, 1984; Raimbault et al., 1993). Mineralization also occurs as interstitial or disseminated pyrrhotite (up to 15%) and scheelite

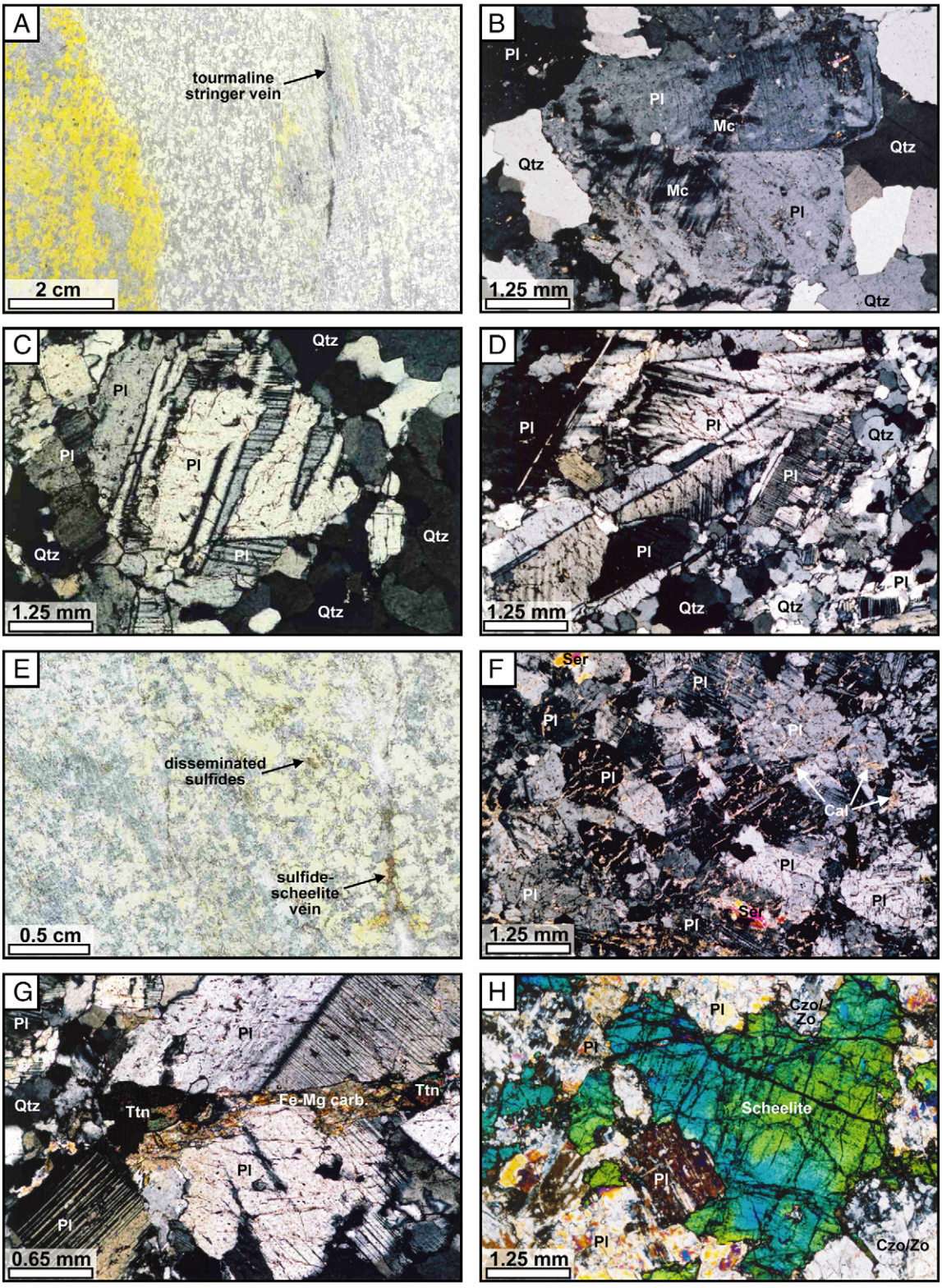

Please cite this article as: Rasmussen, K.L., et al., Felsic magmatic phases and the role of late-stage aplitic dykes in the formation of the world-class Cantung Tungsten skarn deposit, Northwest Territories, Canada, Ore Geol. Rev. (2011), doi:10.1016/j.oregeorev.2011.06.011

(typically <5%, but up to 75%), ±lesser chalcopyrite, pyrite, and trace sphalerite (Fig. 13E). Disseminated scheelite in textural equilibrium with plagioclase and (clino)zoisite (Fig. 13H), and sulfides are typical of aplitic dykes cross-cutting exoskarn mineralization, but scheelite is generally finer grained (<1–3 mm) in the dykes.

3.4.4. Sericitic–calcic metasomatism

A widespread sericitic–calcic metasomatic event has affected samples from all of the FMP and overprinted all other metasomatic mineral assemblages. Sericitic–calcic alteration is characterized by pervasive sericite or coarser-grained muscovite (with δ = 1° and 3°) and calcite ± microcline ± quartz, but is manifested differently in dykes on the basis of pre-existing mineral assemblages. For dykes that were unaltered or had potassic mineral assemblages, a distinct vein or fracture-related late-stage sericite–(muscovite) ± microcline ± quartz ± calcite secondary mineral assemblage is most characteristic of sericitic–calcic alteration. This may be manifested as: (1) narrow fine-grained white mica or Ti-poor muscovite (unpublished results) with microcline ± quartz ± calcite veinlets that cross-cutting large fractured microcline grains; (2) interweaving veinlets around feldspar grains mantled by sericite; and (3) felted to coarse-grained sericite intensely altering or pseudomorphing plagioclase (Fig. 14A, B). Microcline is not destroyed and instead it may be part of the secondary mineral assemblage as it is often relatively large and displays more ordered textures (e.g., perthite-free; sharply tartan-twinned) when located proximal to, or cut by muscovite veinlets (Fig. 14A). This alteration style is roughly analogous to the zones of "greisenization" described by other workers along the apical Mine Stock contact and as the selvages to variably mineralized late quartz–microcline–calcite–tourmaline–apatite veins (e.g., Keith et al., 1989; Mathieson and Clark, 1984; van Middelaar, 1988; Zaw, 1976).

Sericitic–calcic alteration in calcic dykes is characterized by relatively Ti-rich and coarse-grained sericite and muscovite (unpublished results), combined with pervasive disseminated unidirectional and discontinuous calcite blebs with long tails in plagioclase (Figs. 13F, 14C). Muscovite and apatite are also increasingly abundant and coarse grained in samples that have undergone calcic-2 and sericitic–calcic metasomatism, and that are in contact with mineralization (Fig. 14C, D). Therefore, while sericitic–calcic alteration also intensely overprints many samples, it is particularly characteristic of those that are proximal to, or in contact with skarn mineralization (i.e., also have a calcic-2 assemblage); however, this late alteration is not characteristic of all calcic-2 altered dykes adjacent to mineralization.

3.4.5. Alteration summary and zoning

Varying degrees of pervasiveness, and overprinting of one or more styles of metasomatism within the same dyke (Table 1) led to widely variable geochemical compositions, modal and CIPW-normalized mineralogies, and in some cases difficulties in classifying the dykes on the basis of primary magmatic features. Overall though, FMPs that have undergone very minor alteration and that may be classified as unaltered include most samples of the plutonic intrusions, many of the biotite-bearing dykes, and most of the tourmaline-bearing dykes. The biotite-rich dykes have all undergone potassic metasomatism, which is responsible for their higher and heterogeneous biotite content. Some of the later biotite- and tourmaline-bearing dykes have undergone partial to pervasive potassic metasomatism, which may in turn be overprinted by partial to pervasive calcic metasomatism, and sericitic–calcic metasomatism. Essentially all of the aplitic dykes have undergone pervasive calcic metasomatism ± sericitic–calcic metasomatism; however, calcic metasomatism has also locally affected the apical Mine Stock where in contact with the Ore Limestone and skarn mineralization. Not only are alteration types locally zoned with respect to proximity to skarn mineralization (e.g., samples 09–1 through to 09–5, or samples 31–3 through to 31–5; Table 1), but the intensity of both calcic and sericitic–calcic metasomatism also increases with proximity to mineralization.

3.5. Geochemistry of the FMP

3.5.1. Isocon plots

The isocon technique of plotting geochemical data is useful for comparing altered and unaltered samples in order to determine whether or not chemical components have been lost or gained to the system during alteration (Grant, 1986; 2005). These plots are effective because they do not compare absolute quantities, which are affected by bulk mass loss or gain; rather, they allow for the comparison of elemental ratios between unaltered and altered samples. Here, the plutonic intrusions are plotted as unaltered samples, versus the late dyke phases that are plotted as metasomatized (potassic and calcic) samples (Fig. 15), using XRF data from Table 2A. These isocon plots allow for the comparison of the effects of both alteration and magmatic processes (e.g., fractionation) on chemical components from the plutons to the late dykes. Due to the very similar trends amongst the isocons constructed for individual samples, we present averaged concentrations here in order to allow for generalized observations.

Elements that were mobile during potassic metasomatism and concentrated in potassic dykes are U, K, Pb, Mo, and Rb, whereas Ca, Ba, Sr, and Na were either diluted or removed (Fig. 15A). Several of major elements and generally immobile elements do not appear to have been affected by potassic metasomatism (Si, Al, P, Nb, Cr, Y) and they form a relatively tight linear array with a slope of "1." Other elements that are typically regarded as immobile in magmatic-hydrothermal systems (e.g., Jenner, 1996), such as Zr, Ti, La, Ce, V form a relatively tight linear array with a shallower slope of "0.36". As this shallower trend passes through the origin of the isocon plot and is largely defined by immobile elements with other elements that similarly appear to have remained immobile (Th, Zn, Mn, Mg ± Li, Ba, Sr), the overall depletion exhibited by these components is attributed to magmatic differentiation processes from the unaltered plutonic phases to the late dykes. This shallower array will be referred to as a differentiation trend.

Calcic metasomatism is characterized by an enrichment in Ca, P, U ± Cr and an even larger depletion in Na (Fig. 15B). The linear arrays observed in Fig. 15B are less well-defined than those for the unaltered-potassic isocon plot, therefore the fluids responsible for calcic metasomatism may have mobilized most components to some degree. Again, Si and Al remained immobile, as well as Sr, Y, and Nb, during calcic metasomatism. Thorium,

Fig. 13. Characteristic textures and mineral assemblages of calcic metasomatism. A. Polished slab stained for K-feldspar displaying a zoned aplitic dyke that has a central thin tourmaline stringer or vein within a zone of pervasive calcic-1 metasomatism and a fringing potassic mineral assemblage. B. Photomicrograph (CPL) of partial Calcic-1 metasomatism with calcic plagioclase mantling and pseudomorphing sub-phenocrystic, simple-twinned K-feldspar with a relict tartan-twinned core. The matrix comprises coarse-skeletal quartz and anhedral plagioclase. C. Photomicrograph (CPL) of pervasive Calcic-1 alteration displaying skeletal anorthite with untwinned plagioclase infilling embayments in a matrix of fine-grained hexagonal dipyramidal to slightly elongate skeletal quartz. D. Composite anorthite with coarse albite twins displaying a distinct 'herringbone' pattern; note finer-grained skeletal anorthite with fine-patchy albite twinning in the groundmass. E. Polished slab stained for K-feldspar displaying very fine-grained aplitic texture typical of pervasive Calcic-2 metasomatism, comprising anorthite (white), (clino)zoisite (pale blue-gray), and disseminated and fracture-controlled pyrrhotite–chalcopyrite–pyrite ± scheelite. F. Photomicrograph (CPL) of Calcic-2 metasomatism manifested primarily as xenomorphic anorthite (>90%) and lacking epidote-group minerals; note overprinting sericitic–calcic alteration as coarse-grained sericite (δ = 1°) and pervasive unidirectional discontinuous calcite blebs with tails; disseminated apatite and pyrrhotite occur in trace amounts (not visible). G. Photomicrograph (CPL) of 'herringbone' plagioclase cut by a Fe–Mg carbonate vein containing titanite and associated with apatite, and pyrrhotite–scheelite mineralization. H. Photomicrograph (CPL) of equigranular, anhedral to euhedral, coarsely albite-twinned anorthite and (clino)zoisite in equilibrium with a large subhedral disseminated scheelite grain; note that this thin section is above standard thickness. There are steep-dipping fractures sub-parallel to the dyke, and the dyke pinches out just above the frame in skarn. Rock-forming mineral notations are after Kretz (1983) and "Ser" = sericite.

Please cite this article as: Rasmussen, K.L., et al., Felsic magmatic phases and the role of late-stage aplitic dykes in the formation of the world-class Cantung Tungsten skarn deposit, Northwest Territories, Canada, Ore Geol. Rev. (2011), doi:10.1016/j.oregeorev.2011.06.011

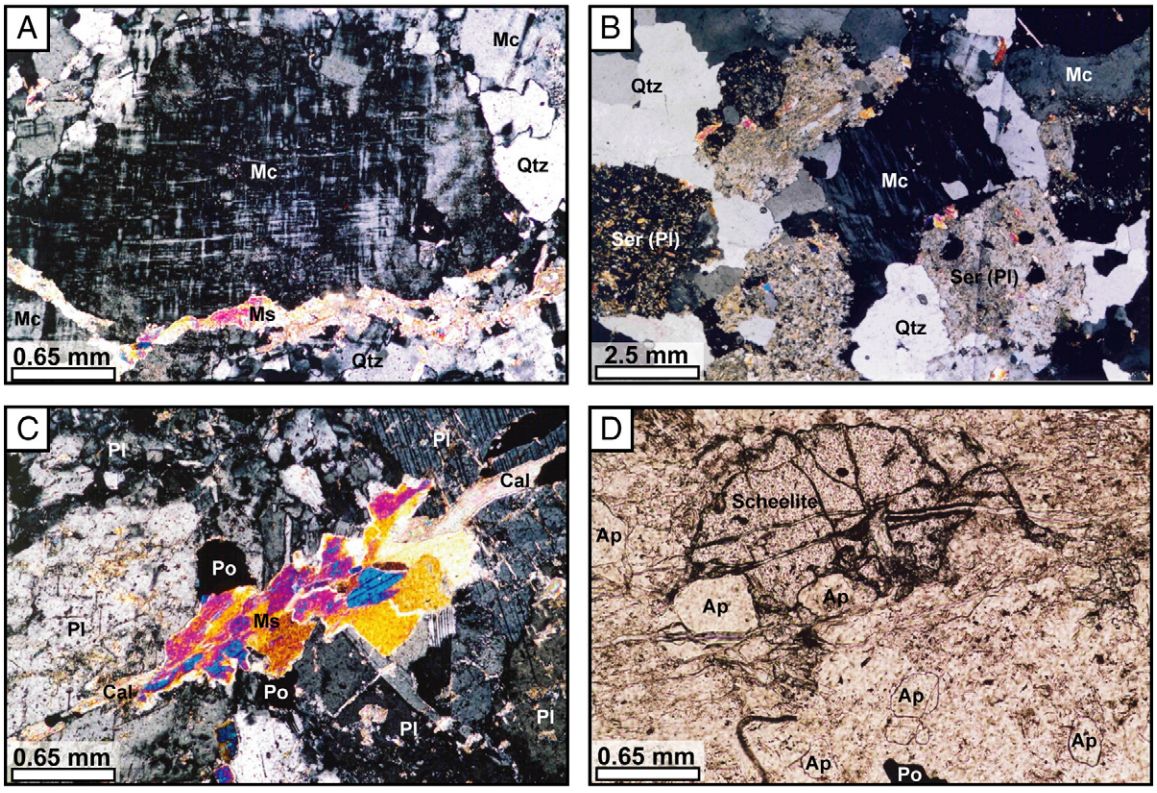

Fig. 14. Characteristic textures and mineral assemblages of sericitic–calcic metasomatism. A. Narrow muscovite ± calcite veinlet cross-cutting large, perthite-free microcline with well-defined tartan twinning. B. Felted sericite intensely pseudomorphing plagioclase within a groundmass of quartz and interstitial perthite-free microcline. C. Coarse-grained muscovite-calcite vein with associated pyrrhotite crosscutting pervasive Calcic-2 mineral assemblage in aplitic dyke. D. Scheelite intergrown with coarse-grained apatite along a Fe-Mg carbonate veinlet in a Calcic-2 metasomatized aplitic dyke. Rock-forming mineral notations are after Kretz (1983) and "Ser" = sericite.

Rb, Ti, Zn, Fe, and to a lesser extent La, V, Mg, K, Pb ± Ce and Mn appear to have been depleted in the dykes due to magmatic differentiation, but have mostly resisted mobilization by calcic fluids; therefore, these elements form a differentiation trend with a slope of "0.34". Zirconium, which plots slightly off-trend, is still grouped with the differentiation trend for two reasons: 1) on the calcic vs. potassic isocon for late dykes (not shown) Zr plots on the equal mass line, implying that the depletion observed in Fig. 15B is related to variation between plutonic and late dyke samples rather than alteration; and 2) Zr has a higher tendency to partition into a crystallizing phase (zircon) than some other immobile elements (e.g., Pearce and Norry, 1979), which slightly affects the relative depletion of Zr when compared to the other elements that lie along the differentiation trend. Conversely, some of the typically mobile elements (e.g., Rb, Pb, K) that plot along or near the differentiation trend are perhaps more likely to

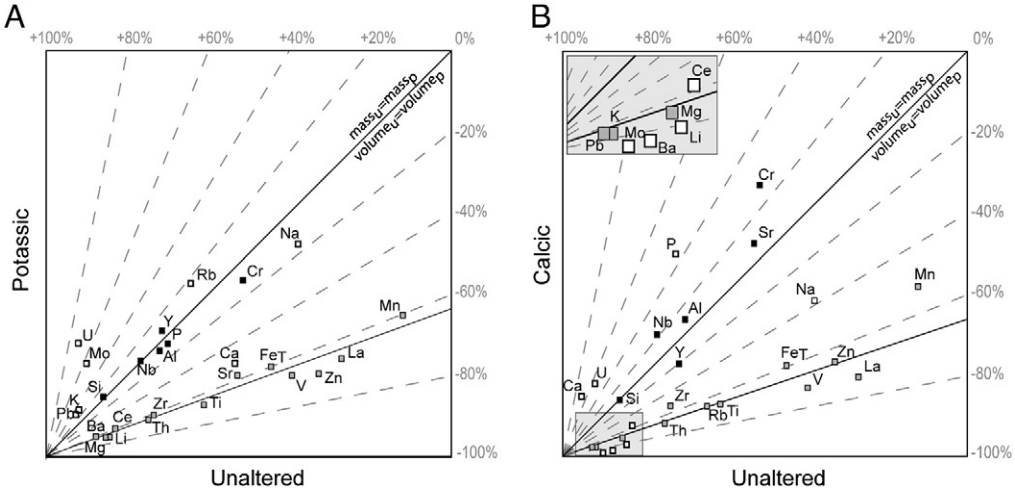

Fig. 15. Isocon plots using *average* major element oxides and trace element concentrations determined by XRF geochemical analysis for unaltered, potassic, and calcic samples (mass equivalent). Components were plotted using a multiplying factor to increase the spread of the data. Elements that were largely unaffected by alteration and magmatic processes are indicated by black symbols; elements affected by magmatic differentiation processes are indicated by gray symbols; and elements affected primarily by alteration are indicated by white symbols. Percent change in the components from unaltered to altered samples are indicated by dashed gray lines. A. Average late, potassic dykes vs. average unaltered plutonic samples; note two distinct linear arrays with zero intercepts and slopes of 1.0 and 0.36. B. Average elemental and oxide concentrations for calcic-altered dykes plotted vs. average concentrations for unaltered samples; note two distinct linear arrays with zero intercepts and slopes of 1.0 and 0.34. The shaded area is expanded in the upper left inset.

Please cite this article as: Rasmussen, K.L., et al., Felsic magmatic phases and the role of late-stage aplitic dykes in the formation of the world-class Cantung Tungsten skarn deposit, Northwest Territories, Canada, Ore Geol. Rev. (2011), doi:10.1016/j.oregeorev.2011.06.011

represent the destruction of K-feldspar in the calcic-altered dykes and partitioning of these components into the metasomatizing fluid (see Eq. (1)). Other significant geochemical markers of dykes that have undergone calcic metasomatism are elevated W, Cu, Zn, Mo, and Bi concentrations when compared to unaltered and potassic intrusions (Rasmussen, 2004).

The similarity of the slopes for both of the differentiation trend lines in Fig. 15 suggests that all of the late dykes are significantly more evolved than the plutons and were derived from highly evolved residual magmas of a relatively similar composition and degree of fractionation. As a secondary check, elemental and oxide concentrations for late calcic (aplitic) dykes vs. late potassic (biotite- and tourmaline-bearing) dykes still form a linear array, although with considerable scatter, that has a zero intercept and a slope approximating one (not shown). Although this late dyke array is more scattered for several of the typically immobile elements than the isocons in Fig. 15, the lack of a distinct differentiation trend in the late dyke isocon plot indicates that all of the late dykes were sourced from highly differentiated magmas relative to the early intrusions at Cantung.

3.5.2. Geochemical evolution of the FMP

In determining the petrogenesis of the intrusions at Cantung, whether or not the plutonic and the dyke phases were sourced from the same parental magma chamber is of primary importance. Examination of the isocon plots indicated that average abundances of several elements (e.g., Si, Al, Y, Nb, Cr) did not undergo significant mass addition or removal between unaltered plutonic phases and potassic or calcic late dyke phases (see Section 3.5.1). Bivariate plots of some of these apparently immobile elements in Fig. 16 display a relatively limited spread of data despite differing degrees of differentiation, although calcic alteration appears to adversely affect their 'immobility' on a sample by sample basis. Overall, the lack of systematic variation in immobile elements between the plutonic and dyke samples indicates that the plutonic phases and the dykes could have been derived from one parent magma (Fig. 16A, b). This is consistent with the small range of Nb/Y (0.65 to 1.1), except in some of the intensely altered samples (Fig. 17A). This also suggests that these intrusive samples at Cantung comprise differentiates of the same parental magma with Nb/Y similar to that of the average rhyolite of Winchester and Floyd (1977). This cogenetic interpretation for the plutonic and dyke intrusions is supported by ca. 97–98 Ma U-Pb ID-TIMS ages for the apical phase of the Mine Stock, a calcic-1 metasomatized late aplitic dyke, and an unaltered late biotite-bearing dyke Ma (Rasmussen et al., 2007).

Given the amount of alteration experienced by most of the dykes, the best indicators of the degree of differentiation that the dykes have undergone from the plutonic phases are HFSE ratios, such as Ti/Zr and Zr/Hf (e.g., Hall and Plant, 1992; Hoskin et al., 2000; Linnen, 1998; Pearce and Norry, 1979; Wang et al., 1996; Winchester and Floyd, 1977; Zaraisky et al., 2009). In Fig. 15, Zr depletion from the plutons to the late dykes is attributed to magmatic differentiation because the Zr concentrations are directly affected by crystal fractionation. Also, despite precipitation of hydrothermal titanite in association with mineralization in calcic-2 altered dykes, the isocon plots in Fig. 15 indicate a closed system behavior for Ti, which is also consistent with the observations of van Middelaar and Keith (1990). Therefore, Ti concentrations are interpreted to reflect primary igneous abundances that remain unaffected by metasomatism at the hand specimen scale. Hafnium was found to be immobile in isocon plots constructed from ICP-MS data (not shown); however, due to the probable effects of incomplete sample dissolution for ICP-MS data in Table 2A, Hf concentrations were recalculated using a correction factor determined from the variation in Zr concentrations measured by ICP-MS and XRF methods (based on the assumption that all Hf and Zr are in zircon in felsic granitic rocks; e.g., Rubin et al., 1993). The corrected Hf

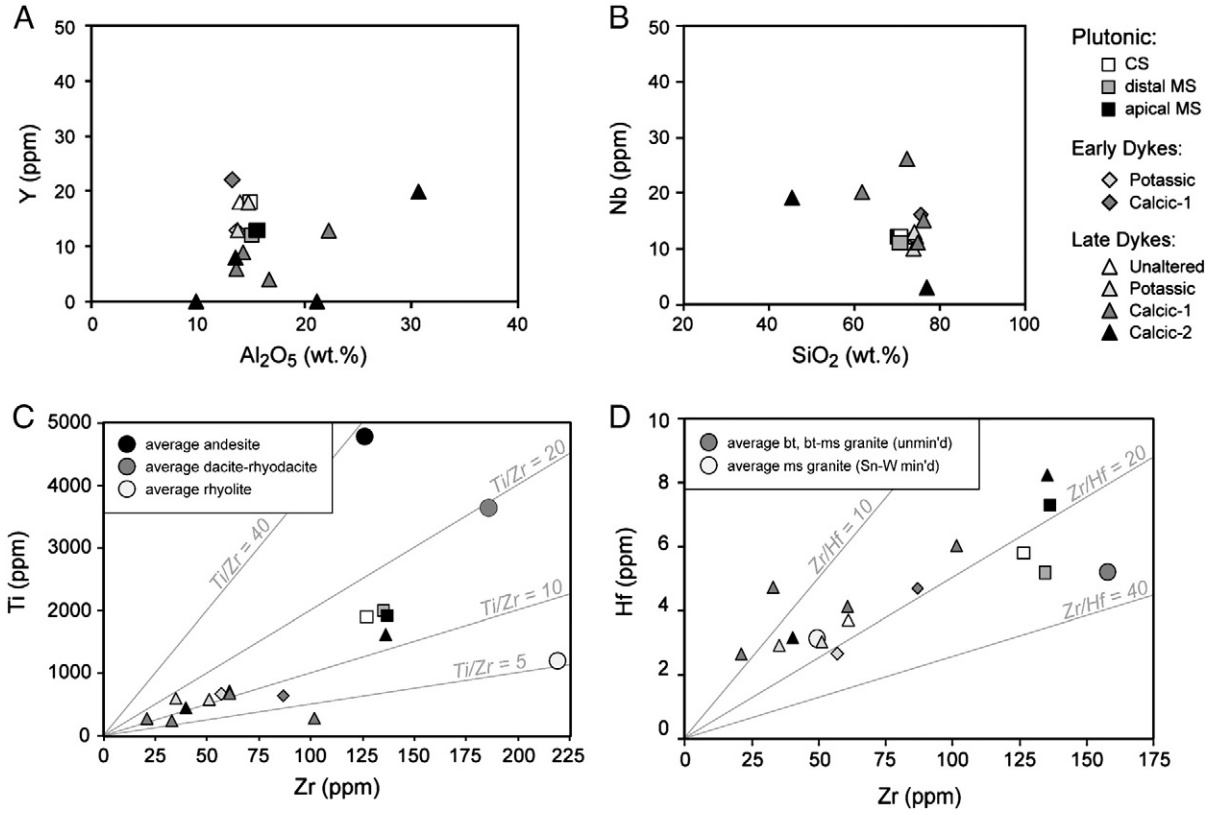

Fig. 16. Bivariate immobile element plots; the plutonic phases are unaltered samples of the Circular Stock (CS) and the Mine Stock (MS). A. Y vs. Al_2O_5. B. Nb vs. SiO_2. C. Ti vs. Zr with the average Ti and Zr concentrations of Winchester and Floyd (1977) for intermediate to felsic volcanic rocks; reference Ti/Zr ratios are indicated. D. $Hf_{recalc.}$ vs. Zr with average Hf and Zr concentrations for leucocratic granites of Zaraisky et al. (2009); reference Zr/Hf ratios are indicated.

Please cite this article as: Rasmussen, K.L., et al., Felsic magmatic phases and the role of late-stage aplitic dykes in the formation of the world-class Cantung Tungsten skarn deposit, Northwest Territories, Canada, Ore Geol. Rev. (2011), doi:10.1016/j.oregeorev.2011.06.011

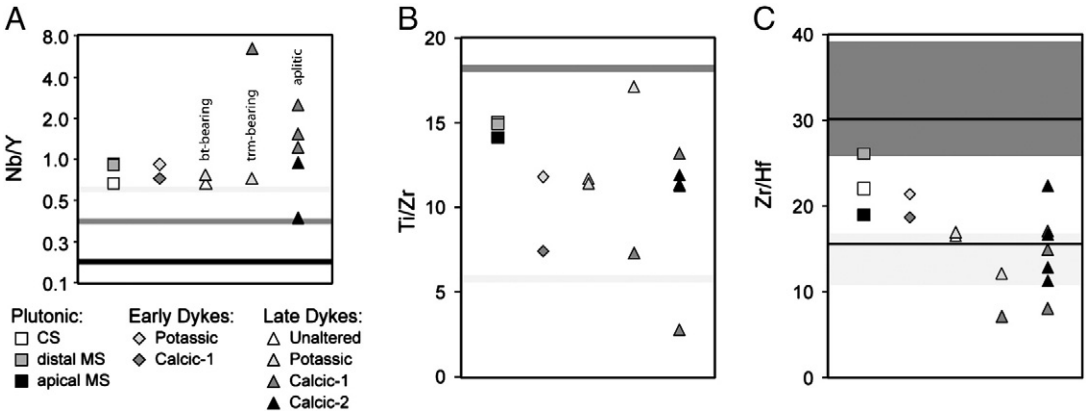

Fig. 17. Immobile element ratio plots; the plutonic phases are unaltered samples of the Circular Stock (CS) and the Mine Stock (MS). A. Nb/Y vs. rock type; average compositions for andesitic (black), dacitic–rhyodacitic (dark gray), and rhyolitic (pale gray) from Winchester and Floyd (1977) indicated. B. Ti/Zr vs. rock type; average dacite-rhyodacite and rhyolitic compositions from Winchester and Floyd (1977) are indicated by the dark gray and pale gray lines, respectively. C. Zr/Hf vs. rock type; range of, and average (black line), compositions for unmineralized biotite and biotite-muscovite granites (dark gray) and for Sn–W mineralized muscovite granites (pale gray) from Zaraisky et al. (2009).

concentrations (0.75–8.25 ppm; Table 2A) are very comparable to those reported in the literature for peraluminous biotite-bearing granites (e.g., Dostal and Chatterjee, 1999; Ishihara and Murakami, 2006; Rasmussen et al., 2007).

Zirconium and Ti are typically compatible elements in intermediate to felsic magmas because of the prevalence of zircon, magnetite or ilmenite, and hornblende or biotite (Pearce and Norry, 1979). Furthermore, Ti/Zr is known to decrease with differentiation such that Ti/Zr or variations of this ratio have been used as differentiation indices (e.g., Hall and Plant, 1992; Winchester and Floyd, 1977). In Fig. 16C, elemental Ti and Zr for the average rhyolitic, dacitic–rhyodacitic, and andesitic compositions of Winchester and Floyd (1977) form a negative trend, whereas the plutonic and dykes phases from Cantung form a positively sloping array. That the samples from Cantung define a linear array between average dacite-rhyodacitic to rhyolitic compositions of Winchester and Floyd (1977) is consistent with fractionation of the Cantung intrusions from a monzogranitic magma. Titanium and Zr have very similar concentrations amongst the plutonic phases at Cantung, but both decrease significantly from the plutonic phases to the dyke phases, probably as a result of zircon and ilmenite ± biotite fractionation. In Fig. 17B, Ti/Zr clearly decreases from the average intermediate to average felsic rock types of Winchester and Floyd (1977). Similarly, plutonic samples at Cantung have a relatively low Ti/Zr of ~15, with the apical Mine Stock phase corresponding to a slightly lower value of ~14. However, nearly all of the dyke phases at Cantung have Ti/Zr<13, which approaches a ratio more typical of rhyolitic (or syenogranitic) rocks. The enrichment in Ti/Zr in the some of the intensely metasomatized (potassic and calcic) late aplitic dykes is likely an effect of elevated Ti in the mineralizing fluids, as evidenced by titanite in skarn mineral assemblages and associated with scheelite-bearing veins cross-cutting some of these dykes. Although subtle, the decreases in Ti/Zr reflect an increasing degree of differentiation from the distal plutonic phases, to the apical plutonic phase, to the various dyke phases.

Zr and Hf typically partition from melt into zircon with very little change in the partition coefficient ratio, therefore Zr/Hf in most plutonic rocks has a range of 30–40 (Dostal and Chatterjee, 1999; Linnen and Keppler, 2002). However, experiments have confirmed in subaluminous to peraluminous granitic magmas that Hf has an increased affinity for melt, and a reduction in Zr/Hf may be another useful differentiation index for felsic intrusions (Linnen, 1998; Linnen and Keppler, 2002). Furthermore, a decrease in Zr/Hf has been correlated to more specialized granites that are prospective for mineralization (e.g., W, Mo, Bi, Sn, Be; Linnen, 1998; Zaraisky et al., 2009). Fig. 16D demonstrates that both Zr and Hf decrease from plutonic to dyke samples at Cantung, from concentrations more typical of a suite of unmineralized biotite and biotite-muscovite granites to concentrations more typical of Sn–W mineralized muscovite granites (e.g., Zaraisky et al., 2009). The plutonic samples at Cantung have elevated Zr/Hf = 18.7–26.0, with the apical Mine Stock sample corresponding to the most differentiated (i.e., lowest value) of these, whereas early dykes have Zr/Hf = 18.4–21.2, and late dyke samples typically have Zr/Hf<17 (Table 2A; Fig. 17C). The notable decrease from early to late dykes indicates a more significant degree of differentiation between these two phases of magmatism than the variation in Ti/Zr would suggest, perhaps due to the monomineralic fractionation of zircon with respect to Zr/Hf. The slight increase to higher Zr/Hf (up to 22) for several mineralized calcic-2 metasomatized aplitic dykes from unmineralized tourmaline-bearing dykes may be attributable to precipitation of Zr by metasomatising fluids. The plutonic and early dyke samples at Cantung lie just below the range and average for Zr/Hf in a suite of unmineralized biotite and biotite-muscovite granites, whereas the majority of the late dykes plot in proximity to the average Zr/Hf for a suite of Sn–W mineralized muscovite granites (Fig. 17C; e.g., Zaraisky et al., 2009).

As the multiple phases of felsic magmatism at Cantung appear to have originated from the same fractionating magma chamber, rare earth element (REE) and trace element profiles for a selection of representative felsic intrusive phases provide further insight into petrogenesis of the plutons and dykes. All of the samples are very similar to the average crustal compositions (Wedepohl, 1995) when normalized to chondritic (Sun, and McDonough, 1989), North American Shale (Gromet et al., 1984), and primitive mantle (Sun, and McDonough, 1989) references (Fig. 18). They are generally most similar to the average upper continental crust (of bulk granodioritic composition), overall continental crust (of bulk tonalitic composition), and North American Shale. Relative to the chondritic composition, the plutonic samples and the early dykes form a very tight and moderately sloping profile with small negative Eu anomalies and minor scatter or depletion with respect to the heavy REEs. A gently sloping pattern with minimal to no Eu anomaly and very similar REE abundances for the early intrusions are evident when compared to the North American Shale. The early biotite-rich dyke was not plotted in the immobile element ratio plots in Figs. 16 and 17 (due to a lack of XRF trace element data), but aside from slightly more depleted HREE and slightly less depleted Eu than the plutonic and QFP intrusions it is nearly identical in composition to the plutonic phases and the early QFP dyke in Fig. 18. This is consistent with the essentially identical plagioclase compositions (ca. An_{30}) exhibited by the plutonic phases and this early dyke (Table 3). Two late dyke samples have relatively depleted profiles on both REE plots, and for the biotite-bearing dyke

Please cite this article as: Rasmussen, K.L., et al., Felsic magmatic phases and the role of late-stage aplitic dykes in the formation of the world-class Cantung Tungsten skarn deposit, Northwest Territories, Canada, Ore Geol. Rev. (2011), doi:10.1016/j.oregeorev.2011.06.011

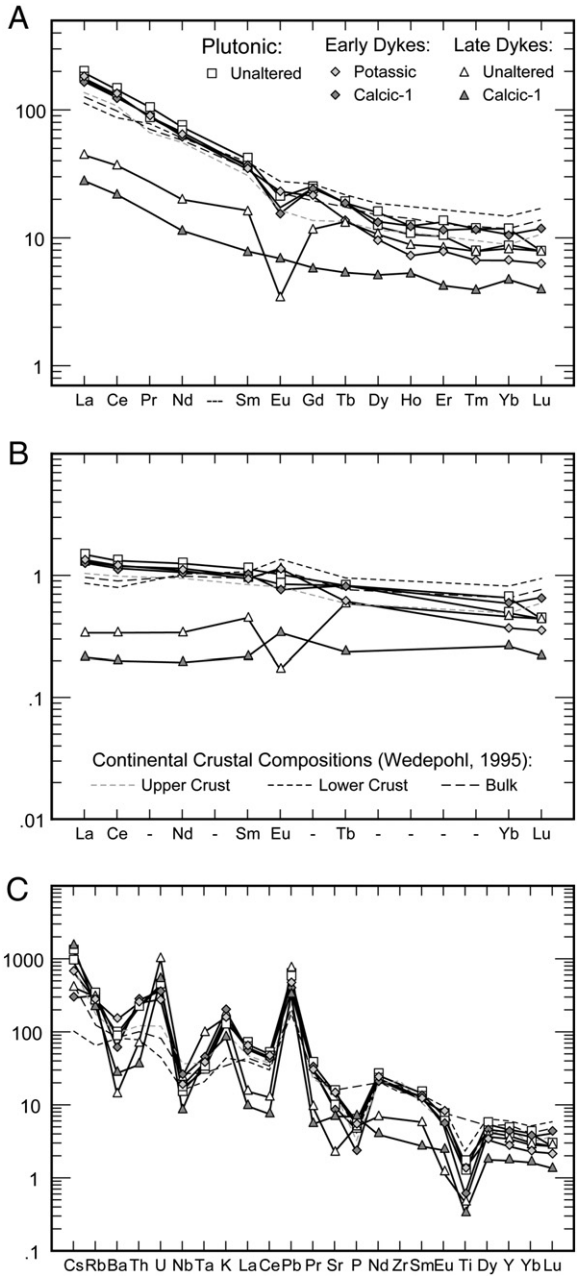

Fig. 18. Rare earth and trace element profiles for representative samples plotted with the average upper continental crust, average lower continental crust, and average bulk continental crust from Wedepohl (1995). Unaltered plutonic samples are KR-05-215 (distal Mine Stock) and 03M-207 (apical Mine Stock); the early potassic dyke is 07–18 (biotite-rich); the early calcic-1 dyke is 03M-212 (Open Pit QFP); the late unaltered dyke is 03M-203 (biotite-bearing); and, the late calcic-1 dyke is 03M-204 (aplitic). A. Rare earth element profile normalized to the chondrite of Sun and McDonough (1989). B. Rare earth element profile normalized to average North American Shale of Gromet et al. (1984). C. Multi-trace element profile normalized to the primitive mantle of Sun and McDonough (1989).

this may be attributed to high degrees of fractionation of monazite, apatite, and zircon (and (or) garnet) from the residual magma. However, the smooth and extremely depleted REE profile exhibited by the late aplitic dyke cannot be explained by selective mineral fractionation, a lack of suitable REE-host minerals (zircon and apatite are both present), or sub-solidus metasomatism as REEs are generally regarded as immobile (e.g., Jenner, 1996). This smoothly depleted REE pattern is likely related to a mass removal due preferential partitioning of REEs into a late-stage H_2S enriched magmatic fluid similar to that which formed the pyrrhotite-rich skarn facies (e.g., Gieré, 1993).

The primitive mantle-normalized multi-trace element profile overall is similar to the REE plots in that the plutonic phases and associated early dykes form a relatively tight profile, and the two late dyke samples once again have generally more depleted trace element concentrations, particularly with respect to the REEs. Relative to the primitive mantle, all of the Cantung samples have pronounced negative HFSE anomalies (e.g., Nb, Ta, Ti, P).

4. Discussion

4.1. Petrogenesis of the FMP

4.1.1. Melt sources

The plutons at Cantung have been interpreted by previous workers to be S-type granites produced by partial melting of over-thickened supracrustal rocks (e.g., Christiansen and Keith, 1996; Gordey and Anderson, 1993). However, relatively low abundances of elements typical of S-type granites (e.g., Sn, Be, Rb, F, As, Y, and Li; Newberry, 1998) and a moderately low peraluminosity (ASI = 1.05–1.15), combined with a lack of highly aluminous minerals in the granitoids (e.g., cordierite, andalusite, sillimanite) led to the suggestion that the intrusions at Cantung were not derived solely from partial melting of supracrustal rocks (Newberry, 1998; Rasmussen, 2004; van Middelaar, 1988). Although geochemical compositions indicate that the plutonic phases at Cantung are very similar to calculated compositions for estimates of upper continental crust and bulk continental crust compositions (e.g., Gromet et al., 1984; Wedepohl, 1995), the negative Eu anomalies on chondrite-normalized REE plots and negative HFSE anomalies when normalized to the primitive mantle (Sun, and McDonough, 1989) are more indicative of fractionation of plagioclase and hornblende in the evolution of the magma, or the presence of a plagioclase and hornblende-bearing restite in the melt source. Either way, these data are inconsistent with previous interpretations that the Cantung intrusions may be classified solely as S-type granites.

Radiogenic isotopic data for the Tungsten suite intrusions argue for a mixed melt source in radiogenic Proterozoic quartzo-feldspathic sedimentary rocks and interlayered intermediate-mafic sills and volcanic rocks (Rasmussen et al., 2010). This is not inconsistent with previous interpretations of melt sources for Cretaceous magmatism in the northern Cordillera (Driver et al., 2000; Morris and Creaser, 2008), and reports of hornblende- and biotite-rich igneous xenoliths in most of the other Tungsten suite intrusions (e.g., Anderson, 1983). A hybrid I–S type partial melt should have compositional characteristics very similar to those of a low-temperature I-type granite derived solely from partial melting of infracrustal rocks (e.g., Chappell et al., 1998). The high SiO_2 content (70.39–71.16 wt.%), a lack of associated intermediate composition granitoid phases, very similar trace element and REE abundances, and relatively low incompatible element ratios (e.g., Ti/Zr, Zr/Hf) for the Mine and Circular stocks plutonic phases are features that are shared by many of the other Tungsten suite plutons in the region (e.g., Rasmussen et al., 2007). These features suggest that the monzogranitic plutonic rocks at Cantung and other members of the Tungsten plutonic suite, were derived primarily from partial melting of a bulk crustal source of intermediate (e.g., hornblende-bearing) composition. A hybrid I–S type or low-temperature I-type granitic parent magma for the intrusions at Cantung is more consistent with reviews of mineralogical, compositional, and radiogenic isotopic data for other granitoids associated with W skarns (Meinert, 1995; Newberry, 1998; Newberry and Swanson, 1986), as well as work on S- and I-type granitoids (e.g., Chappell et al., 1998; Chappell and White, 1992) and on ore-forming intrusions in general (Keith et al., 1998; Vigneresse, 2006, 2007). Newberry and Swanson (1986) and Newberry (1998) have also suggested that economic W deposits are not associated with magmas solely derived from partial melting of metasedimentary rocks and that true S-type magmas are not capable of producing economic W mineralization.

Please cite this article as: Rasmussen, K.L., et al., Felsic magmatic phases and the role of late-stage aplitic dykes in the formation of the world-class Cantung Tungsten skarn deposit, Northwest Territories, Canada, Ore Geol. Rev. (2011), doi:10.1016/j.oregeorev.2011.06.011

4.1.2. Magma evolution

The plutonic Mine and Circular stocks do not appear to have undergone a significant degree of plagioclase fractionation (as a proxy for differentiation) from the inferred parental monzogranitic magma composition, based on their relatively small Eu anomalies (Fig. 18A). Additionally, the apical Mine Stock and early biotite-rich and QFP dykes underwent only marginal to minor amounts of zircon ± ilmenite ± biotite fractionation based on the small decreases in Ti/Zr and Zr/Hf ratios from the distal Mine and Circular stocks, to the apical Mine Stock, to the early dykes (Fig. 17). This fractionation may have occurred in a larger crystallizing magma chamber at depth and (or) upon injection and emplacement (e.g., Ishihara and Murakami, 2006; Tartèse and Boulvais, 2010; Webster et al., 2004). If multiple magma chambers were involved they must have been very similar compositionally, varying only minimally in their overall degree of fractionation.

The late leucocratic dykes are significantly more depleted with respect to the REEs (particularly the light REEs), Eu, several compatible elements (e.g., Th, La, V, etc.), and immobile element ratios (Ti/Zr, Zr/Hf), which implies a much greater degree of differentiation for these later intrusions. The depleted elements in the leucocratic biotite- or tourmaline-bearing dykes were removed from the magma as the crystallization of REE-hosting accessory mineral phases (e.g., zircon, ilmenite, monazite, apatite) proceeded at depth after emplacement of the plutonic phases and early dyke suites. An even greater mass removal of REEs from the calcic aplitic dykes is attributed to preferential partitioning of the REE and other incompatible elements into a H_2S-rich magmatic fluid that may have been involved in formation of skarn facies bearing REE-rich minerals (e.g., allanite, apatite; Marshall et al., 2003). Overall, geochemical (and geochronological) evidence indicates that the dyke phases at Cantung are genetically linked to the plutonic phases and were emplaced over a relatively short period. Although the late leucocratic dykes may have originated from the same monzogranitic magma chamber as the earlier intrusions, they are significantly more evolved than the plutonic and the early dyke magmas and were derived from segregated residual magma(s). The aplitic dykes in particular appear to be massively depleted in some chemical components that are enriched in the mineralized skarn.

4.1.3. Magma mixing and metallogenic implications

Moderately calcic ($An_{35–42}$) euhedral plagioclase grains (referred to previously as xenocrysts) have euhedral to rounded and irregular cores, range from unzoned to coarsely reverse-zoned to rare finely oscillatory-zoned, and frequently have unzoned to normally zoned sodic grain margins. Other workers attributed sodic plagioclase overgrowths and selective replacement of cores to high temperature sub-solidus metasomatism (Mathieson and Clark, 1984; van Middelaar, 1988; van Middelaar and Keith, 1990). While this is a possibility, it is curious that this mainly affects large, euhedral plagioclase grains, and that many other large euhedral grains and anhedral groundmass grains do not appear to have been altered. An alternative explanation for the partially resorbed andesine cores with sodic overgrowths is that they may represent an intermediate restitic component to the magma that was later overgrown by more sodic plagioclase in a felsic granitic magma (e.g., Castro et al., 1999; Chappell et al., 1998). Evidence for entrained restite at Cantung includes “dark inclusions” of more intermediate composition within the apical Mine Stock granite reported by van Middelaar (1988); similarly, mafic-rich igneous xenoliths are also reported for most of the Tungsten plutonic suite intrusions in the region (e.g., Anderson, 1983).

However, the textural and compositional variations in xenocrystic plagioclase could have another explanation. The zoning patterns, and particularly the sieve-textures exhibited by many of the andesine plagioclase grains before overgrowth of the latest sodic rim, may also be suggestive of complex dynamics in the magma chamber related to magma mixing (e.g., Gagnevin et al., 2004; Janoušek et al., 2004; Kontak and Clark, 2002). These large plagioclase xenocrysts may have been introduced during, or formed by, early mixing with a mafic to intermediate magma, causing resorption and overgrowth patterns and the associated sieve textures (e.g., Gagnevin et al., 2004; Janoušek et al., 2004; Kontak and Clark, 2002). Mixing would have occurred at depth, likely in the source region of the parental monzogranitic magma, due to the lack of evidence for magma mixing in the exposed Mine Stock and the apparent widespread distribution of these xenocrysts throughout the Mine and Circular stocks. A xenocrystic source (from either restite or magma mixing, or both) appears to be the most likely explanation for the andesine plagioclase grains with sodic rims ± intermediary sieve-textures.

Post-emplacement mixing of magmas with significantly different compositions and temperatures, however, can have significant effects on the volatile and metal budget of a pluton, even if changes in whole rock or mineral compositions are not evident due to the very high timescales of chemical diffusion in partially crystallized felsic magmas (Vigneresse, 2006, 2007). For example, if a hotter mafic magma intrudes a cooler felsic magma (inducing a large temperature gradation), the diffusion coefficients and oxygen fugacity of the felsic magma will increase, partition coefficients in the felsic magma will decrease, and elements with the highest activation energies (including W) will migrate into the felsic magma and (or) segregate from the existing magma into a coexisting fluid phase (Hibbard, 1981; Keith et al., 1998; Vigneresse, 2006, 2007). Although actual metal transfer from relatively small batches of an intermediate to mafic magma into a larger silicic magma chamber may not be particularly significant, another effect is that the volatile species, some of which are much more concentrated in mafic magmas (e.g., CO_2, Cl, S), can exsolve from the mafic magma as its temperature decreases during interaction with the cooler felsic magma (Keith et al., 1998; Litvinovsky and Podladchikov, 1993; Vigneresse, 2006, 2007). Although the increase in the temperature of the felsic magma will also increase the solubility of most of the volatile species in the felsic magma (e.g., H_2O, CO_2), any added S and halogen species will remain insoluble and will migrate upwards or diffuse into the magma chamber to enrich the felsic magmatic fluid phase (Keith et al., 1998; Meinert, 1993; Vigneresse, 2006, 2007). In this way relatively small inputs of mafic magma may substantially increase the volatile, and potentially the metal budget, of the felsic magma.

At Cantung, the late (post-mineralization) shoshonitic lamprophyre dykes and breccias could be compositional equivalents to earlier injections of hot volatile-rich mafic magmas into the crystallizing and fractionating felsic monzogranitic magma chamber at depth. Field evidence for the addition and mixing of mafic magmas may not be evident due to the limited exposures of only the uppermost levels of the Mine Stock, particularly if the mafic magma batches are small and localized. However, volatiles and metals derived from mafic dykes may have been added to the Mine Stock magmatic system (e.g., Keith et al., 1998; Litvinovsky and Podladchikov, 1993; Vigneresse, 2006, 2007) and may help to explain the exceptionally high water/rock ratios required for the observed W mineralization (Bowman et al., 1985) and the anomalously abundant and ubiquitous pyrrhotite found throughout all of the skarn facies at Cantung (e.g., Dick and Hodgson, 1982). Although the objective of this study was not to determine whether or not late-stage magma mixing occurred at Cantung, the possibility that lamprophyric or similar mafic magma(s) may have interacted with the felsic magma chamber at Cantung could have interesting implications regarding the formation of this world-class W skarn deposit.

4.2. Emplacement and crystallization of the FMP

In addition to macroscopic features of dykes (i.e., orientation, textures, cross-cutting relationships, etc.), detailed documentation of petrographic textures in the FMPs may also provide a significant amount of information on the mechanisms of emplacement, cooling histories, and whether or not a volatile phase was exsolved from these intrusive phases (e.g., MacLellan and Tremblath, 1991; Lentz and Fowler, 1992;

Please cite this article as: Rasmussen, K.L., et al., Felsic magmatic phases and the role of late-stage aplitic dykes in the formation of the world-class Cantung Tungsten skarn deposit, Northwest Territories, Canada, Ore Geol. Rev. (2011), doi:10.1016/j.oregeorev.2011.06.011

Lowenstern and Sinclair, 1996; Webber et al., 1997; Breiter, 2002; Leonard et al., 2006; Bineli Betsi and Lentz, 2010). One method of determining approximate cooling histories of felsic intrusions is to document crystal morphologies for quartz and feldspar, and then relate these observations to the results of experimental studies on morphology and cooling (e.g., Baker and Freda, 2001; Lofgren, 1971, 1974; MacLellan and Tremblath, 1991; Swanson, 1977; Swanson and Fenn, 1986). This allows us to estimate the degree of undercooling (supercooling) a magma may have experienced, and provides an alternate explanation for textures that might otherwise be attributed to changes in pressure, temperature, or fluid content (MacLellan and Tremblath, 1991). Although the magnitude of undercooling (ΔT) is difficult to estimate, relative variations can be determined from mineral morphologies and crystallization sequences. The ΔT values below are provided for comparative purposes, but are only estimates based on the work of MacLellan and Tremblath (1991) for intrusions with similar (but not identical) relative Q–K–Ab–An content to those at Cantung. Caution is also required when interpreting degrees of undercooling as small changes in magma composition, or longer cooling rates may have major effects on the resultant textures (MacLellan and Tremblath, 1991). As quartz is less subject to sub-solidus recrystallization than feldspars (e.g., MacLellan and Tremblath, 1991), we focus this discussion mainly on quartz morphology.

4.2.1. Early underground FMP

Quartz textures characteristic of the early plutonic and biotite-rich dyke phases include large composite aggregates with coarse-skeletal intergrain boundaries, finer-grained quartz in the groundmass with anhedral to euhedral elongate prismatic skeletal morphology, and rare recrystallized micropoikilitic quartz and spherulitic K-feldspar. It is unclear here if the skeletal quartz preceded anhedral quartz, which would suggest an increase in the degree of undercooling with time (MacLellan and Tremblath, 1991), or if they formed at the same time and indicate a relatively high, but stable degree of undercooling. Overall, though, the majority of quartz in these intrusions has anhedral grain boundaries and likely started to crystallize at moderate undercooling conditions (e.g., ΔT = 100–150 °C for slow to high rates of cooling, respectively). However, the rare micropoikilitic quartz also observed in the Mine Stock and early biotite-rich dykes is a late texture that requires a very high degree of undercooling (e.g., ΔT>210 °C), and could be related to isolated pockets of very late-stage fluid-rich melt in these intrusions approaching near complete crystallization. These early magmatic phases likely cooled primarily by conductive heat loss at a relatively slow rate in the Mine Stock pluton and a more moderate rate in the biotite-rich dykes, due to an elevated geothermal gradient in the region resulting from magma emplacement at moderate depths (e.g., at a minimum pressure of 2 kbar) and ongoing nearby plutonism. The rarity of micropoikilitic quartz textures in these early intrusions implies that mainly moderate undercooling conditions (e.g., ΔT = 125 °C) dominated, which is typical of granitic magmas (Baker and Freda, 2001; MacLellan and Tremblath, 1991; Swanson, 1977).

4.2.2. QFP dykes

The large QFP dykes exposed on the surface were derived from a deep magma chamber experiencing high fluid pressures (>2.5 kbar; see Martin and Bonin, 1976) related to the early crystallization of the mainly anhydrous phenocrysts (e.g., London, 1992, and references therein). These high fluid pressures at depth are inferred to have led to magmatic overpressuring and rapid, far-ranging fracture propagation (at least 300–700 m vertical, and very likely more) involving ongoing depressurization and devolitization upon ascension of the magma (Burnham, 1985; Downey and Lentz, 2006; Leonard et al., 2006). Dipyramidal quartz phenocrysts indicate that minimal to no undercooling occurred in the magma chamber at depth prior to injection as dykes, although the development of skeletal protrusions on these crystals could imply a slight increase in the degree of undercooling as crystallization proceeded (e.g., ΔT<55 °C). However, skeletal quartz textures could also be interpreted as embayments resulting from a depressed liquidus and consequent resorption of the quartz crystals during decompression related to magma ascension (e.g., Burnham, 1985; Swanson and Fenn, 1986; Hibbard, 1994, and references therein; Leonard et al., 2006). In the case of the QFP dykes, other textures and observations suggest that depressurization was the main mechanism for forming the skeletal quartz textures. Following emplacement, crystallization of the melt to what is now an exceptionally fine-grained K-feldspar-rich groundmass (with lesser quartz, plagioclase, and accessory biotite) is ascribed to granular recrystallized magmatic fibrolites (e.g., Bineli Betsi and Lentz, 2010; Leonard et al., 2006; MacLellan and Tremblath, 1991). Extremely high degrees of undercooling (e.g., ΔT>210 °C) will produce intergrown fibrolitic textures in magmas similar in composition to the QFP dykes (MacLellan and Tremblath, 1991), which are induced by the exsolution and immediate escape of a volatile phase causing a near-instantaneous quenching of the remaining melt (Leonard et al., 2006). Therefore, the potassic microcrystalline groundmass, the embayed quartz phenocrysts, and the absence of chill margins point mainly to depressurization of a relatively hot, likely fluidized magma during ascension and emplacement. This magma experienced continued exsolution and loss of volatiles to the upper levels of the system, and the remaining extremely supercooled potassic melt was quenched essentially instantaneously.

Unlike the other QFP dykes, the Open Pit dyke exhibits pervasive micrographic to coarse-granophyric textures rimmed by later axiolitic to spherulitic microcline-quartz intergrowths extending from locally resorbed quartz and microcline phenocrysts to throughout the groundmass. Dipyramidal quartz phenocrysts in this dyke first underwent extensive resorption, followed by pervasive quartz–feldspar intergrowths ranging from those typical of moderate degrees of undercooling (e.g., micrographic, granophyric) to those that normally indicate very high degrees of undercooling (e.g., spherulitic). The development of micrographic-granophyric intergrowths requires a restricted range of undercooling conditions (ΔT = 150–200 °C) as these textures are not preserved at high ΔT. However, crystallization of felsic magmas in the presence of an exsolved fluid has also been linked to granophyric to micrographic K-feldspar overgrowths on quartz phenocrysts (Fenn, 1986; Lentz and Fowler, 1992; Lowenstern and Sinclair, 1996). Therefore, the pervasive magmatic quartz–microcline intergrowth textures in Open Pit QFP may be the result of less extreme disequilibrium crystallization compared to the other QFP dykes, related to the presence of an exsolved sodic fluid (e.g., Pirajno, 2010; Yuvan et al., 2007) that was not immediately lost from the system. The presence of a fluid-phase during crystallization may have reduced the degree of undercooling and perhaps the rate of cooling experienced by the Open Pit QFP dyke. Calcic metasomatism, or the replacement of microcline to plagioclase from the dyke margins inwards may be the result of interaction between this fluid and the Ore Limestone into which the dyke is emplaced.

4.2.3. Late underground FMP

Highly fractionated biotite- or tourmaline-bearing dykes were emplaced into the country rocks predominantly along bedding and joint planes. The relatively fine-grained textures of these dykes, combined with the dominance of anhedral quartz, lesser coarse-skeletal grain boundaries, and rare recrystallized micropoikilitic quartz, are indicative of moderately high degrees of undercooling (e.g., ΔT>150 °C). Although a range of cooling rates is possible, a moderate rate is assumed for most of these dykes due to the overall thermally elevated regime and the dyke textures. The lack of graphic or granophyric textures in these dykes could be either a result of magma composition (e.g., feldspar on the liquidus), or extremely high undercooling (e.g., ΔT>200 °; MacLellan and Tremblath, 1991). However, these dykes were relatively enriched in volatile species, based on localized late exsolution and entrapment of B–F–Fe rich fluid

Please cite this article as: Rasmussen, K.L., et al., Felsic magmatic phases and the role of late-stage aplitic dykes in the formation of the world-class Cantung Tungsten skarn deposit, Northwest Territories, Canada, Ore Geol. Rev. (2011), doi:10.1016/j.oregeorev.2011.06.011

phase (Sinclair and Richardson, 1992), as both miarolitic cavities with aplitic margins and tourmaline-infilled cores in the biotite- and tourmaline-bearing dykes, and as finer grained tourmaline–muscovite pockets in the tourmaline-bearing dykes. Therefore, although the high degrees of undercooling experienced by these late dykes (e.g., $\Delta T > 200$ °C) may be responsible for the micro-textures documented here, an undersaturated fluid- or volatile-rich residual melt could have contributed to the localized and highly undercooled crystallization textures by suppressing the solidus. Conversely, the coarse granophyric and graphic textures exhibited by rare pegmatitic equivalents of the tourmaline-bearing dykes would suggest crystallization in these particular dykes at a lower restricted range of undercooling (e.g., $\Delta T = 125$–200 °C) and a moderate rate. It should also be noted that crystallization of leucogranitic magma in equilibrium with an exsolved fluid will also produce similar textures (Fenn, 1986; Lentz and Fowler, 1992), which is similar to the explanation given for these textures in the Open Pit QFP dyke.

Aplitic dykes are generally finer grained than the other dykes at Cantung; however, at least small K-feldspar and possibly plagioclase crystals appear to have been present in the injected magma due to relatively large, simply twinned plagioclase pseudomorphs after K-feldspar ± plagioclase. If both feldspars were injected with melt then the source magma was probably volatile-rich, implying a lowered solidus and a relatively high fluid pressure (e.g., > 2.5 kbar; Martin and Bonin, 1976; London, 1992, 1995). Where quartz is present (i.e., fresh to calcic-1 metasomatized dykes), abundant small equant hexagonal quartz dipyramids transitioning to slightly elongate coarse-skeletal quartz morphologies are observed. Both types of calcic alteration lack granophyric, micropoikilitic, and anhedral quartz and feldspar morphologies, and display larger skeletal and boxy cellular plagioclase grains with untwinned anhedral plagioclase infilling embayments. Although dipyramidal quartz is stable at very low to no undercooling, experimental work by MacLellan and Tremblath (1991) would suggest that the skeletal textures in quartz are produced only above moderately high undercooling conditions in K-feldspar-poor haplogranitic magmas, which is also relatively consistent with the initiation of skeletal plagioclase crystallization (Lofgren, 1974). This could reflect either a large increase in the degree of undercooling if quartz morphologies are truly transitional from dipyramidal to skeletal; however, both of these morphologies occupy the same stability field at $\Delta T > 150$ °C and may also form at the same time. Granophyric textures will not be preserved in these intrusions if $\Delta T > 200$ °C, or if the dykes cooled at an extremely fast rate (MacLellan and Tremblath, 1991). Since it is unlikely that the dykes were cooled quickly, due in part to the elevated geothermal gradients inferred for the other intrusions at Cantung, a very high degree of undercooling ($\Delta T > 200$ °C) is proposed for these dykes, which may have been enhanced to some degree by an initially depressed solidus due to high volatile contents prior to fluid exsolution (e.g., London, 1995) and (or) minor depressurization upon emplacement. However, the aplitic dykes also may not have produced quartz–feldspar intergrowth textures due to their magmatic compositions or to the effects of subsolidus metasomatism. Granophyric to micropoikilitic intergrowths were not produced, or were only produced very sporadically, in experimental haplogranitic magmas with plagioclase and (or) K-feldspar on the liquidus (MacLellan and Tremblath, 1991), which is consistent with the presence of one or both of these feldspars (and the apparent lack of quartz) as early phenocryst phases injected with the aplitic magma. Therefore, the degree of undercooling experienced by these dykes could have been from ca. 150 °C to > 200 °C.

4.2.4. Circular Stock breccia pipe

The Circular Stock breccia pipe is a sub-vertical elliptical body of up to several tens of meters wide that occurs at the northeast margin of the K-feldspar megacrystic biotite monzogranitic Circular Stock intrusion along its contact with the Upper Argillite. The Circular Stock and its associated breccia body were not studied in detail here; however, a description of their textures and compositions are warranted due to a possible connection with magmatic processes responsible for mineralization at Cantung. Although the Circular Stock macroscopically appears to be a hypidiomorphic-granular, K-feldspar megacrystic, coarse-grained biotite granite, petrographic examination reveals a pronounced seriate texture consisting of microcline megacrysts, large composite quartz grains, and plagioclase and biotite phenocrysts set within a very fine-grained or quenched quartz–feldspar groundmass related to depressurization and rapid crystallization of the groundmass upon emplacement. The pipe-shaped geometry of the Circular Stock granite also suggests that the emplacement of this crystal-rich magma occurred along a zone of structural weakness. Exposures of the adjacent breccia body consist mainly of rounded to sub-rounded clasts of cohesive, coarse-grained K-feldspar megacrystic monzogranite to leucogranite, with bleaching and broken K-feldspar crystals along margins. Fractured feldspars ± chloritized biotite within the clasts are healed by bladed sericite, zoisite/epidote, or chlorite. Less abundant, but locally highly concentrated angular clasts of pale green (epidotitic) carbonate with dark green chloritized margins, and angular to sub-angular clasts of dark brown argillite are also present. Clasts are commonly fractured and infilled with or rimmed by Fe-oxides or Fe-sulfides ± malachite. Rare calc-silicate-altered (skarnified) fragments may also be mineralized with scheelite. Breccia fragments range from mm- to dm-sizes and are unsorted. The presence of epidote-carbonate clasts where the breccia is in contact with the Upper Argillite suggests that some upward (or downward) transport of calcareous clasts is likely to have occurred. The breccia has three main texturally and mineralogically distinct matrices: (1) a coarse-grained K-feldspar megacrystic monzogranitic matrix with a strongly seriate texture identical to that of the Circular Stock described above and containing only sub-rounded granitic to leucogranitic clasts; (2) a widespread pale green matrix comprising very fine-grained equigranular quartz–carbonate ± very fine-grained muscovite, large scattered resorbed plagioclase and K-feldspar phenoclasts with minor to moderate sericitization/saussuritization, ragged resorbed biotite altered to chlorite and associated with coarse-grained apatite, and mottled with zoisite/epidote–chlorite patches replacing small calc-silicate clasts or possibly plagioclase; and, (3) a black tourmaline cement related to syn- or post-breccia fluids. Spatial relationships between the breccia matrix phases were not observed, although the very fine-grained, pale green matrix appears to be dominant and is associated with the precipitation of sulfides and Cu-oxides. Based on its texture the strongly seriate granitic matrix is transitional to the Circular Stock intrusion and the Circular Stock breccia pipe, and observed textures that are intermediate to the granitic and pale green matrices suggest a gradational variation between these two end-member matrix types.

Classic magmatic-hydrothermal breccias are formed by overpressuring of a magmatic volatile phase (i.e., fluid, or fluid + vapor) in a magma chamber at moderate to shallow depths, causing hydrofracturing of overlying wall rocks followed by a larger exsolution of vapor due to associated depressurization (e.g., Breiter, 2002; Burnham, 1985; Oliver et al., 2006; Tosdal and Richards, 2001). Magmatic breccias contain angular to rounded clasts of wall rock, frequently from higher or lower levels, supported within a fine-grained to microcrystalline or tuffisitic matrix composed of pressure-quenched melt (e.g., Breiter, 2002; Burnham, 1985; Tosdal and Richards, 2001). They are considered to have a hydrothermal component, or to be hydrothermal if, instead of an igneous groundmass, a cement precipitated from fluid forms the breccia matrix (e.g., Oliver et al., 2006; Tosdal and Richards, 2001). Magmatic ± hydrothermal breccias are propagated from the bottom up. A second distinct set of breccia type are the phreatomagmatic breccia pipes (or cones), formed by the explosive interaction between hot magma and sub-surface or surface water, which produces steam and explosively ruptures the surrounding rock (Wolfe, 1980). Repeated explosions fracture the rock downwards such that the result is a sub-vertical pipe extending up to 3 km depth and containing an intensely milled rock flour matrix supporting μm- to m-size, subrounded to

Please cite this article as: Rasmussen, K.L., et al., Felsic magmatic phases and the role of late-stage aplitic dykes in the formation of the world-class Cantung Tungsten skarn deposit, Northwest Territories, Canada, Ore Geol. Rev. (2011), doi:10.1016/j.oregeorev.2011.06.011

rounded, equidimensional clasts from various levels of the pipe, with or without an overprinting hydrothermal cement (Oliver et al., 2006; Wolfe, 1980). Frequently, distinguishing between magmatic-hydrothermal and phreatomagmatic breccias can be difficult due to late percolation of fluids and destruction of matrix textures.

The Circular Stock breccia appears to be the product of magmatic-hydrothermal processes based on the presence of igneous and hydrothermal end-member matrices, and due to the re-interpreted depth of essentially coeval magmatism and mineralization at Cantung (e.g., 6–8 km; Marshall et al., 2003). Localized tourmalinization in the Circular Stock breccia is also typical of magmatic-hydrothermal breccia pipes formed in association with W-mineralizing systems since excess B indicates overpressuring of magmatic volatiles resulting in the formation of tourmaline-cemented breccias (Breiter, 2002; Pirajno, 2010). Timing of the breccia is interpreted to be very shortly after the emplacement of the ca. 97 Ma crystal-rich Circular Stock magma as an overpressured, a steeply dipping cylindrical body injected vertically into overlying country rocks and rapidly quenched, 'plugging' the system. Continued build-up of volatile-rich (e.g., B) magma at depth eventually led to hydro-fracturing along the contact of the Circular Stock and adjacent cooler country rocks, and injection of magma and exsolved fluid ± vapor to form the breccia body. Rounded granitic clasts with seriate textures in the breccia suggest that brecciation of the Circular Stock occurred after quenching of the magma while it was still hot, whereas cooler carbonate and argillite country rocks formed more angular clasts. Depressurization of injected magma and fluid during the formation of the marginal breccia body produced a very fine-grained tuffisitic matrix containing larger resorbed magmatic crystals and a localized tourmaline cement. The tuffisitic matrix, feldspar phenoclasts, and carbonate clasts were altered to quartz, carbonate, muscovite, and epidote, or were displaced/replaced by a localized tourmaline cement by the passage of late to post-breccia fluids.

4.2.5. Mechanics of emplacement of the FMP

Localized deformation and penetrative foliation in the wall rocks within a few meters of the relatively flat-topped Mine Stock contact (Mathieson and Clark, 1984), and mineralogically and texturally similar off-shooting granitic apophysies cross-cutting bedding indicate a semi-forceful emplacement of the apical Mine Stock, probably in part related to pressure anisotropies produced by the emplacement of a larger magma body at depth. However, the early and shallow-dipping biotite-rich dykes are suggestive of a low lithostatic load at the time of their emplacement (e.g., Breiter, 2002; Derre et al., 1986). The apical Mine Stock and biotite-rich dykes may have been emplaced just above the critical depth of Brisbin (1986) under the influence of a vertically directed minimum normal stress field.

Evidence for most of the injection of QFP dykes as a fluidized, crystal-poor melt-vapor phase includes their emplacement ranging from 300 to 700 m above the top of the apical Mine Stock (a minimum estimate for the vertical distance traveled), angular granitic xenoliths displaced at least 300 m vertically, the lack of chill margins, a microcrystalline groundmass, and one intensely flow-banded dyke. Anhydrous crystallization-related saturation of a vapor phase in the QFP magma at relatively high fluid pressures at depth (e.g., > 2.5 kbar; Martin and Bonin, 1976) may have caused the initial volatile exsolution and vesiculation of the magma, which would have led to volume expansion at a critical fluid pressure, overpressuring, and the initiation of far-ranging fractures in the overlying rocks (e.g., Burnham, 1985; Downey and Lentz, 2006). Rapid ascension and depressurization of the crystal-poor fluidized magma caused quenching, an additional and probably greater exsolution of the remaining magmatic volatiles, and further fracture propagation upwards (Bineli Betsi and Lentz, 2010; Burnham, 1985; Candela, 1997; Downey and Lentz, 2006; Swanson, 1977). A similar process of magmatic overpressuring and volatile exsolution may also be responsible for the emplacement of the cylindrical Circular Stock as a crystal-rich and partially crystallized magma 'pipe', followed by the formation of a breccia along its northern margin. However, the Open Pit QFP dyke appears to have experienced a more moderate degree of undercooling and a slower rate of cooling, probably due to the presence of an exsolved supercritical fluid, and therefore is not thought to have experienced boiling and the catastrophic loss of its volatile phase causing extensive fracturing and fluid-escape (e.g., Yuvan et al., 2007).

The late biotite- and tourmaline-bearing dykes were emplaced under slightly higher lithostatic loads just below the critical depth, which favors multiple dyke orientations focused along pre-existing country rock anisotropies such as bedding and joint planes (Brisbin, 1986). Many of these dyke orientations define a near-conjugate set with a sub-vertical principal stress axis, whereas other dykes are emplaced sub-parallel to folded bedding in the hinge zone of the recumbent anticline. These dykes were not injected with enough force to systematically fracture or brecciate the country rock and there is no evidence for a principal far-field stress control on these particular dyke orientations. The apparent increase in the lithostatic pressure prior to emplacement of the late dykes could be related to an increase in magmatic overpressuring at depth resulting from increased fluid pressure as a result of magmatic differentiation, or to an increase in volume resulting from a influx of magma into the deeper chamber (e.g., Moore, 1975; Tosdal and Richards, 2001).

The orientation of late aplitic dykes parallel to NE-trending, sub-vertical normal faults and fractures underground implies significantly different emplacement conditions when compared to the other dyke suites. These aplitic dykes were emplaced below the critical depth, suggesting that stress fields were largely altered by strong magmatic overpressuring (e.g., Shinohara and Kazahaya, 1995, and references therein; Tosdal and Richards, 2001; Pirajno, 2010). Although increased magmatic overpressuring of residual magma in a highly crystallized felsic magma at depth increases lithostatic pressure and leads to vertical fracturing (e.g., Burnham, 1985; Dingwell, 1997), the emplacement and orientation of the sheeted aplitic dykes at Cantung were also highly influenced by regional stress controls (e.g., Tosdal and Richards, 2001). Due to ongoing NE-directed continental margin shortening through the mid- to Late Cretaceous, the least principal stress field would have been oriented NW–SE across much of the northern Cordillera. Therefore, a combination of regional stress regimes and an increased fluid pressure in the magma led to the propagation of steep-dipping NE-trending fractures through the plutonic carapace of the felsic magma chamber, including the apical Mine Stock, and into the overlying country rocks. A fluid-rich residual magma, or an equilibrated residual magma and exsolved supercritical magmatic fluid were injected into the fractures. The lack of evidence for large phenocrysts in these dykes upon emplacement suggests that the magma was near its ternary minimum, which was probably significantly reduced by the volatile enrichment prior to exsolution of the magmatic fluid (e.g., London, 1992, and references therein). However, based on the fluid inclusion evidence summarized below and unlike most of the QFP dykes, fracture propagation and depressurization was not fast enough or great enough to cause the magmatic fluid to intersect the saturated vapor curve in P–T space; therefore, boiling of the magmatic fluid upon ascent did not occur (e.g., Candela and Piccoli, 1995; Meinert et al., 2003). A lack of vapor exsolution during ascension may also explain why the aplitic dykes did not form large and far-ranging fractures like those created by the QFP dykes, although competency contrasts in the wall rocks at the time of aplitic dyke emplacement may also have been a limiting factor in the size and distance of fracture propagation (Shinohara and Kazahaya, 1995).

4.3. Skarn mineralization processes

4.3.1. Composition of skarn-forming fluids

Early fluids leading to the formation of reduced anhydrous W–(Cu) skarns are generally primary or non-boiling hot magmatic brines with <10% NaCl and low $f(O_2)$, which are thought to strongly partition W from the melt (Candela, 1997; Manning and Henderson,

Please cite this article as: Rasmussen, K.L., et al., Felsic magmatic phases and the role of late-stage aplitic dykes in the formation of the world-class Cantung Tungsten skarn deposit, Northwest Territories, Canada, Ore Geol. Rev. (2011), doi:10.1016/j.oregeorev.2011.06.011

1984; Meinert et al., 2003; Newberry, 1998; Newberry and Swanson, 1986). At Cantung, two low to moderate salinity non-boiling fluids were detected (Marshall et al., 2003; Mathieson and Clark, 1984; Yuvan et al., 2007; Zaw, 1976): (1) a widespread brine with 4–14% NaCl and $CaCl \pm CO_2 \pm CH_4$ interpreted to be the main mineralizing fluid; and (2) a relatively insignificant $CO_2 \pm CH_4$, 3-phase fluid with varying proportions of vapor found only in apatite from the biotite skarn and thus suggested to indicate only local and episodic venting of CO_2 from the underlying intrusion. The main mineralizing fluid at Cantung was also modestly enriched in $FeCl_2$, $MgCl_2$, and KCl (Mathieson and Clark, 1984) and elements that behave incompatibly in highly differentiated magmas, including P (Bea et al., 1992; van Middelaar and Keith, 1990), B (based on the presence of tourmaline veins; Pirajno, 2010), and possibly F (based on rare fluorite in the Cantung skarn assemblages and unpublished apatite-biotite-muscovite compositions). A large enrichment in H_2S in the mineralizing fluid is inferred on the basis of the positive association between pyrrhotite and scheelite mineralization in all skarn facies. These fluid compositions are consistent with the experimentally determined preferential partitioning of W into $NaCl \pm KCl$–CaCl brines (Burnham and Ohmoto, 1980; Candela and Piccoli, 1995; Foster, 1977; Keppler and Wyllie, 1991; Manning and Henderson, 1984; Mathieson and Clark, 1984). Deposition of scheelite with pyrrhotite was attributed to the increase in aCa^{2+} and pH of the mineralizing fluid as a result of calcite break-down during pyrrhotite precipitation in the host calcareous country rocks (Mathieson and Clark, 1984). A range in homogenization temperatures (500–270 °C) and a remarkably small range in stable isotopic compositions of magmatic and skarn minerals suggests that anhydrous and early hydrous skarn initially formed together, although only the hydrous skarn facies persisted to lower temperatures (e.g., Bowman et al., 1985; Mathieson and Clark, 1984), although this model has since been questioned (Newberry, 1998). In a study of fluid inclusions in quartz veins and aplitic dykes, Yuvan et al. (2007) noted that underground aplitic dykes and the QFP dyke in the Open Pit have similar fluid compositions to those found in the E-zone skarn and the Open Pit quartz veins. None of the fluid inclusions studies found any evidence for boiling at Cantung.

4.3.2. Relationship between metasomatism of the FMP and skarn mineralization

Potassic mineral assemblage(s) and associated textures may be attributed to an open-system loss of high temperature autometasomatic sodic ($Na \pm Si$) magmatic fluid related to a build-up of volatile species like B in late-stage melt/fluids within the dykes (Hibbard, 1980; Pirajno, 2010, and references therein). This leaves a residual melt that crystallizes a relatively potassic mineral assemblage and (or) metasomatizes earlier-formed minerals. This autometasomatism of the dykes (with the exception of rare potassic aplitic dykes, discussed next) is particularly pronounced along micro-fractures that may have provided escape structures for fluids, and macroscopic fractures with bleached margins and lined with tourmaline and quartz cross-cutting all but the aplitic dyke phases, but may also be more pervasive (e.g., the biotite-rich dykes). Evidence for sodic fluid flow and entrapment along dyke margins is also present and includes the cm-scale bleached plagioclase–quartz margins of the early biotite-rich dykes (Fig. 6B; as well as the bleached halo around the biotite-rich phase in the apical Mine Stock, Fig. 5B) and dm-scale pods of albite–tourmaline–(quartz) pooling along late biotite- and tourmaline-bearing dyke contacts (Fig. 7B). Although this type of metasomatism is described as potassic, very fine-grained turbid and mottled albite $\pm$ quartz may be precipitated along the grain boundaries of pristine microcline in some of the dykes. This minor albitization represents the last precipitates of trapped of sodic fluid in these dykes, as does the prevalence of coarse-flame (overprinting film perthite) and (or) bleb perthite in most of these samples. However, despite the evidence for some fluid flow and potentially loss from the potassic dykes, any association between this type of metasomatism and the localization of W mineralization is lacking. This suggests that exsolved autometasomatic sodic fluids from potassically metasomatized dykes were probably of relatively low volume and not particularly significant with respect to skarn mineralization processes.

The calcic metasomatic mineral assemblages in steeply dipping aplitic dykes are attributed to an increase in the aCa^{2+} in the exsolved magmatic fluids due to bimetasomatic interaction between marble and the magmatic fluid in equilibrium with or exsolving from the aplitic dykes (Brown et al., 1985; Einaudi and Burt, 1982; Pirajno, 2010). Aplitic dykes affected by partial to pervasive calcic-1 metasomatism may still have relatively sodic compositions, but frequently display evidence for fluid exsolution and flow, such as a calcic-1 core $\pm$ central tourmaline vein(s) and marginal zones of pervasive potassic metasomatism (Fig. 13A). The exsolution of a sodic fluid from these dykes is encouraged by the accumulation of B in the residual melt or fluid during crystallization (Pirajno, 2010), and causes a sharp juxtaposition of calcic-1 and potassic mineral assemblages. However, the pervasive metasomatism experienced by most of these dykes appears to supersede the volume of fluid that can be exsolved from the potassic dyke margins, suggesting an ongoing influx of magmatic fluid from greater depths. Similarly, sub-vertical tourmaline stringers or veins localized in (rare) zones of intense calcic metasomatism cross-cutting the apical Mine Stock suggest volatile-rich magmatic fluid flow also sourced from greater depths in these areas. Furthermore, the development of calcic mineral assemblages in these intrusive phases requires an interaction between magmatic fluid and calcareous country rocks. While dykes that have been altered to calcic-1 assemblages are not directly associated with mineralization, they are interpreted to have experienced high fluid fluxes and to represent more distal equivalents to aplitic dykes displaying the pervasive calcic-2 metasomatic mineral assemblage. Calcic-2 dykes have been affected more strongly by an increased aCa^{2+} in the exsolved fluid due to an increased proximity to calcareous country rocks and a documented spatial association with mineralization (i.e., adjacent to or cross-cutting the skarn orebody); these dykes are frequently mineralized themselves. Overall, evidence for high fluid flow and the evolution of the exsolved magmatic fluids to more calcic compositions during interaction with carbonate units intrinsically links the metasomatism of the aplitic dykes to W mineralization at Cantung.

Similarly, the increased intensity of sericitic–calcic alteration proximal to most aplitic dykes associated with mineralization suggests that a relationship exists between the lower temperature responsible for this alteration and skarn mineralization processes. This late alteration of the dykes is suggested to be analogous to previously described quartz–microcline–calcite–tourmaline–apatite veins with locally abundant scheelite $\pm$ powellite or molybdenite and greisenization (Keith et al., 1989; Mathieson and Clark, 1984; van Middelaar, 1988; Zaw, 1976), which were in turn related to magmatic fluids associated with lower temperature stages of hydrous skarn formation and mineralization (Keith et al., 1989; Mathieson and Clark, 1984). The sericitic–calcic fluids are also bimetasomatic and although they may have a lower aK^+ and fluid temperature when compared to the early autometasomatic magmatic fluids responsible for potassic metasomatism (e.g., Pirajno, 2010), they are not as strongly affected by high aCa^{2+} either. This suggests that as the lower temperature skarn facies at Cantung evolved to more siliceous and hydrous compositions, the later fluids became less Ca-rich. As demonstrated by Foster (1977), scheelite solubility can actually be enhanced in KCl-rich brines buffered by muscovite–K–feldspar–quartz mineral assemblages, therefore the relative increase in aK^+ in the sericitic–calcic fluids have played a major role with respect to lower temperature W precipitation and (or) remobilization (e.g., Mathieson and Clark, 1984; Zaw and Clark, 1978).

4.3.3. Association between emplacement of the FMP and mineralizing processes

Although thermal metamorphism leading to skarnoid mineral assemblages (Mathieson and Clark, 1984) and undoubtedly some metasomatic alteration occurred in the country rocks during the

Please cite this article as: Rasmussen, K.L., et al., Felsic magmatic phases and the role of late-stage aplitic dykes in the formation of the world-class Cantung Tungsten skarn deposit, Northwest Territories, Canada, Ore Geol. Rev. (2011), doi:10.1016/j.oregeorev.2011.06.011

emplacement of the apical Mine Stock and the associated early biotite-rich dykes (that exsolved some sodic fluid), it is improbable that significant W skarn could have developed from these early intrusions. Exsolution of fluid from the apical Mine Stock upon or shortly following emplacement appears to be limited to a thin unmineralized quartz margin and related localized veining. Additionally, the lack of widespread, intense and pervasive potassic or calcic metasomatism resulting from a loss of fluid from these intrusive phases and (or) consequent interaction with calcic country rocks suggests that neither the apical Mine Stock or early biotite-rich dyke magmas were capable of exsolving enough fluid to generate a large mineralized orebody at the time of their emplacement (particularly one with a water/rock ratio averaging 40; Bowman et al., 1985). Finally, the apical Mine Stock and the early biotite-bearing dykes have not undergone a high degree of differentiation, which significantly reduces the likelihood of elevated W concentrations sequestered by their magmatic fluid phase (e.g., Candela, 1997; Candela and Piccoli, 1995; Keith et al., 1989; Meinert, 1995; Newberry and Swanson, 1986).

The Open Pit QFP dyke likely exsolved a single-phase sodic fluid (e.g., Yuvan et al., 2007) that remained in equilibrium with the crystallizing dyke, based on the pervasive development micrographic and granophyric throughout the groundmass (Downey and Lentz, 2006; Lentz and Fowler, 1992; Lowenstern and Sinclair, 1996; Pirajno, 2010), and therefore it is permissive that the Open Pit QFP is directly related to skarn mineralization in the Open Pit orebody. However, as with the plutonic phases and the early biotite-rich dykes observed underground the QFP dykes are early, relatively unevolved intrusions, therefore they are unlikely to have been a source of significant W-rich fluid at the time of their emplacement (e.g., Candela, 1997; Candela and Piccoli, 1995; Keith et al., 1989; Meinert, 1995; Newberry and Swanson, 1986). An alternate role for the QFP dyke in the localization of mineralization in the Open Pit orebody is that the dyke may have propagated a far-ranging fracture that was later utilized as a particularly efficient conduit for ascending and non-boiling mineralizing fluid(s) sourced at depth. This could resolve the contradiction of the prevalence of a relatively high temperature anhydrous skarn facies in the Open Pit orebody, which is so distal to the probable granitic source at depth. Evidence for later fluid passage along the Open Pit QFP dyke contacts includes the post-metasomatic saussuritization of calcic plagioclase and associated brecciation along the hanging-wall contact. Similarly, mineralized en-echelon quartz veins in the floor of the Open Pit actually cross-cut and overprint earlier mineralized skarn assemblages (e.g., Yuvan et al., 2007, and references therein). Overall, the possibility that the QFP dyke in the Open Pit may have caused or contributed to early skarn mineralization cannot be entirely discounted, although the dyke may have had a more indirect influence on later mineralization processes in the Open Pit.

Evidence of a B-rich sodic fluid pooling along the margins of late biotite-bearing and tourmaline-bearing dykes, or cross-cutting these dykes as tourmaline veins with bleached selvages, indicates that these late, non-aplitic dykes exsolved small quantities of magmatic fluid. The potassic mineral assemblages of many of the biotite- and tourmaline-bearing dykes are the result of this sodic fluid loss, due to a late stage build-up of volatiles in the crystallizing magma that would encourage Na to concentrate in magmatic fluid (e.g., B, F; Hibbard, 1980; Pirajno, 2010, and references therein). However, these sodic fluids appear to have been largely trapped in the dykes along their contacts, or within flame perthite and late intergranular albite. The preservation of magmatic textures in the potassic dykes also suggests that these sodic fluids did not have an exceptionally high flux, nor did significant bimetasomatic interaction with calcareous country rocks occur. Together these observations negate a significant association between the late biotite- and tourmaline-bearing dykes, and skarn mineralization processes at Cantung. Although these late dykes appear to be as highly fractionated as the aplitic dykes geochemically, they are more likely to have been sourced from local entrapments or pockets of intergranular crystals and melt ± fluid in the underlying magma chamber that did not segregate to form a significant volume of incompatible metals and other species (Hibbard, 1980).

Conversely, pinching out of the steeply dipping aplitic dykes in mineralized skarn, as well as ribboned textures indicating multiple fluid pulses and pervasive and intense development of calcic metasomatism suggests that emplacement of the aplitic dykes coincided with extensive interaction between a large quantity of magmatic fluid(s) and calcareous country rocks. Rare examples of relatively unmetasomatized aplitic dykes have a leucocratic haplogranitic mineralogy with minor to trace ferro-magnesian components (Fe-poor biotite and garnet), which combined with geochemical compositions indicates that these dykes are highly fractionated. A source of highly fractionated magma and metal-rich fluid is a deep chamber in the underlying felsic magma body, where incompatible elements (such as metals and volatiles) and highly fractionated residual magma were segregated and concentrated during normal crystallization of the parental magma to near-solidus conditions. A lowered solidus in the residual magma due to high concentrations of incompatible volatile species may have allowed segregation of incompatible elements over an extended period of time, and allowed for particularly efficient scavenging and concentration of W from the main magma body (Candela, 1997; Meinert et al., 2005; Newberry, 1998; Newberry and Swanson, 1986; Vigneresse, 2006). This is important as it has been estimated that if over 99% of a monzogranitic batholith has crystallized before a fluid phase saturates, the concentration of W in the magmatic fluid can increase by up to two orders of magnitude (Newberry and Swanson, 1986). Eventually, overpressuring initiated by, or leading to the exsolution of the magmatic fluid from the residual magma created and propagated sub-vertical fractures through the plutonic carapace. The injection of supercritical fluid and co-existing magma into the overlying country rocks must have involved minimal depressurization and cooling in order to avoid vapor exsolution (boiling). Local ribboned aplitic dykes also indicate that this was a sustained process with more than one phase of magma and (or) fluid injection. Abundant sub-vertical fractures in skarn and sub-vertical tourmaline veins cutting locally calcic-metasomatized Mine Stock near its upper contact also indicate that in many cases the residual magma did not ascend as high as, or with the supercritical magmatic fluid. However, where present the crystallizing residual magma exchanged chemically with the fluid as it interacted with calcareous country rocks to form scheelite-mineralized calc-silicate skarn. This led to an increased $a\mathrm{Ca}^{2+}$ (as $\mathrm{Ca(OH)_2}$, $\mathrm{CaCl_2}$) in the fluid and caused the pervasive calcic metasomatism of the aplitic dykes that increases in intensity with proximity to mineralization. A similar process of geochemical exchange between magmatic fluid and calcic country rocks demonstrated by bimetasomatic endoskarn formation is also evident in several other scheelite-bearing skarns, including Rudi and Ivo in the NWT, and the Pine Creek deposit in California (Brown et al., 1985).

Late-stage bimetasomatic calcic–sericitic metasomatism of all of the dykes, but particularly the aplitic dykes associated with mineralization, may be related to an increased pH and $a\mathrm{K}^{+(\mathrm{KOH,\ KCl})}$ of the mineralizing fluids, particularly as $a\mathrm{Ca}^{2+}$ decreased during the development of more hydrous and siliceous skarn facies at lower temperatures. This later increase in pH may have enhanced the solubility of scheelite in the fluid (e.g., Foster, 1977), and may be responsible for the voluminous pyrrhotite and increased scheelite grades in the amphibole- and biotite-bearing skarn facies (Mathieson and Clark, 1984). The earlier development of anorthite ± quartz endoskarn in the aplitic dykes may have also helped to focus mineralization or remobilization by these later-stage bimetasomatic fluids (as evidenced by overprinting sericitic-calcic metasomatism) by increasing the permeability of the aplitic dykes and reducing fluid pressure in proximity to the skarn orebodies (Lentz, 2005b; Yardley and Lloyd, 1995).

Please cite this article as: Rasmussen, K.L., et al., Felsic magmatic phases and the role of late-stage aplitic dykes in the formation of the world-class Cantung Tungsten skarn deposit, Northwest Territories, Canada, Ore Geol. Rev. (2011), doi:10.1016/j.oregeorev.2011.06.011

4.3.4. Aplitic dykes as an exploration tool

Altered zones in intrusions and country rocks observed in drill core at Cantung are not predictable (i.e., they do not follow a regular fracture or vein set) and are typically immediately adjacent to unaltered rocks (Mathieson and Clark, 1984; van Middelaar, 1988). Therefore, alteration of any type at Cantung is not a widespread phenomena and cannot be effectively used as an exploration tool during exploration drilling and (or) driving drifts. However, the aplitic dykes and rare margins of the underlying pluton in contact with skarn mineralization are affected by systematic calcic metasomatism that increases in intensity with proximity to mineralization. Even if metasomatized steeply dipping aplitic dykes are not always directly involved in W skarn mineralizing processes, permeability contrasts resulting from their emplacement and calcic metasomatism resulting from interaction with calcareous country rocks may have led to the focusing of later mineralizing magmatic fluids along the same structures (e.g., Atkinson, 1984; Lentz, 2005b; Yardley and Lloyd, 1995; Zaw, 1976). Recognition of the steeply dipping aplitic dykes or tourmaline-lined fractures and veins in the apical Mine Stock that have undergone pervasive calcic metasomatism may be one of the few techniques available for delineating mineralizing fluid pathways at Cantung. Careful identification of dyke phases, metasomatic mineral assemblages, and orientations has the potential to aid in future exploration for mineralization at Cantung, as well as other W skarn deposits and prospects in the northern Cordillera (Dawson, 1996; Rasmussen, 2004).

4.4. A model for magmatism and mineralization

Most workers now interpret metals to be entirely magmatically derived for W skarn systems (e.g., Meinert et al., 2003, 2005; Newberry, 1998; Newberry and Swanson, 1986), including Cantung (e.g., Bowman et al., 1985; Mathieson and Clark, 1984; McDougall, 1977; Zaw, 1976). The low background concentrations of W in the Mine and Circular stocks (e.g., 1–2 ppm; Table 2) relative to other Tungsten plutonic suite intrusions in the region suggests that W behaved very incompatibly and that the partitioning of W into melt or fluid was exceptionally efficient at Cantung. However, rather than the initial metal content or composition of the magma, the most important controls on the formation of large W skarn orebodies are indicators that the magma underwent a high degree of fractionation coupled with evidence for very late fluid exsolution (related to deep emplacement of a H_2O-poor magma; Newberry and Swanson, 1986; Keith et al., 1989; van Middelaar and Keith, 1990; Newberry, 1998). A late-stage, segregated residual magma in equilibrium with a volatile-rich magmatic fluid derived from anhydrous crystallization of a larger granitic intrusion will have a significantly suppressed solidus, allowing for the extraction of W from the intrusion at the latest stages of crystallization of the larger intrusion. Therefore, large buried bodies of coarser grained granitic intrusions lacking abundant minerals that incorporate W (e.g., ilmenite, titanite), and associated with highly evolved or late stage dykes and vein swarms emplaced into the apical pluton and overlying country rocks would be inherently more prospective for significant W mineralization. The multiple intrusive phases and deposit size at Cantung are suggestive of a deep and a large magmatic system at depth experiencing ongoing differentiation. The presence of such a deeper batholithic body capped by the exposed Mine Stock intrusions and felsic dykes at Cantung is supported by the remarkable geochemical similarities between the Mine Stock and the Circular Stock, the explosively emplaced QFP dykes and the Circular Stock pluton with its associated marginal breccia, the early crystallization of two feldspars in most or all of the FMPs (e.g., Martin and Bonin, 1976), the exceptionally high fluid/rock ratios calculated by Bowman et al. (1985), and the presence of two separate, high-grade orebodies (the E-Zone and the Open Pit). Although undoubtedly the injection of dykes at various stages of magmatic differentiation and the influx magmatic fluid(s) during the evolution of the Cantung orebody is more complicated than presented here, the evolution of magmatism and mineralization at Cantung can be simplified to represent four main magmatic events.

Initially, a relatively anhydrous sub-horizontal monzogranitic magma sourced from or capping a larger monzogranitic body at depth was emplaced as a relatively flat-topped pluton into recumbently folded sedimentary rocks. This was accompanied by a younger and finer-grained monzogranitic apical phase and at least two early dyke phases (biotite-rich and QFP) over a period of approximately 3 m.y. These early FMP represent the main stages of magmatism at Cantung and were emplaced at lithostatic conditions with a vertical minimum normal stress field at or just below the critical point of Brisbin (1986). Predominantly moderate undercooling combined with a relatively slow rate of cooling due to the elevated geothermal gradient at Cantung are the primary mechanisms for the textures observed in the apical Mine Stock and early biotite-rich dykes. However, the QFP dykes exposed only on the surface initially evolved as hot, hydrous, crystal-poor magma injected as highly pressurized magma or melt-vapor mixtures. Very high degrees of undercooling in these dykes are the result of extremely rapid pressure-quenching and extensive volatile exsolution and escape along propagating far-ranging fractures, although the Open Pit QFP may instead have crystallized at more moderate degrees of undercooling in equilibrium with a supercritical fluid that did not escape or diffuse as quickly. The exsolved magmatic fluids from these early or 'main-stage' intrusions at Cantung may have caused some metasomatization and perhaps early skarnification in the Open Pit orebody, but they are regarded as incapable of producing significant W skarn mineralization due to the lack of geochemical evidence for extensive magmatic fractionation in these FMPs (e.g., Hibbard, 1980; Newberry and Swanson, 1986).

Ongoing crystallization of the Mine Stock or underlying felsic magma chamber segregated local and relatively small pockets of highly fractionated fluid-rich magma (Candela and Piccoli, 1995). These localized residual magma pockets may have been released in pulses along dilational joints resulting from cooling of the magma (e.g., Hibbard, 1980; Mathieson and Clark, 1984) to form episodically emplaced leucocratic dykes at multiple orientations (e.g., at lithostatic conditions), but emplaced mainly along pre-existing anisotropies in the country rocks. High degrees of undercooling at fluid undersaturated ± saturated conditions, a relatively slow cooling rate, and sub-solidus potassic metasomatism resulting from the exsolution of B-rich sodic fluids characterize these dykes. However, the loss of relatively minor amounts of sodic fluid (much of which may have been trapped within the dykes) is not likely to be responsible for generating the extensive and high-grade W skarn mineralization at Cantung, despite geochemical evidence for the highly fractionated nature of these late dykes (cf. Hibbard, 1980).

The distinct suite of steeply dipping aplitic dykes was a result of the particularly effective segregation of a highly differentiated residual magma trapped in a nearly completely solidified monzogranitic magma chamber. The segregation of a fluid-rich residual magma also enriched in elements that behave incompatibly at low oxygen fugacities, including W, with the possible addition of volatile material (specifically S and H_2O) related to injections of hot lamprophyric magmas, eventually led to very late overpressuring of the residual magma and fluid. This initiated and propagated a set sub-vertical fractures through the plutonic carapace and into the surrounding country rocks, leading to a decrease in the lithostatic load and allowing the influence of far-field stresses related to regional dextral oblique transpression on the NE-trending fracture orientations. The very highly evolved residual magma comprised melt, small feldspar crystals, and an exsolved incompatible element-enriched magmatic brine that were injected along the fractures. A relatively slow ascent rate combined with a moderately deep level of emplacement (2 kbar, or greater) prevented the magmatic fluid from intersecting its solvus and boiling. Instead, a calcic fluid gradient was developed in the brine between the residual melt and the

Please cite this article as: Rasmussen, K.L., et al., Felsic magmatic phases and the role of late-stage aplitic dykes in the formation of the world-class Cantung Tungsten skarn deposit, Northwest Territories, Canada, Ore Geol. Rev. (2011), doi:10.1016/j.oregeorev.2011.06.011

calcareous country rocks reacting with the magmatic fluid to form calc-silicate W skarn mineralization. This caused the pervasive calcic metasomatism of the moderately highly undercooled crystallizing aplitic dykes. Most of the metals and incompatible elements appear to have partitioned preferentially into the brine and infiltrated the host limestone to form the skarn orebody, although some of the incompatible species (e.g., W, Cu, Bi, Au, P) were still moderately enriched in the aplite dykes. For example, even though P is incompatible in highly peraluminous residual magmas, the increased $a\mathrm{Ca}^{2+}$ in the magmatic system overall likely led to the precipitation of abundant apatite in the calcic-2 metasomatized dykes (cf. Bea et al., 1992; Breiter, 2002). The aplitic dykes and the associated exsolved incompatible element-enriched magmatic brine comprise 'early post-magmatic intrusions and fluids' that are primarily responsible for the extensive and high-grade mineralization at Cantung (cf. Hibbard, 1980).

Finally, the bimetasomatic sericitic–calcic mineral assemblage overprinting all the dyke phases and the other alteration styles were derived largely from late post-magmatic fluids (cf. Hibbard, 1980) with increased $a\mathrm{K}^{+}/a\mathrm{Ca}^{2+}$ due to a reduced interaction with calcareous country rocks during the lower temperature stages of mineralization. These late fluids were mainly injected along the steeply dipping and more permeable calcic-metasomatized dykes (e.g., Yardley and Lloyd, 1995), although in less permeable intrusions (unaltered or potassic) these fluids created muscovite–microcline–quartz–calcite micro-veins and larger quartz–tourmaline–scheelite–(powellite/molybdenite)–sulfide veins (Keith et al., 1989; Mathieson and Clark, 1984; Rasmussen, 2004; van Middelaar, 1988; Zaw, 1976; Zaw and Clark, 1978). Due to increased $a\mathrm{K}^{+}$, these late post-magmatic fluids may have had a significant role in continued W mineralization and (or) remobilization at lower temperatures (Foster, 1977; Hibbard, 1980; Mathieson and Clark, 1984; Newberry and Einaudi, 1981; Zaw, 1976; Zaw and Clark, 1978), which could explain the intensity of this type of alteration in many dykes in contact with mineralization.

Ultimately, the careful documentation of field relationships, orientations, petrographic textures, and trace element compositions of intrusive phases, but particularly of felsic dykes associated with magmatic-hydrothermal mineral deposits (e.g., Lentz, 2005a), may lead to refinements in our understanding of these systems and help to better define metallogenic models and focus exploration efforts.

Acknowledgments

We extend our sincere gratitude to an anonymous reviewer for their time and effort in reviewing this manuscript, and their pertinent comments. The authors would also like to gratefully acknowledge the assistance of D. Tenney (North American Tungsten Ltd.), B. Mann (Klondike Star Resources), Dr. D. Kontak (Laurentian University) for sharing their insight on mineralization at Cantung and mineralizing processes in general. North American Tungsten and its employees at the Cantung mine site in 2003 kindly provided generous support in the field and access to the mine workings and company reports. Funding for this project was provided by the Northwest Territories Geoscience Office, the Polar Continental Shelf Project, the Aurora Research Institute Research Assistant Program, a Natural Resources Canada and Natural Science and Engineering Research Discovery Grant to Drs. D. R. Lentz and J. K. Mortensen, and the Department of Geology and Geophysics (now the Department of Geosciences) at the University of Calgary. This manuscript is largely derived from a B.Sc. thesis completed at the University of Calgary, and is the Northwest Territories Geoscience Office Contribution 0057.

References

Adie, L., Allen, T., Ball, C.W., 1959. Report on the Geology and Ore Reserves, Canada Tungsten Mining Corporation Ltd. Property, Flat Lake, NWT. Canada Tungsten Mining Corporation Ltd.

Aitken, J.D., Cook, D.G., 1974. Carcajou Canyon map-area, District of Mackenzie, Northwest Territories. Geological Survey of Canada Paper 74–13, 28p.

Aitken, J.D., Cook, D.G., Yorath, C.J., 1982. Upper Ramparts River (106G) and Sans Sault Rapids (106H) map areas, District of Mackenzie. Geological Survey of Canada Memoir 388.

Report, Amax Internal, 1983. Technological Assessment Report of Canada Tungsten Mining Corporation Limited, Tungsten. N.W.T, Canada. 184p.

Anderson, R.G., 1983. Selwyn plutonic suite and its relationship to tungsten skarn mineralization, southeastern Yukon and District of Mackenzie. Geological Survey of Canada Paper 83-1B, pp. 151–163.

Armstrong, D.W., Harris, F.R., Kerrigan, J.E., Kiehn, O.A., Johnson, R.E., 1983. Technological Assessment Report of Canada Tungsten Mining Corporation Ltd., Tungsten, NWT. Amax Engineering and Management Services Company, Canada.

Atkinson, D., 1984. Comments and Observations on Cantung geology with comparison to Mactung based on March 19–22, 1984 mine visit. Amax Northwest Mining Company Ltd., Inter-office memorandum.

Baker, D.R., Freda, C., 2001. Eutectic crystallization in the undercooled orthoclase–quartz–H_2O system: experiments and simulations. Eur. J. Mineral. 13, 453–466.

Bartlett, S.C., 1982. Report on Surface Exploration Program 1982: Tungsten Area. Northwest Territories, Bema Industries. 45p.

Bea, F., Fershtater, G., Corretgé, L.G., 1992. The geochemistry of phosphorus in granite rocks and the effect of aluminium. Lithos 29, 43–56.

Bineli Betsi, T., Lentz, D.R., 2010. The nature of "quartz eyes" hosted by dykes associated with Au–Bi–As–Cu, Mo–Cu, and base-metal-Au–Ag mineral occurrences in the Mountain Freegold region (Dawson Range), Yukon, Canada. J. Geosci. 55, 347–368.

Blusson, S.L., 1968. Geology and tungsten deposits near the headwaters of the Flat River, Yukon Territory and District of Mackenzie, Canada. Geol. Surv. Can. Pap. 67–22, 77p.

Bowman, J.R., Covert, J.J., Clark, A.H., Mathieson, G.A., 1985. The Cantung E zone scheelite skarn orebody, Tungsten, Northwest Territories: oxygen, hydrogen, and carbon isotope studies. Econ. Geol. 80, 1872–1895.

Breiter, K., 2002. From explosive breccia to unidirectional solidification textures: magmatic evolution of a phosphorus- and fluorine-rich granite system (Podlesí, Krušné hory Mts., Czech Republic). Bull. Czech. Geol. Surv. 77, 67–92.

Brisbin, W.C., 1986. Mechanics of pegmatite intrusion. Am. Mineral. 71, 644–651.

Brown, P.E., Bowman, J.R., Kelly, W.C., 1985. Petrologic and stable isotope constraints on source and evolution of skarn-forming fluids at Pine Creek, California. Econ. Geol. 80, 72–95.

Burnham, C.W., 1985. Energy release in subvolcanic environments: implications for breccia formation. Econ. Geol. 80, 1515–1522.

Burnham, C.W., Ohmoto, H., 1980. Late-stage processes of felsic magmatism. Mining Geology Special Issue 8, pp. 1–11.

Candela, P.A., 1997. A review of shallow, ore-related granites: textures, volatiles, and ore metals. J. Petrol. 38, 1619–1633.

Candela, P.A., Piccoli, P.M., 1995. Model ore-metal partitioning from melts into vapor and vapor/brine mixtures. In: Thompson, J.F.H. (Ed.), Magmas, fluids and ore deposits. Mineralogical Association of Canada Short Course Series 23, pp. 101–128.

Castro, A., Patiño Douce, A.E., Corretgé, L.G., de la Rosa, J.D., El-Biad, M., El-Hmidi, H., 1999. Origin of peraluminous granites and granodiorites, Iberian massif, Spain: an experimental test of granite petrogenesis. Contrib. Mineral. Petrol. 135, 255–276.

Cathro, B.J., 1969. Tungsten in Yukon. Third Northern Resource Conference, Whitehorse, Yukon. 8p.

Chappell, B.W., White, A.J.R., 1992. I- and S-type granites in the Lachlan Fold Belt. Transactions of the Royal Society of Edinburgh. Earth Sci. 83, 1–26.

Chappell, B.W., Bryant, C.J., Wyborn, D., White, A.J.R., Williams, I.S., 1998. High- and low-temperature I-type granites. Resour. Geol. 48, 225–235.

Christiansen, E.H., Keith, J.D., 1996. Trace Element Systematics in Silicic Magmas: A Metallogenic Perspective. In: Wyman, D.A. (Ed.), Trace element geochemistry of volcanic rocks: applications for massive sulphide exploration: Geological Association of Canada Short Course Notes 12, pp. 115–151.

Covert, J.J., 1983. The origin of skarn-forming fluids and wall rock-skarn interaction at Cantung, Northwest Territory, Canada. Unpublished M.Sc. thesis, University of Utah, Salt Lake City

Crawford, W.J.P., 1963. Geology of the Canada Tungsten Mine, SW District of Mackenzie, Canada. Unpublished M.Sc. thesis, University of Washington, Seattle

Cummings, W.W., Bruce, D.E., 1977. Canada Tungsten: change to underground mining and description of mine-mill procedures. Can. Inst. Min. Metall. Bull. 70, 94–101.

Dawson, K.M., Dick, L.A., 1978. Regional metallogeny of the northern Cordillera: tungsten and base metal-bearing skarns in southeastern Yukon and southwestern Mackenzie. Geological Survey of Canada Paper 78-1A, pp. 287–292.

Dawson, K.M., 1996. Skarn deposits. In: Eckstrand, O.R., Sinclair, W.D., Thorpe, R.I. (Eds.), Geological Survey of Canada Geology of Canada 8, pp. 447–502.

Derre, C., Lecolle, M., Roger, G., de Freitas, Tavares, Carvalho, J., 1986. Tectonics, magmatism, hydrothermalism and sets of flat joints locally filled by Sn–W aplite-pegmatite and quartz veins; southeastern border of the Serra de Estrela granitic massif (Beira Baixa, Portugal). Ore Geol. Rev. 1, 43–56.

Dick, L.A., 1978. Tungsten Skarns in the Northern Cordillera. Western Miner. April, 68–73.

Dick, L.A., 1979. Tungsten and base metal skarns in the northern Cordillera. Current Research, Part A, Geological Survey of Canada Paper 79-1A, pp. 259–266.

Dick, L.A., 1980. A comparative study of the geology, mineralogy, and conditions of formation of contact metasomatic mineral deposits in the northeastern Canadian Cordillera. Unpublished Ph.D. thesis, Queens University, Kingston.

Dick, L.A., Hodgson, C.J., 1982. The Mactung W–Cu(Zn) contact metasomatic and related deposits of the northeastern Canadian Cordillera. Econ. Geol. 77, 845–867.

Dingwell, D.B., 1997. The brittle-ductile transition in high-level granitic magmas: material constraints. J. Petrol. 38, 1635–1644.

Please cite this article as: Rasmussen, K.L., et al., Felsic magmatic phases and the role of late-stage aplitic dykes in the formation of the world-class Cantung Tungsten skarn deposit, Northwest Territories, Canada, Ore Geol. Rev. (2011), doi:10.1016/j.oregeorev.2011.06.011

Dostal, J., Chatterjee, A.K., 1999. Contrasting behavior of Nb/Ta and Zr/Hf ratios in a peraluminous granitic pluton (Nova Scotia, Canada). Chem. Geol. 163, 207–218.
Downey, W.S., Lentz, D.R., 2006. Modelling of deep submarine pyroclastic volcanism: a review and new results. Geosci. Can. 33, 5–24.
Driver, L.A., Creaser, R.A., Chacko, T., Erdmer, P., 2000. Petrogenesis of the Cretaceous Cassiar batholith, Yukon-British Columbia, Canada: implications for magmatism in the North American cordilleran interior. Geol. Soc. Am. Bull. 112, 1119–1133.
Einaudi, M.T., Burt, D.M., 1982. Introduction — terminology, classification, and composition of skarn deposits. Econ. Geol. 77, 745–754.
Fenn, P.M., 1986. On the origin of graphic granite. Am. Mineral. 71, 325–330.
Foster, R.P., 1977. Solubility of scheelite in hydrothermal chloride solutions. Chem. Geol. 20, 27–43.
Gabrielse, H., Murphy, D.C., Mortensen, J.K., 2006. Cretaceous and Cenozoic dextral orogen-parallel displacements, magmatism, and paleogeography, north-central Canadian Cordillera. In: Haggart, J.W., Enkin, R.J., Monger, J.W.H. (Eds.), Paleogeography of the North American Cordillera: Evidence For and Against Large-Scale Displacements: Geological Association of Canada Special Paper 46, pp. 255–276.
Gagnevin, D., Daly, J.S., Poli, G., 2004. Petrographic, geochemical and isotopic constraints on magma dynamics and mixing in the Miocene Monte Capanne monzogranite (Elba Island, Italy). Lithos 78, 157–195.
Gieré, R., 1993. Transport and deposition of REE in H2S-rich fluids: evidence from accessory mineral assemblages. Chem. Geol. 110, 251–268.
Gordey, S.P., Anderson, R.G., 1993. Evolution of the Northern Cordilleran Miogeocline, Nahanni Map Area (105I), Yukon and Northwest Territories. Geological Survey of Canada Memoir, 428.
Gordey, S.P., Makepeace, A.J., 1999. Yukon digital geology. In: Gordey, S.P., Makepeace, A.J. (Eds.), Geological Survey of Canada Open File D3826.
Grant, J.A., 1986. The isocon diagram: a simple solution to Gresen's equation for metasomatic alteration. Econ. Geol. 81, 1976–1982.
Grant, J.A., 2005. Isocon analysis: a brief review of the method and applications. Phys. Chem. Earth 30, 997–1004.
Gromet, L.P., Dymek, R.F., Haskin, L.A., Korotev, R.F., 1984. The "North American shale composite": its compilation, major and trace element characteristics. Geochim. Cosmochim. Acta 48, 2469–2482.
Hadlari, T., Thomson, D., Schröder-Adams, C.J., Lemieux, Y., MacLean, B., Gabites, J., 2009. Evolution of a Northern Cordilleran foreland basin inferred from cretaceous stratigraphy. Seismic Sections, and Detrital Zircons, Mackenzie Mountains, NWT. Frontiers + Innovation, CSPG CSEG CWLS Convention, pp. 128–130.
Hall, G.E.M., Plant, J.A., 1992. Application of geochemical discrimination diagrams for the tectonic interpretation of igneous rocks hosting gold mineralization in the Canadian Shield. Chem. Geol. 95, 157–165.
Hammarstrom, J.M., Elliott, J.E., Kotlyar, B.B., Theodore, T.G., Nash, J.T., John, D.A., Hoover, D.B., Knepper Jr., D.H., 2004. Sn and (or) W skarn and replacement deposits. In: du Bray, E.A. (Ed.), Preliminary Compilation of Descriptive Geoenvironmental Mineral Deposit Models, Version 1.0. United States Department of the Interior, United States Geological Survey. http://pubs.usgs.gov/of/1995/ofr-95-0831.
Hart, C.J.R., Goldfarb, R.J., Lewis, L.L., Mair, J.L., 2004a. The northern cordilleran mid-Cretaceous plutonic province: ilmenite/magnetite-series granitoids and intrusion-related mineralization. Resour. Geol. 54, 253–280.
Hart, C.J.R., Mair, J.L., Goldfarb, R.J., Groves, D.I., 2004b. Source and redox controls on metallogenic variations in intrusion-related ore systems, Tombstone-Tungsten Belt, Yukon Territory, Canada. Trans R. Soc. Edinb. Earth Sci. 95, 339–356.
Hibbard, M.J., 1980. Indigenous source of late-stage dikes and veins in granitic plutons. Econ. Geol. 75, 410–423.
Hibbard, M.J., 1981. The magma mixing origin of mantled feldspars. Contrib. Mineral. Petrol. 76, 158–170.
Hibbard, M.J., 1994. Petrographic classification of crystal morphology. J. Geol. 102, 571–581.
Hodgson, C.J., 2000. Exploration Potential at Cantung Mine, District of Mackenzie, NWT. Andean Engineering.
Hoskin, P.W.O., Kinny, P.D., Wyborn, D., Chappell, B.W., 2000. Identifying accessory mineral saturation during differentiation in granitoid magmas: an integrated approach. J. Petrol. 41, 1365–1396.
Ishihara, S., Murakami, H., 2006. Fractionated ilmenite-series granites in southwest Japan: source magma for REE–Sn–W mineralizations. Resour. Geol. 56, 245–256.
Janoušek, V., Braithwaite, C.J.R., Bowes, D.R., Gerdes, A., 2004. Magma-mixing in the genesis of Hercynian calc-alkaline granitoids: an integrated petrographic and geochemical study of the Sázava intrusion, Central Bohemian Pluton, Czech Republic. Lithos 78, 67–99.
Jenner, G., 1996. Trace element geochemistry of igneous rocks: geochemical nomenclature and analytical geochemistry. In: Wyman, D.A. (Ed.), Trace Element Geochemistry of Volcanic Rocks: Applications for Massive Sulphide Exploration. Geological Association of Canada Short Course Notes 12, pp. 51–77.
Keith, J.D., van Middelaar, W., Clark, A.H., Hodgson, C.J., 1989. Granitoid textures, compositions, and volatile fugacities associated with the formation of tungsten-dominated skarn deposits. In: Whitney, J.A., Naldrett, A.J. (Eds.), Ore Deposition Associated with Magmas. Society of Economic Geologists Reviews in Economic Geology 4, pp. 235–250.
Keith, J.D., Christiansen, E.H., Maughan, D.T., Waite, K.A., 1998. The role of mafic alkaline magmas in felsic porphyry Cu and Mo systems. In: Lentz, D.R. (Ed.), Mineralized intrusion-related skarn systems: Mineralogical Association of Canada Short Course Series, 26, pp. 211–243.
Keppler, H., Wyllie, P.J., 1991. Partitioning of Cu, Sn, Mo, W, U, and Th between melt and aqueous fluid in the systems haplogranite–H_2O–HCl and haplogranite–H_2O–HF. Contrib. Mineral. Petrol. 109, 139–150.
Kontak, D.J., Clark, A.H., 2002. Genesis of the giant, bonanza San Rafael lode tin deposit, Peru: origin and significance of pervasive alteration. Econ. Geol. 97, 1741–1777.
Kretz, R., 1983. Symbols for rock-forming minerals. Am. Mineral. 68, 277–279.
LaCroix, P.A., Cook, R.B., 2007. Technical Report on the Mactung Tungsten Deposit. MacMillan Pass, Yukon.
Lang, J., 2000. Chapter 2: Tombstone-Tungsten magmatic belt. Mineral Deposit Research Unit Magmatic-Hydrothermal Project, Special Publication Number 2. Mineral Deposit Research Unit, Vancouver, B.C, pp. 7–49.
Lentz, D.R., 2005a. Examination of dikes in ore-forming systems: analysis of geological, petrochemical, and geotectonic constraints. Actas Del XVI Congreso Geologico Argentina, LaPlata, pp. 403–411.
Lentz, D.R., 2005b. Mass-balance analysis of mineralized skarn systems: implications for replacement processes, carbonate mobility, and permeability evolution. In: Mao, J., Bierlein, F.P. (Eds.), Mineral Deposit Research: Meeting the Global Challenge. Springer Berlin Heidelberg, pp. 421–424.
Lentz, D.R., Fowler, A.D., 1992. A dynamic model for graphic quartz–feldspar intergrowths in granitic pegmatites in the southwestern Grenville Province. Can. Mineral. 30, 571–585.
Leonard, P.R.R., Lentz, D.R., Poujol, M., 2006. Petrology, geochemistry, and U-Pb (zircon) age of the quartz–feldspar porphyry dyke at the Lake George antimony mine, New Brunswick implications for origin, emplacement process, and mineralization. Atl. Geol. 42, 13–29.
Linnen, R.L., 1998. The solubility of Nb–Ta–Zr–Hf–W in granitic melts with Li and Li + F: constraints for mineralization in rare metal granites and pegmatites. Econ. Geol. 93, 1013–1025.
Linnen, R.L., Keppler, H., 2002. Melt composition control of Zr/Hf fractionation in magmatic processes. Geochim. Cosmochim. Acta 66, 3293–3301.
Litvinovsky, B.A., Podladchikov, Yu.Yu., 1993. Crustal anatexis during the influx of mantle volatiles. Lithos 30, 93–107.
Lofgren, G., 1971. Experimentally produced devitrification textures in natural rhyolitic glass. Geol. Soc. Am. Bull. 82, 111–124.
Lofgren, G., 1974. An experimental study of plagioclase crystal morphology: isothermal crystallization. Am. J. Sci. 274, 243–273.
London, D., 1992. The application of experimental petrology to the genesis and crystallization of granitic pegmatites. Can. Mineral. 30, 499–540.
London, D., 1995. Geochemical features of peraluminous granites, pegmatites, and rhyolites as sources of lithophile metal deposits. In: Thompson, J.F.H. (Ed.), Magmas, fluids and ore deposits: Mineralogical Association of Canada Short Course Series, 23.
Lowenstern, J.B., Sinclair, W.D., 1996. Exsolved magmatic fluid and its role in the formation of comb-layered quartz at the Cretaceous Logtung W–Mo deposit, Yukon Territory, Canada. Trans. R. Soc. Edinburgh Earth Sci. 87, 291–303.
MacLellan, H.E., Tremblath, L.T., 1991. The role of quartz crystallization in the development and preservation of igneous texture in granitic rocks: experimental evidence at 1 kbar. Am. Mineral. 76, 1291–1305.
Manning, D.A.C., Henderson, P., 1984. The behaviour of tungsten in granitic melt — vapour systems. Contrib. Mineral. Petrol. 86, 286–293.
Marshall, D., Falck, H., Mann, B., Kirkham, G., Mortensen, J., 2003. Geothermometry and fluid inclusion studies of the E-zone biotite skarn, Cantung Mine, Tungsten, NWT. Abstract Volume of Talks and Posters, Yellowknife Geoscience Forum, 60.
Martin, R.F., Bonin, B., 1976. Water and magma genesis: the association hypersolvus granite — subsolvus granite. Can. Mineral. 14, 228–237.
Mathieson, G.A., Clark, A.H., 1984. The Cantung E Zone scheelite skarn orebody, Tungsten, Northwest Territories: a revised genetic model. Econ. Geol. 79, 883–901.
McDougall, G.F.E., 1977. Trace element bedrock geochemistry around the Cantung skarn-type scheelite deposits at Tungsten, Northwest Territories. Unpublished M.Sc. thesis, Queen's University, Kingston.
Meinert, L.D., 1993. Igneous petrogenesis and skarn deposits. In: Kirkham, R.V., Sinclair, W.D., Thorpe, R.I., Duke, J.M. (Eds.), Mineral Deposit Modeling. Geological Association of Canada Special Paper, 40, pp. 569–583.
Meinert, L.D., 1995. Compositional variation of igneous rocks associated with skarn deposits — chemical evidence for a genetic connection between petrogenesis and mineralization. In: Thompson, J.F.H. (Ed.), Magmas, fluids and ore deposits. Mineralogical Association of Canada Short Course Series, 23, pp. 401–418.
Meinert, L.D., Hedenquist, J.W., Satoh, H., Matsuhisa, Y., 2003. Formation of anhydrous and hydrous skarn in Cu–Au ore deposits by magmatic fluids. Econ. Geol. 98, 147–156.
Meinert, L.D., Dipple, G.M., Nicolescu, S., 2005. World skarn deposits. In: Hedequist, J.W., Thompson, J.F.H., Goldfarb, R.J., Richards, J.P. (Eds.), Economic Geology 100th Anniversary Volume. Society of Economic Geologists. Littleton, Colorado, pp. 299–336.
Menzie, D.W., Jones, G.M., 1986. Grade and tonnage models of tungsten skarn deposits. In: Cox, D.P., Singer, D.A. (Eds.), Mineral Deposit Models. United States Geological Survey Bulletin, 1693, pp. 55–57.
Moore, J.M., 1975. A mechanical interpretation of the vein and dyke systems of the S.W. England Orefield. Miner. Deposita 10, 374–388.
Morris, G.A., Creaser, R.A., 2008. Correlation of mid-Cretaceous granites with source terranes in the northern Canadian Cordillera. Can. J. Earth Sci. 45, 389–403.
Mortensen, J.K., Hart, C.J.R., Murphy, D.C., Heffernan, S., 2000. Temporal evolution of Early and mid-Cretaceous magmatism in the Tintina Gold Belt. In: Jambor, J. (Ed.), The Tintina Gold Belt: Concepts, Exploration and Discoveries. British Columbia and Yukon Chamber of Mines Special Volume, 2, pp. 49–57.
Nelson, J., Colpron, M., 2007. Tectonics and metallogeny of the British Columbia, Yukon and Alaska Cordillera, 1.8 Ga to present. In: Goodfellow, W.D. (Ed.), Mineral Resources of Canada: A Synthesis of Major Deposit-types, District Metallogeny, the Evolution of Geological Provinces, and Exploration Methods: Geological Association of Canada Special Publication, 5, pp. 755–792.

Please cite this article as: Rasmussen, K.L., et al., Felsic magmatic phases and the role of late-stage aplitic dykes in the formation of the world-class Cantung Tungsten skarn deposit, Northwest Territories, Canada, Ore Geol. Rev. (2011), doi:10.1016/j.oregeorev.2011.06.011

Newberry, R.J., 1998. W- and Sn-skarn deposits: a 1998 status report. In: Lentz, D.R. (Ed.), Mineralized Intrusion-Related Skarn Systems. Mineralogical Association of Canada, Short Course Series, 26, pp. 289–335.
Newberry, R.J., Einaudi, M.T., 1981. Tectonic and geochemical setting of tungsten skarn deposits in the Cordillera. Arizona Geol. Soc. Digest 14, 99–112.
Newberry, R.J., Swanson, S.E., 1986. Scheelite skarn granitoids: an evaluation of the roles of magmatic source and process. Ore Geol. Rev. 1, 57–81.
Oliver, N.H.S., Rubenach, M.J., Fu, B., Baker, T., Blenkinsop, T.G., Cleverley, J.S., Marshall, L.J., Ridd, P.J., 2006. Granite-related overpressure and volatile release in the mid crust: fluidized breccias from the Cloncurry District, Australia. Geofluids 6, 346–358.
Pearce, J.A., Norry, M.J., 1979. Petrogenetic implications of Ti, Zr, Y, and Nb variations in volcanic rocks. Contrib. Mineral. Petrol. 69, 33–47.
Pirajno, F., 2010. Hydrothermal processes and mineral systems. Springer Science + Business Media B.V., Geological Survey of Australia, Perth. 1250p.
Pouchou, J.L., Pichoir, F., 1985. PAP $\phi(\rho Z)$ procedure for improved quantitative microanalysis. In: Armstrong, J.T. (Ed.), Microbeam Analysis Proceedings, pp. 104–106.
Raimbault, L., Baumer, A., Dubru, M., Benkerrou, C., Croze, V., Azhm, A., 1993. REE fractionation between scheelite and apatite in hydrothermal conditions. Am. Mineral. 78, 1275–1285.
Rasmussen, K.L., 2004. The aplitic dykes of the Cantung Mine, NWT: Petrology, geochemistry, and implications for the mineralization process. Unpublished B.Sc. thesis, Department of Geology and Geophysics, The University of Calgary, Calgary, Alberta, Canada.
Rasmussen, K.L., Mortensen, J.K., Falck, H., Ullrich, T.D., 2007. The potential for intrusion-related mineralization within the South Nahanni River MERA area, Selwyn and Mackenzie Mountains, Northwest Territories. In: Wright, D.F., Lemkow, D., Harris, J.R. (Eds.), Mineral and Energy Resource Assessment of the Greater Nahanni Ecosystem under Consideration for the Expansion of the Nahanni National Park Reserve, Northwest Territories: Geological Survey of Canada Open File 5344, pp. 203–278.
Rasmussen, K.L., Mortensen, J.K., Arehart, G., 2010. Radiogenic and stable isotopic compositions of mid-Cretaceous intrusions in the Selwyn Basin, Yukon and Northwest Territories. GeoCanada 2010, 4p.
Reid, J.B., Baldwin, R.D., Bakker, F.J., 2009. Technical Report on the Cantung Mine, Northwest Territories. Canada for North American Tungsten Corporation Ltd., Report for NI 43–101, August 18, 2009. accessed at http://www.northamerican-tungsten.com/i/pdf/Tech-Report-CanTung-Mine.pdf on November 1, 2010.
Rubin, J.N., Henry, C.D., Price, J.G., 1993. The mobility of zirconium and other immobile elements during hydrothermal alteration. Chem. Geol. 110, 29–47.
Shinohara, H., Kazahaya, K., 1995. Degassing processes related to magma-chamber crystallization. In: Thompson, J.F.H. (Ed.), Magmas, fluids and ore deposits. Mineralogical Association of Canada Short Course Series 23, pp. 47–70.
Sinclair, W.D., Richardson, J.M., 1992. Quartz–tourmaline orbicules in the Seagull batholith, Yukon Territory. Can. Mineral. 30, 923–935.
Štemprok, M., Seifert, T., Holub, F.V., Chlupáčová, M., Dolejš, D., Novák, J.K., Pivec, E., Lang, M., 2008. Petrology and geochmemistry of Variscan dykes from the Jáchymov (Joachimsthal) ore district, Czech Republic. J. Geosci. 53, 65–104.
Stott, D.R., Yorath, C.J., Dixon, J., 1991. The Foreland Belt, Upper Jurassic to Paleogene assemblages, Chapter 9. In: Gabrielse, H., Yorath, C.J. (Eds.), Geology of the Cordilleran Orogen in Canada. Geological Survey of Canada: Geology of Canada 4, pp. 335–344.
Streckeisen, A.L., 1976. To each plutonic rock its proper name. Earth Sci. Rev. 12, 1–33.
Sun, S.-s., McDonough, W.F., 1989. Chemical and isotopic systematic of oceanic basalts: implications for mantle compositions and processes. In: Saunders, A.D., Norry, M.J. (Eds.), Magmatism in the Ocean Basins. Geological Society, London, pp. 313–345.
Swanson, S.E., 1977. Relation of nucleation and crystal growth to the development of granitic textures. Am. Mineral. 62, 966–978.
Swanson, S.E., Fenn, P., 1986. Quartz crystallization in igneous rocks. Am. Mineral. 71, 331–342.
Tartèse, R., Boulvais, P., 2010. Differentiation of peraluminous leucogranites "en route" to the surface. Lithos 114, 353–368.
Tosdal, R.M., Richards, J.P., 2001. Magmatic and structural controls on the development of porphyry Cu ± Mo ± Au deposits. In: Richards, J.P., Tosdal, R.M. (Eds.), Structural Controls on Ore Genesis. Society of Economic Geologists Reviews, 14, pp. 157–181.
Vallance, J., Cathelineau, M., Boiron, M.C., Fourcade, S., Shepherd, T.J., Naden, J., 2003. Fluid-rock interactions and the role of late Hercynian aplite intrusion in the genesis of the Castromil gold deposit, northern Portugal. Chem. Geol. 194, 201–224.
van Middelaar, W.T., 1988. Alteration and mica chemistry of the granitoid associated with the Cantung scheelite skarn, Tungsten, Northwest Territories, Canada. Unpublished Ph.D. dissertation, University of Georgia, Athens
van Middelaar, W.T., Keith, J.D., 1990. Mica chemistry as an indicator of halogen and oxygen fugacities in the CanTung and other W-related granitoids in the North American Cordillera. In: Stein, H.J., Hannah, J.L. (Eds.), Ore-bearing granite systems: petrogenesis and mineralizing processes: Geological Society of America Special Paper, 246, pp. 205–220.
Vigneresse, J.-L., 2006. Element mobility in melts during successive intrusion of crustal-derived magmas and Sn–W mineralization. Resour. Geol. 56, 293–314.
Vigneresse, J.-L., 2007. The role of discontinuous magma inputs into felsic magma and ore generation. Ore Geol. Rev. 30, 181–216.
Wang, R.C., Fontan, F., Xu, S.J., Chen, X.M., Monchoux, P., 1996. Hafnian zircon from the apical part of the Suzhou Granite, China. Can. Mineral. 34, 1001–1010.
Watson, B., 1981. Cantung Internal Map.
Webber, K.L., Falster, A.U., Simmons, W.B., Foord, E.E., 1997. The role of diffusion-controlled oscillatory nucleation in the formation of line rock in pegmatite–aplite dikes. J. Petrol. 38, 1777–1791.
Webster, J., Thomas, R., Föster, H.-J., Seltmann, R., Tappen, C., 2004. Geochemical evolution of halogen-enriched granite magmas and mineralizing fluids of the Zinnwald tin–tungsten mining district, Erzgebirge, Germany. Miner. Deposita 39, 452–472.
Wedepohl, K.H., 1995. The composition of the continental crust. Geochim. Cosmochim. Acta 59, 1217–1232.
Winchester, J.A., Floyd, P.A., 1977. Geochemical discrimination of different magma series and their differentiation products using immobile elements. Chem. Geol. 20, 325–343.
Wolfe, J.A., 1980. Fluidization versus phreatomagmatic explosions in breccia pipes. Econ. Geol. 75, 1105–1111.
Yardley, B.W.D., Lloyd, G.E., 1995. Why metasomatic fronts are really metasomatic sides. Geology 23, 53–56.
Yorath, C.J., 1991. Upper Jurassic to Paleogene assemblages. In: Gabrielse, H., Yorath, C.J. (Eds.), Geology of the Cordilleran Orogen in Canada. Geological Survey of Canada, Geology of Canada, 4, pp. 329–371.
Yuvan, J., Shelton, K., Falck, H., 2007. Geochemical investigations of the high-grade quartz–scheelite veins of the Cantung Mine, Northwest Territories. In: Wright, D.F., Lemkow, D., Harris, J.R. (Eds.), Mineral and Energy Resource Assessment of the Greater Nahanni Ecosystem under Consideration for the Expansion of the Nahanni National Park Reserve, Northwest Territories: Geological Survey of Canada Open File 5344, pp. 177–190.
Zaraisky, G.P., Aksyuk, A.M., Devyatova, V.N., Udoratina, O.V., Chevychelov, V.Yu., 2009. The Zr/Hf ratio as a fractionation indicator of rare-metal granites. Petrology 17, 25–45.
Zaw, U.K., 1976. The Cantung E-zone orebody, Tungsten, Northwest Territories: a major scheelite skarn deposit. Unpublished M.Sc. thesis, Queen's University, Kingston, Ontario, Canada.
Zaw, U.K., Clark, A.H., 1978. Fluoride-hydroxyl ratios of skarn silicates, Cantung E-zone scheelite orebody, Tungsten, Northwest Territories. Can. Mineral. 16, 207–221.

Please cite this article as: Rasmussen, K.L., et al., Felsic magmatic phases and the role of late-stage aplitic dykes in the formation of the world-class Cantung Tungsten skarn deposit, Northwest Territories, Canada, Ore Geol. Rev. (2011), doi:10.1016/j.oregeorev.2011.06.011